

Multi Miner



www.multiminer.eu



[@company/multiminer](https://www.linkedin.com/company/multiminer)



[@MultiMiner_EU](https://twitter.com/MultiMiner_EU)

Grant Agreement No: 101091374

Project Start Date: 1st January 2023

Project Duration: 42 Months

Deliverable No 4.1

Part 1: Field Guidebook



Grant agreement	101091374
Project title	Multi-Source and Multi-Scale Earth Observation and Novel Machine Learning for Mineral Exploration and Mine Site Monitoring
Project acronym	MultiMiner
Project coordinator	Dr. Maarit Middleton, GTK
Project start date	Jan 1, 2023
Project duration	42 months
Related work packages	WP 4 – Site Demonstrations
Related task(s)	Task 4.1 In situ data standardization and databases
Lead organization	Geosphere Austria
Contributing partners	GTK, BGR, VTT, RHI, MUL, EFTAS, HSGME, CGS
Submission date	May 31, 2024
File name	D4_1_MultiMiner_Field_Guidebook_V1_4.docx
Organisation responsible for deliverable	Geosphere Austria
Author name(s)	Holger Paulick, Kati Laakso, Matthieu Molinier, Michaela Frei, Veronika Kopačková-Strnadová, Piotr Lipiarski, Pauliina Liwata-Kenttälä, Marianthi Anastasatou, Constantinos Mavrogonatos, Alexandros Liakopoulos, Gerald Schuberth-Hlavac, Neea Heino, Martin Schodlok, Maarit Middleton, Alireza Hamedianfar, Oleg Antropov, Miradije Rama, Martin Kýhos, Jan Jelének, Patrick Reschke, Kai Hahne, Panagiotis Daoultzis
Date	June 30, 2024
Version	1.1
Status	Complete
Dissemination Level	Public

Revision History

Version	Date	Modified By	Comments
V1	01.05.2023	The task team	First version
V1.1	01.12.2023	The task team	An updated version
V1.2	15.01.2024	The task team	An updated version
V1.3	24.02.2024	Holger Paulick	Clean version
V1.4	16.03.2024	Kati Laakso	Clean version
V1.5	30.06.2024	Holger Paulick	Final version

Disclaimer



The contents of this publication are the sole responsibility of its author and do not necessarily reflect the opinion of the European Union.

Contents

Revision History	2
Disclaimer	2
1. Executive Summary.....	6
2. Introduction	7
2.1 Project summary	7
2.2 Purpose of the Field Guidebook	10
2.3 The general workflow	11
2.4 Relation to other project documents and deliverables.....	12
3. The field guidebook	12
3.1 Field work.....	12
3.1.1 Spatial localization of in-situ data	12
3.1.2 Geological mapping	12
3.1.3 Geochemical analyses of rock surfaces in the field.....	12
3.1.4 Spectral data acquisition – Field spectroscopy on rock surfaces and tailings material	13
3.1.5 Spectral data acquisition - Field spectroscopy on substrates/minerals in the context of Acid Mine Drainage (AMD) investigation	13
3.1.6 Spectral data acquisition - Field spectroscopy to monitor dust covering on vegetation	14
3.1.7 In-situ vegetation measurements	14
3.1.8 Water quality measurements in the context of Acid Mine Drainage (AMD) investigation	16
3.1.9 Ground moisture measurements	16
3.1.10 Characterization of tailings.....	19
3.1.11 In-situ dust measurements.....	19
3.2 Mineralogical and geochemical characterization of samples – laboratory data	19
3.2.1 Rock sampling strategy for integrated spectral, mineralogical and geochemical analyses.....	19
3.2.2 Laboratory analysis of substrate/minerals in the context of Acid Mine Drainage (AMD) investigation	20
3.2.3 Spectral analyses of individual rock samples and tailings material in the laboratory	21
3.2.4 X-ray powder diffraction (XRD, XRPD) analyses	21



3.2.5 Geochemical analyses (XRF analyses; ICP-MS analyses)	21
3.2.6 Micro-XRF analyses.....	22
3.2.7 Petrographic description of rock sample thin sections	22
3.2.8 Micro-scale mineralogical analyses of rock and tailings samples (SEM-EDS)	22
3.2.9 Geochemical analyses of individual minerals (EMPA).....	23
3.3 UAV data acquisition	23
3.3.1 UAV data acquisition in the context of vegetation monitoring (Hochfilzen test site)	24
3.3.2 UAV data acquisition: in the context of mineral mapping and TSF monitoring.....	25
3.3.2.1 Hyperspectral UAV HySpex Mjöl­nir VS620 System	25
3.3.2.2 Photogrammetry DJI Mavic 3 RTK System	25
3.3.2.3 Rules and Regulations.....	26
3.3.2.4 Before the flight.....	26
3.3.2.5 During the flight.....	27
3.3.3 UAV data acquisition for water and AMD monitoring	29
3.3.3.1 Parrot Sequoia multispectral data + RGB photogrammetric products	29
3.3.3.2 Before the flight.....	30
3.3.3.3 Setting up the calibration targets (spectral and geometric)	31
3.3.3.4 Data acquisition	31
3.3.4 Water spectrum acquired by UAV's based microspectrometer OceanOptics STS-VIS.....	31
3.3.4.1 Before the flight.....	32
3.3.4.2 Data acquisition	33
3.3.5 PIKA L hyperspectral data.....	34
3.3.5.1 Before the flight.....	34
3.3.5.2 Setting up the calibration targets.....	35
3.3.5.3 Data acquisition	36
4. References	36



List of Figures

Figure 1. Organic soil dielectric constant measurement using hand-held percometer.....	18
Figure 2. IoT soil moisture sensor installation. In the left image, the soil moisture sensor is attached to the wooden pole, and in the right image, the probe is situated 5 cm below the surface of the ground...19	19
Figure 3. An example of a size sample cut to sizes 1/3 and 2/3.	20
Figure 4. BFD XQ - 1400S with Gimbal and Mjolnir.....	25
Figure 5. DJI Mavic 3E with RTK antenna.	26
Figure 6. A base station with white reference targets.	28
Figure 7. Parrot Sequoia with solar irradiance sensor.	29
Figure 8. A Parrot Sequoia UAV setup (Kopačková-Strnadová et al., 2021).	30
Figure 9. An Airinov calibration target.	31
Figure 10. STS Development Kit.	32

List of Tables

Table 1. A list of acronyms used in this document.....	6
Table 2. The Consortium Partners and the Associated Partner (RHI Magnesita) of the MultiMiner project.	9
Table 3. The MultiMiner applications and sites.	11
Table 4. Overview of the Perrot Sequoia spectral band setting.	29

List of Appendices

Appendix 1: Description of MultiMiner database for in-situ metadata
Appendix 2: Field guide to the regional geology of Hochfilzen test site (Austria)
Appendix 3: Field guide to the regional geology of Kallyntiri test site (Greece)
Appendix 4: Hyperspectral data acquisition, field
Appendix 5: Hyperspectral data acquisition, laboratory



List of Acronyms

Table 1. A list of acronyms used in this document.

Abbreviation	Meaning
AMD	Acid Mine Drainage
EO	Earth Observation
CRM	Critical Raw Material
DMP	Data Management Plan
EDS	Energy Dispersive X-ray Spectroscopy
EMPA	Electron Microprobe Analysis
EO	Earth Observation
FVC	Fractional Vegetation Cover
GO	General Objective
LAI	Leaf Area Index
NIR	Near Infrared
SEM	Scanning Electron Microscope
SO	Strategic Objective
SWIR	Short-wavelength Infrared
TMF	Tailings Management Facility
TSF	Tailings Storage Facility
TOC	Total Organic Carbon
VWC	Volumetric Water Content
XRF	X-Ray Fluorescence
XRPD	X-ray Powder Diffraction

1 Executive Summary

The Multi-source and Multi-scale Earth observation and Novel Machine Learning Methods for Mineral Exploration and Mine Site Monitoring (MultiMiner) project develops novel data processing algorithms for cost-effective utilization of Earth Observation (EO) technologies for mineral exploration and mine site monitoring. The project focuses on new EO-based exploration technologies for critical raw materials (CRM) to increase the probability of finding new sources within EU thereby strengthening the EU autonomy in the area of raw materials.

In this document, the field work and laboratory work protocols of the MultiMiner project are described. This relates to the actual materials and parameters measured and includes protocols for geological mapping, geochemical analysis, vegetation mapping, water analyses, spectral analyses, ground moisture measurements, dust monitoring, as well as dam stability and open pit stability monitoring.

In terms of laboratory measurements spectral data acquisition protocols, X-Ray Fluorescence (XRF), X-Ray Diffraction (XRD), inductively coupled plasma mass spectrometry (ICP-MS), petrographic description of rock samples in thin section, scanning electron microscope-energy dispersive X-ray spectroscopy (SEM-EDS) and electron probe microanalysis (EMPA) are described. Furthermore, Appendix 1, describes the structure of the metadata database of the project. The regional geology of the Hochfilzen test site and



the Kallyntiri test site are presented in Appendices 2 and 3, respectively. In Appendices 4 and 5, the hyperspectral field and laboratory protocols are documented.

2 Introduction

2.1 Project summary

The Multi-source and Multi-scale Earth observation and Novel Machine Learning Methods for Mineral Exploration and Mine Site Monitoring (MultiMiner) project develops novel data processing algorithms for cost-effective utilization of Earth Observation (EO) technologies for mineral exploration and mine site monitoring. MultiMiner unlocks the potential of EO data, including Copernicus, commercial satellites, upcoming missions, airborne and low altitude as well as in situ data, to support the entire mining life cycle including mineral exploration, operational, closure and post-closure stages. This is achieved by creating generic but highly innovative machine learning solutions. The project focuses on new EO based exploration technologies for critical raw materials (CRM) to increase the probability of finding new sources within EU thereby strengthening the EU autonomy in the area of raw materials. MultiMiner EO based exploration solutions have extremely low environmental impact, and are thus socially acceptable, economically efficient and improve safety. The project's solutions for mine site monitoring increase the transparency of mining operations as environmental impacts can be detected as early as possible. Also, digital information of currently unexploitable raw materials can be stored for future generations. The applicability of the developed algorithms is demonstrated in five European test sites. MultiMiner is a pan-European consortium consisting of 12 partners and 1 associated partner from research institutes, academia, consulting businesses and mining industry with interdisciplinary backgrounds in geology, remote sensing and machine learning. The members come from five EU member states which represent mining regions across Europe with diverse geology with evident potential for various types of CRM resources and abundant operational and closed mines.

The strategic aim of MultiMiner is to provide Europe with novel scalable, robust and integrated mineral exploration and mine site monitoring solutions based primarily on multi-source EO data, facilitating discovery of critical raw materials (CRM) and their safe and environmentally sustainable exploitation in Europe. To enable the transition towards the MultiMiner strategy, the following two strategic objectives (SO) have been defined to address the expected outcomes of the call HORIZON-CL4-2022-RESILIENCE-01-08:

(SO1) To develop scalable methods combining extensive Earth Observation (EO) data at multiple spectral, spatial and temporal resolutions, and making the most efficient use of scarcely available in situ measurements, while improving the efficiency and timeliness of EO-assisted critical raw material exploration, and monitoring of mine operations and environmental impacts.

(SO2) To demonstrate the added-value of the novel products and services covering the whole mining life cycle across Europe and providing mining stakeholders and EO value-adding industry with pathways contributing to increasing access to critical raw materials in Europe in a sustainable way.

In order to achieve the strategic objectives (SO1) and (SO2), we have specified four general objectives (GO1) to (GO4), each operationalized by specific objectives:



(GO1) To develop scalable and automated approaches for mineral exploration based on multi-source EO data and sparse in situ data, focused on mineral deposits hosting CRMs across EU.

(GO2) To leverage novel EO data analysis methods to make the most of scarcely available in situ data for timely mine site monitoring, reducing both disruptions to mining activities and environmental impacts.

(GO3) To demonstrate novel exploration and monitoring methods for the whole mining life cycle in five test sites across Europe, emphasizing their potential to increase access to critical raw materials across Europe.

(GO4) To share the innovative MultiMiner methods broadly with European value-adding industry to stimulate further research and developments and ensure their exploitation by the European mining industry.

The project comprises the Consortium Partners listed in **Table 2**.



Table 2. The Consortium Partners and the Associated Partner (RHI Magnesita) of the MultiMiner project.

Name	Short name	Country	
GEOLOGIAN TUTKIMUSKESKUS	GTK	Finland	
TEKNOLOGIAN TUTKIMUSKESKUS VTT OY	VTT	Finland	
Nordkalk Oy Ab	Nordkalk	Finland	
ELLINIKI ARCHI GEOLOGIKON KAI METALLEFTIKON EREVNON	HSGME	Greece	
FONDATION EUROPEENNE DE LA SCIENCE	ESF	France	
CESKA GEOLOGICKA SLUZBA	CGS	Czechia	
MONTANUNIVERSITAET LEOBEN	MUL	Austria	
BUNDESANSTALT FUER GEOWISSENSCHAFTEN UND ROHSTOFFE	BGR	Germany	
GEOSPHERE AUSTRIA	GeoSphere Austria	Austria	
HELLAS GOLD S.A	HG	Greece	
EFTAS FERNERKUNDUNG TECHNOLOGIETRANSFER GMBH	EFTAS	Germany	
TECHNISCHE UNIVERSITAET MUENCHEN	TUM	Germany	



Name	Short name	Country
RHI Magnesita	RHI	Austria



2.2 Purpose of the Field Guidebook

The field guidebook is a contribution of MultiMiner Task 4.1: *In Situ* data standardization and databases to Deliverable D4.1: “Field work protocols for in-situ data collection and review of accuracy assessment methods. Description of the data collection standards and protocols to be used in accuracy assessment of the multi-scale and multi-source data products and test site specific ground truth activities.”

The MultiMiner Projects aims to integrate multiple sources and scales of data from the ground to space at several test sites (Ihalainen, Finland; Hochfilzen, Austria; Chalkidiki, Greece; Kallyntiri, Greece; Kirki, Greece). In this context, data collection on the ground (“in-situ”) serves two principal purposes: *calibration* and *validation* of remote data interpretation. Here we use the term “in-situ” to imply direct observation and/or measurement in the field as well as laboratory analyses of samples. The sampled materials include water, rock, soil, substrate and tailings.

Within the scope of MultiMiner work package 2 (“Scalable mineral prospectivity tools”) the main focus is on characterization of changes in mineralogical composition of rocks which can be interpreted in the context of mineral systems as prospectivity indicators in exploration. Hence, a combination of field-based measurements and observations (geological field work, field spectrometry, geochemical analyses of rock surfaces in the field), laboratory analyses (spectrometry, X-ray powder diffraction, thin section petrography, geochemical analyses of rock samples and individual minerals) and remote spectral measurements (drones, aircraft, and satellite) will be applied. In this deliverable the protocols for field measurements and observations as well as laboratory analyses are described. These data feed into Task 2.1 MultiMiner Mineral Mapping Algorithm and 2.2 MultiMiner workflows for multiscale data interpretation.

Within the scope of MultiMiner work package 3 (“Timely mine site monitoring”) the parameters and materials collected as “in-situ” data are diverse, and include vegetation measurements, water quality samples, ground moisture measurements, analyses of rock, soil, stream sediments and substrate samples, information on volume and composition development of tailings, reference measurements for dam stability monitoring, and samples and measurements for dust monitoring. These data feed into Tasks 3.2 Vegetation monitoring, Task 3.3 Water quality, Acid Mine Drainage and ground moisture monitoring, 3.4 Integrated 3D mine site monitoring and 3.5 combined atmospheric and surface dust monitoring.

Mineral prospectivity mapping is conducted in Chalkidiki and Kallyntiri. Vegetation monitoring will be carried out at Hochfilzen (Austria). In-situ data regarding water quality will be obtained at Chalkidiki and Kirki sites (Greece) which includes investigation of acid mine drainage at Kirki (Greece). Measurements regarding monitoring of dams, ground moisture and open pit are planned for at Ihalainen site in Finland. In situ measurements for dust monitoring will be taken at Ihalainen and Chalkidiki sites. Samples and in situ measurements for monitoring tailings volume and composition will be collected at the tailings storage



facility of Olympias mine (Chalkidiki; Greece), where material is already under the process of being transported to Kokkinolakkas tailings management facility, Stratoní (Chalkidiki; Greece). The applications and the sites where the work is conducted are shown in Table 3.

Table 3. The MultiMiner applications and sites.

	Mineral prospectivity mapping	Vegetation monitoring	Water quality / AMD*	Dam stability monitoring / ground moisture monitoring / open pit monitoring	Dust monitoring	TSF monitoring
Ihalainen				X	X	
Hochfilzen	X	X				
Chalkidiki	X		X		X	X
Kallyntiri	X					
Kirki			X			

*) AMD monitoring is done in Kirki only.

The aim of this fieldwork guide is to ensure that each type of in-situ data collected within the scope of the MultiMiner project are described appropriately. This includes appendices to this document that describe in more detail certain parameters, field measurement instructions or laboratory procedures. Furthermore, a metadata database structure is designed to link the various types of data to a geographically defined point. This is in addition to any naming systematics used by individual researchers working in the field. A description of the database structure is part of this field work guide (Appendix 1). The responsibility for imports into the MultiMiner database lies with the organisation responsible for the coordination of field work at the specific test site.

2.3 The general workflow

The field work protocols for the remote sensing studies, in particular those that involve geology, follow specific workflows. In such studies, field spectral measurements are often collected at the same time as samples that will later be analyzed in a laboratory. Here, field spectroscopy refers to spectral measurements that are acquired in contact with the sample or acquired from some distance. The latter is often referred to as proximal remote sensing. Sometimes field spectral measurements are complemented by handheld XRF geochemical analyses or other field analytical measurements. Sample collection is commonly accompanied by drone data acquisition and, if possible, satellite data acquisition. The collected samples, field spectral measurements, field analytical measurements and later laboratory analytics are commonly used as validation data.

The structure of this document follows the common workflow of field work in geological studies. In section 3.1 the field work protocols of different applications of the project (geological field mapping, spectral analyses / geochemical analyses using field instruments, vegetation monitoring, measurements of water quality, ground moisture, dam stability, dust and tailing) are discussed. Section 3.2 comprises the laboratory analytical methods of the project (laboratory spectroscopy, XRD, XRF, ICP-MS, thin section analysis, SEM-EDS, EMPA). Finally, in section 3.3, the protocols of UAV data acquisition are discussed.



2.4 Relation to other project documents and deliverables

The data_management_plan (DMP; deliverable D5.4) of the project describes how the MultiMiner project processes and shares its data and other research outputs internally and externally. In the DMP the following aspects are discussed, among other: i) metadata formats, ii) data types and data formats iii) sharing of physical samples, and thus the deliverable has links to D4.1 (this document). This document also links to part 2 of D.1: *Review of accuracy assessment methods* and D4.2: *Report on evaluation of the novel products in terms of their accuracy and applicability in mineral exploration and mine site monitoring*, which discusses how field data are used to assess the accuracy of research results extracted from remotely sensed data.

3 The field guidebook

3.1 Field work

3.1.1 Spatial localization of in-situ data

All in-situ data must be accompanied by information on where the measurement or sample was obtained. This must be documented as X,Y coordinates in WGS 84 coordinate system (EPSG: 4326) together with a Z- coordinate (in meters above sea-level).

3.1.2 Geological mapping

Geological field mapping is carried out at the test sites of Hochfilzen (Austria) and Kallyntiri (Greece). Mapping of the lithological and structural setting is of great importance to mineral deposit exploration on a regional scale and can define vectors to hidden mineralization in the subsurface. This work is in the expertise of field geologists mapping rocks outcropping in the area of interest. From the geological perspective, mapping of rock types involves visual inspection on the ground with the aim to characterize different rock types (“lithologies”), their contact relationships and any tectonic structures that may be present. Mineralogical characterizations can be done in the field, provided that the grain size is sufficient for mineral recognition with a hand lens. This, however, relies on the expertise and experience of the individual geologist and is commonly accompanied by sampling representative rock types in order to back-up field characterizations with analytical data such as thin section petrography, X-ray diffraction or geochemical analyses. Such analytical data are used as validation to characterize the accuracy of field mapping information.

3.1.3 Geochemical analyses of rock surfaces in the field

X-ray fluorescence (XRF) spectroscopy is a standard analytical technique for geochemical analysis (e.g., Beckhoff et al. 2006). In the last decades, manufacturers have deployed portable (handheld) XRF (pXRF) instruments. Before 2000, pXRF applications in mineral exploration were rarely reported (Young et al., 2016); nevertheless, nowadays, it is a routine method in the field. During the last years, the pXRF method has improved in analytical precision matters. However, critical parameters, such as matrix homogeneity, calibration and normalization (e.g., trace and major concentrations, Compton normalization) and



operation safety remain challenges of constant improvement (Young et al., 2016). Portable X-ray Fluorescence (pXRF) spectra are collected in the field at the Kallyntiri area (Greece) by HSGME with a Thermo Scientific Niton XL5 Plus handheld XRF analyzer.

3.1.4 Spectral data acquisition – Field spectroscopy on rock surfaces and tailings material

Spectral measurements on rock and tailings surfaces provide information on the mineralogical composition of the rocks and the chemical composition of the minerals. Diagnostic spectral patterns can be observed for different types of minerals depending on the wavelength and characteristics of associated spectral features. Most commonly, visible-near infrared (VNIR) to short-wave infrared (SWIR) spectra are used to discriminate and characterize carbonate, sulphate and phyllosilicate minerals in the field.

Spectral analyses of rocks in the field are of critical importance for integration of in-situ data and remote spectral data (sourced from drone, aircraft or satellite). The conditions of the measurements need to be documented including date and time, weather conditions, instrument type, general characteristics of rock material analyzed etc. Detailed instructions for spectral analyses carried out in the field are provided in the “Hyperspectral field guide manual” (Appendix 4). This type of in-situ data are collected at the test sites Hochfilzen (Austria), Chalkidiki (Greece) and Kallyntiri (Greece).

3.1.5 Spectral data acquisition - Field spectroscopy on substrates/minerals in the context of Acid Mine Drainage (AMD) investigation

To ensure representative AMD spectral libraries and measurements, soil/substrate plots are carefully chosen to reflect the most homogeneous patches and a wide range of mineral types. Additionally, each soil/substrate plot is photographed alongside a reference person. Measurements are conducted during cloudless moments. Field measurements take place when the sun's elevation is at its highest (between 11 am and 2 pm). During the spectral measurements, photographs of the sky are taken to accurately document the prevailing sky conditions at the time of data collection.

Spectral data is collected in natural illumination conditions using a spectro-radiometer device (Spectral Evolution SR2500), and the collected spectra (400-2500 nm) are normalized using a Spectralon panel. To ensure precision, the Spectralon plate is leveled using a spirit-level and remains steady with the help of a tripod. The data collection process involves a sweeping motion, wherein the stick with the attached spectrometer sensor is moved across the target. To achieve consistent measurement parameters (e.g., Field Of View - FOV), the sensor head is attached to a 1m stick. When measuring the field spectrum of "pure" AMD indicator minerals, the sensor is positioned close to the sample surface to reduce the FOV. In cases where a small area needs to be measured, a contact probe is utilized.

In the LWIR wavelength range, spectral data are acquired using the Agilent 4300 Handheld FTIR spectrometer. The measurements are frequently normalized against a diffuse gold reference. Care is taken that the foreoptics of the instrument do not get wet or dirty during the measurements. Any dust is removed from the foreoptics using lint-free tissues. The measurements are carried out using a contact probe of a diameter of 8 mm. A few measurements are collected from each sample, the exact amount of



which depends on the size of the sample. In the Kirki site (Greece), the Agilent instrument is used for AMD investigations.

3.1.6 Spectral data acquisition - Field spectroscopy to monitor dust covering on vegetation

Optical spectrum of the leaves is collected using the SR2500 spectrometer (400–2500 nm). To ensure standardized measurement conditions and comparability across spectral measurements, the collected spectra are normalized using a Spectralon panel. Additionally, a benchtop reflectance probe is utilized to measure under control conditions the reflectance of the leaves, which are covered with varying quantities of dust as well as completely clean and dry leaves.

3.1.7 In-situ vegetation measurements

Rationale for in-situ vegetation measurements in the MultiMiner context

Vegetation cover around Weissenstein open pit at the Hochfilzen (Austria) test site includes pasture and other type of grasslands, recultivated meadows, as well as vegetation in natural transition (bushes, young trees). To accommodate this wide range of vegetation types and ensure upscaling from in situ to drone and EO can be achieved for all vegetation types, two commonly used in situ measurements were selected for their complementarity in the context of vegetation monitoring:

- Leaf Area Index (LAI) quantifies the amount of foliage in the plant canopy and corresponds to the projected area of leaves over a unit of land (m^2). It is an important structural property of vegetation that is strongly linked to canopy structure and ecological functions, such as net primary production, water and nutrient use, and carbon balance.
- Fraction of Vegetation Cover (FVC) is a biophysical parameter, generally defined as the ratio of the vertical projection area of above-ground vegetation on the ground to the total measurement area. FVC is a key indicator of grassland health.

Both LAI and FVC can be upscaled to drone and satellite imagery through e.g. vegetation indices and either regression or inversion models. LAI and FVC measures fulfil the scope of the proposed vegetation monitoring activity, enabling comparison of vegetation characteristics and growing patterns at recently revegetated areas of the active mine site, compared to surrounding vegetated areas under different management regimes (either in natural succession or from other land uses).

At the beginning of MultiMiner project, it was found that monitoring plant biodiversity at Weissenstein site was of high interest, since revegetation of grasslands took into account the natural mix of plant species in the area, which was not the case of all other land uses in the vicinity. Monitoring plant biodiversity was also deemed feasible and a relevant activity for MultiMiner. Linking EO derived features to measures of plant biodiversity is challenging, but several successful studies were found for drone hyperspectral images and Sentinel-2 images time series. Therefore, additional in situ measurements were collected in connection to plant biodiversity:

- species richness: simply estimated as the amount of different plant species covering a given ground measuring unit
- dominant species: the main plant species covering the ground measuring unit



Vegetation measurements at Hochfilzen (Weissenstein)

The locations for in situ vegetation measurements were selected before field work, using the following sampling scheme.

Polygons (shapefile) were delineated in QGIS for 3 vegetation cover types within the Weissenstein mine site (Pasture recultivated, Meadow recultivated, Natural succession) and 2 control classes next to the mine site (Control - “ski slope” and Control - “natural”).

A 10x10m grid was created, aligned with Sentinel-2 pixels. Within each polygon, buffers were applied to avoid edge effects – near the border between polygons or next to dirt roads, and minimizing shading effects of shrubs. From the remaining candidate cells within the grid (centre of S2 pixel), locations were selected randomly, with a minimum distance of 60m between each centre pixel (to reduce auto-correlation). Six to eight centre locations were selected for polygons within the mine site, three to five centre locations for control classes. A total of 32 centre locations were thus selected quasi randomly (with the additional distance constraints) and by class, forming a sampling scheme close to stratified random sampling, a gold standard in vegetation studies in remote sensing.

For each 32 centre locations, the 4-neighboring pixel centres were also preliminarily selected. This allows the study of local variations both in situ and in EO data.

The measurement unit adopted at each location is a 1x1 m square, called quadrat. This is a standard measurement unit for in situ biodiversity measures and vegetation studies in general. For each quadrat, delineated in situ with a 1x1 m square, measurements were assigned in this way:

- species richness: number of plant species within the quadrat
- dominant species: the main plant species (from 1 to 3) within the quadrat
- LAI was measured within the quadrat with a LAI2000 device, either at the centre, or when needed in several points then averaged
- a digital photo of the quadrat was taken (standard phone camera), and analysed later to derive FVC with simple thresholding of green vegetation index based on RGB image

In August 2023, in situ vegetation measurements were collected only for the 32 centre quadrats. A wider scale in situ campaign is planned for summer 2024, for 75 quadrats (including the original 32 centre quadrats, one set of 4 neighbouring quadrats per polygon, and additional quadrats).

In connection to in situ measurements campaign in 2023, drone flights were carried out in August 2023 to collect multispectral imagery over all vegetated polygons defined in sampling stage. Imagery includes Red, Green, Blue and NIR bands, has been ortho-rectified and pre-processed, and vegetation indices were computed to allow upscaling of LAI and FVC measures. More details on drone imagery pre-processing and analysis can be found in other documents related to WP3, e.g. D3.1 and D3.2.

In connection to in situ measurement campaign in 2024 HS drone flights and spectral field data are collected



3.1.8 Water quality measurements in the context of Acid Mine Drainage (AMD) investigation

Water quality investigations in MultiMiner, containing water spectral and water physical properties' measurements as well as analytical work, are carried out in the context of Acid Mine Drainage (AMD) investigations. The term "acid mine drainage" (AMD) refers to the outflow of acidic water from mining sites. It occurs when water and oxygen comes into contact with certain minerals, particularly sulfide minerals like pyrite, during mining operations. When these sulfide minerals are exposed to air and water, they can react and produce sulfuric acid, causing the water to become highly acidic. This acid drainage can have harmful environmental effects, as it may contaminate nearby rivers, streams, and groundwater with toxic metals and lower the pH levels of the affected water bodies. The formation of the AMD process can naturally slow down if the rock material contains minerals with neutralizing potential that prevent acidity such as calcite and certain silicates, and therefore measures to reduce AMD and monitoring are important.

At the Chalkidiki (Greece) test site, time series of extensive water quality measurements are available from Hellas Gold Environment monitoring platform. Additional in situ water quality measurements were collected during MultiMiner field work. These new sampling locations were selected using GIS/ image analysis techniques, to identify areas with potentially different pollutant concentrations or potential sources of contamination. More specifically the hydrological analysis of DEM (water flow parameters) and unsupervised soil/substrate pre-classification were employed to optimize positioning of sampling locations to capture the variability of water quality parameters across the study area.

At the Kirki (Greece) test site, the sampling will be carried out from several selected locations: from the shallow creeks by hand, and from the AMD lake using Drosens, a drone-borne open water sampler with a total sample size of 1,5 litres. Simultaneously The physical properties of water (pH, redox, conductivity, temperature, dissolved oxygen) are measured in the field with WTW MultiLine 3620 IDS and WTW 315i portable multi-parameter and pH-meters.

At both sites (Chalkidiki and Kirki), water spectral data is acquired with a drone (see chapter UAV data acquisition for water and AMD monitoring). The spectral measurements will be calibrated/validated with the basic water parameters (e.g, total dissolved solids, dissolved iron) determined in the Hellas Gold laboratories (Chalkidiki samples) and in HSGME laboratories (Kirki samples) following the standard operation procedures. In addition, VTT provided in situ estimates of water turbidity and Secchi depth, using a device developed earlier for citizen science. This approach was validated in a previous study versus more than 1000 measurements in Finnish lakes ($R^2=0.942$ for Secchi depth, Toivanen et al. 2013).

For the Kirki water samples additional analysis will be conducted to determine dissolved elements. Samples for multi-element analysis will be filtered at 0.45 mm on site and preserved using ultra-pure HNO_3 in 100mL polyethylene bottles. Dissolved elements will be analysed in HSGME laboratories by ICP-MS (ASTM D5673:2003). Major elements in the water will also be analysed in HSGME laboratories on raw unfiltered samples by wet chemical methods, according to ASTM standards.

3.1.9 Ground moisture measurements



Rationale for in-situ moisture measurements in MultiMiner context

Volumetric water content (VWC) can be used to monitor wide areas and identify and delineate sudden changes in surface soil moisture not explained by rainy conditions or snow-melt. Those can be potentially associated with dam leakages and lead to increased subsidence. SAR sensors are a commonly used remote sensing technique for retrieving surface soil moisture at high spatial resolution. SAR sensors mounted on satellites, airborne or drone platforms emit radio wave signals and measure the backscatter from the Earth's terrain. The multiparametric backscatter contains information about surface properties, including soil moisture. Other important contributors are scattering contributions caused by soil roughness and short vegetation (if present). For separating those effects, auxiliary information from optical and thermal imagery, topography, soil texture information can help improve accuracy of soil moisture retrievals when combined with SAR data.

Many analytical, semi-empirical and machine learning models establishing connection between SAR observables (multifrequency, multipolarization, interferometric) or multi-source EO-data and soil moisture (SM) and suitable for producing SM predictions need calibration and/or teaching with representative in-situ measurements. To enable wall-to-wall mapping based on SAR imagery and semi-empirical models for soil moisture retrievals, the sampling of in-situ measurements should include representative wide range of soil moisture values (from dry soils with 0% VWC to saturated 100% VWC), various soil textures (sand, loam, clay) and coincide in time domain with SAR image datatake (satellite or drone).

Ground moisture measurements at Ihalainen

Field work for calibration and validation of the ground moisture involved 1) single time measurements of dielectric permittivity (ϵ_r) with a capacitance probe and 2) time series data with field installed soil moisture sensors (Figure 1). The in-situ ground moisture measurements (0 – 0,40 m depth) are targeted for sand, clay, gravel sand, and organic soil texture types at locations where the initial soil moisture modelling shows contrast to the surroundings. The data is collected with an electrical capacitance probe, Percometer (Plakk, 1994), which simultaneously and non-destructively measures soil ϵ_r , electrical conductivity, and soil temperature. ϵ_r depends on the soil water content, which can be determined computationally from the measurement data. GTK has two types of Percometer devices; 1) a down-hole probe which requires augering of a 32 mm hole to the ground for the tip of the probe, and 2) a flat surface probe which has a diameter of 60 mm, making it possible to measure rough surfaces, such as vertical sandy sections. For the surface moisture measurements, the flat probe is recommended because the measurement space better reflects the surface ϵ_r as measured with the remotely sensed SAR systems. Percometer (Adek Ltd., Tallinn, Estonia; abbreviation from Permittivity and Conductivity) was chosen and this uses electrical capacitive probes to measure the in-situ ϵ_r at 40-50 MHz frequencies and bulk electrical conductivity of soil at 1 kHz.





Figure 1. Organic soil dielectric constant measurement using hand-held percometer.

To increase the sampling locations and number of representative soil moisture measurements, relatively cheap systems using buried capacitance probes can be used. One possible option is Finnish produced “Soil scout” system, where soil moisture sensors (3-prong integrated capacitive and resistivity) are buried to 10-50 cm depth and periodically transmit temperature, soil moisture and salinity measurements to base station. Soil moisture sensors (EM500-SMT-868M, LoRaWAN, Milesight, Finland) were installed to acquire time-series data (Figure 2). Each sensor has 5 cm measurement radius, 2% measurement accuracy, and typical radius of operation around 200 meters (10cm deep buried sensor, 50% VWC, omnidirectional base antenna). The data transmitters were set up on wooden poles that were 5 cm thick and about 1 m high above the ground to guarantee good data transmission to the nearest receiving stations. The probe was placed approximately 5 cm below the ground surface, approximately 1 m away from the wooden pole. LoRaWAN IoT devices are used to transmit measured data from soil moisture probes to receiver stations. A sample of auxiliary locations was measured in the vicinity of the soil moisture sensors for data calibration purposes of IoT sensor installations. At these locations ϵ_r was measured using the hand-held capacitance probe to provide an estimate on spatial autocorrelation of soil moisture of the soil textural classes.



Figure 2. IoT soil moisture sensor installation. In the left image, the soil moisture sensor is attached to the wooden pole, and in the right image, the probe is situated 5 cm below the surface of the ground.

3.1.10 Characterization of tailings

Tailings are fine-grained processing waste resulting from the enrichment of ore, from which valuable materials such as metals or industrial minerals have been enriched. However, some valuable material often remains in the tailings, because it may be impossible to enrich all the valuable material in terms of beneficiation technology or economics. In responsible and modern mining operations, tailings are piled or spread in appropriate and monitored tailings storage facilities (TSF). This is distinguished from unmanaged, historic mine waste dumps. In-situ characterization of the tailings storage facility will focus on composition measurements and sampling tailings material in the Olympias TSF, Chalkidiki (Greece). During the sampling campaign tailing samples will be collected to calibrate and validate the hyperspectral drone and hyperspectral and multispectral satellite data collected from the same area. The sampling locations will be adjusted based on the preliminary satellite data. The sampling area does not cover the entire TSF area, because the sampling must be concentrated in the same area as the drone flights. The drone's limited flight range defines the area. At the same time as sampling and drone flights, field spectral measurements are made from tailings.

3.1.11 In-situ dust measurements

Passive dry dust deposition collectors (Pas-DDs) with the polyurethane foam disk configuration will be used (e.g., <https://tisch-env.com/product/te-pas-dd-passive-air-sampler-outdoor>). Around each mine site 3 dust traps will be installed to capture seasonal trends (April – October and December-March) and spatial extent (Cleaver et al. 2022).

In addition, during the field visit simple dust sample collection is planned to be done. Samples with a range of dust quantity will be collected to conduct an independent measure of the dust weights on the leaves. Dust will be removed from the leaves with a wet tissue of known weight and then will be carefully inserted into sealable plastic bags. Tissues will be air dried in a temperature-controlled lab and weighted (Ong et al. 2013). Test sites are Ihalainen (Finland) and Chalkidiki (Greece).

3.1 Mineralogical and geochemical characterization of samples – laboratory data

3.1.1 Rock sampling strategy for integrated spectral, mineralogical and geochemical analyses

To ensure that the spectral, mineralogical and chemical laboratory analytical results are comparable, all analyses must be carried out consistently from the same sample sections, the MultiMiner project follows the laboratory protocol described in this section. The protocol must be taken into account already in the field, mainly by collecting large enough samples. The rock samples are in the first step analyzed at the spectral labs in Hannover, then further petrographic analyses (e.g. thin sections) or further mineralogical and geochemical analyses are performed on the same piece of the rock fraction. Bulk rock geochemical



or mineralogical analyses, however, require the preparation of a rock powder at a first step. Hence, it is paramount to ensure that the rock fraction taken from the whole sample is representative of the material.

The protocol comprises two steps. First, the sample is split into two. Here, 2/3 of the sample is kept as a reference and 1/3 is going into spectral and analytical work. Second, the latter piece is further split into two in a way that the center piece (approximately 2 cm in size) represents the fresh and weathered rock surface. This piece (fresh/weathered) is then given to spectral (1) and mineralogical and chemical analytical (2) (e.g. XRD) work, in this order. The final setup of three rock pieces is shown in Figure 3.



Figure 3. An example of a size sample cut to sizes 1/3 and 2/3.

3.2.2 Laboratory analysis of substrate/minerals in the context of Acid Mine Drainage (AMD) investigation

Substrate samples are collected from acid mine drainage (AMD) areas of the Kirki site. For selected samples of the surface material (0–2 cm depth) is collected at 50 selected points. The collected samples are dried and sieved to <2 mm and the abundance of trace elements including major heavy metals is measured using a portable Innov-x Alpha RFA spectrometer. Furthermore, the samples are subjected to determination of laboratory pH, sulphur (S total wt%), and total organic carbon (TOC%). The phase analysis of the studied samples is based on the powder X-ray diffraction patterns (whole-rock random powder samples and oriented clay fraction specimens) and voltammetry. The X-ray powder diffraction patterns were obtained on the Philips X'Pert diffractometer using CuK α radiation and graphite secondary monochromator. Moreover, the mineralogical composition (qualitative and semi-quantitative) can be defined using a powder X-ray diffractometer (PXRD) PANALYTICAL X'Pert MRD PRO with a CuK α radiation source at 40 kV, 40 mA and a graphite monochromator (HSGME). The XRD patterns are evaluated using the EVA DIFFRACplus software package.

3.2.3 Spectral analyses of individual rock samples and tailings material in the laboratory

In addition to spectral measurements carried out during field work, rock samples are taken for analyses in the lab. Here, the conditions of spectral measurement are controlled in order to adhere to certain standards. For the MultiMiner project, such spectral measurements are carried out at the lab facilities of BGR at Hannover. The particular conditions and analytical steps are documented in Appendix 5.

3.1.2 X-ray powder diffraction (XRD, XRPD) analyses

The X-ray powder diffraction (XRD, XRPD) method applies X-ray scattering by the sample to resolve its crystal structure(s). The underlying principles are the systematics of constructive interferences by the crystal lattice, as described by the Bragg's Law (e.g. Waseda et al., 2011). Mineral composition of a sample powder is first determined qualitatively, by assigning all diffraction peaks in a measured diffractogram to mineral phases using extensive reference databases. At this stage, it is already seen in X-ray diffraction pattern which minerals are major, minor or trace constituents.

Depending on the characteristics of the mineral assemblage of the sample, it is normally possible to use full powder pattern fitting methods to model a calculated diffraction pattern that matches the measured one. Using this Rietveld refinement method (e.g. Young 1995), the quantitative phase composition of the sample can be extracted from the model. Limiting factors include complications from non-identified and amorphous phases, extensive peak overlaps, varied chemical compositions of most minerals, and stacking disorders in some phyllosilicates (clay minerals).

The tailings samples from Chalkidiki (Greece) will be analyzed by the XRPD method in the GTK Espoo research laboratory (Finland) using a Bruker D8 Discover instrument. Because of the limitations described above, the results are semi-quantitative. The same samples will be analyzed using field-emission scanning-electron-microscope energy-dispersive spectroscopy FE-SEM-EDS. This complements the data set with another independent semi-quantitative method that is based on mineral chemical compositions. The combined information of mineral chemistries and crystal structures is needed to characterize complex mineral materials.

3.1.3 Geochemical analyses (XRF analyses; ICP-MS analyses)

The geochemical composition of bulk rock sample powders are typically determined by X-ray fluorescence (XRF) analyses for the major elements as oxides (i.e., SiO₂; TiO₂; Al₂O₃; Fe₂O₃; MgO, MgO; MnO; CaO; K₂O and Na₂O) in weight % (wt.%). This involves the preparation of fused disks and/ or pressed powder disks that are exposed to gamma ray causing the emission of characteristic "secondary" radiation with element-specific energy characteristics (Beckhoff et al., 2006). In conjunction, the content of volatile elements is determined as "loss on ignition" by heating sample powder to 1000 °C. The total of major element oxides and "loss on ignition" should add up to close to 100 wt. %; in practice values between 98% and 102 wt.% are commonly consider acceptable results.

Trace elements are characterized by concentrations << 1 wt.% and are expressed as parts per million (ppm). For rock samples, they are commonly determined using ICP-MS (inductively coupled plasma – mass spectrometry) analyses. This method applies mass spectroscopy on an ionized plasma stream which



allows for low detection limits (Thompson and Walsh, 1989). Importantly, the rock powder must be completely dissolved prior to analyses which, for silicate rocks, is achieved used treatment with hydrofluoric acid. Recent developments have established laser ablation as an option to generate small volumes of ionized sample plasma from individual spots of single minerals (Nelms, 2005).

For the scope of the MultiMiner project, geochemical analyses of rock samples are part of the geological studies in the frame of the mineral prospectivity investigations at Hochfilzen and Kallyntiri test sites.

3.1.4 Micro-XRF analyses

One of the objectives of MultiMiner is to test the applicability of the M4 Tornado AMICS μ -XRF instrument of GTK for the detection of small amounts of dust impurities on leaves. The technology is based on X-ray fluorescence spectroscopy, discussed in section 3.1.3. Dust collected from are placed in a sample chamber for measurements without coatings or other sample preparation. The instrument produces multi-element maps of the sample with a maximum spatial resolution of 20 μ m. Here, the objective is to study the quantities of different types of particles on collected leaves to obtain information about the different sources of dust in the area. The protocol of dust collection is described in more detail in section 3.1.6.

3.1.5 Petrographic description of rock sample thin sections

Optical microscopy on thin slices of rock (30 μ m) is referred to as “petrography”. A section of rock specimen is prepared on a mounting glass typically 26 mm x 46 mm in size. A variety of optical features can be observed in order to identify different types of minerals and to characterize their textural features (e.g., MacKenzie et al., 2017). This includes grain size, shapes orientation and contact relationships to other minerals. As such, petrography is particularly useful for investigations of mineral reactions and replacement sequences. For the scope of the MultiMiner project, petrographic analyses of rock samples are part of the geological studies in the frame of the mineral prospectivity investigations at Hochfilzen and Kallyntiri test sites.

3.1.6 Micro-scale mineralogical analyses of rock and tailings samples (SEM-EDS)

Scanning Electron Microscopy, commonly referred to as “SEM”, is a technique used to acquire high-resolution images of various samples and applies to a wide spectrum of scientific fields (e.g., biology, medicine, geology, materials science, etc.). The main principle behind the SEM technique is a focused beam of high-energy electrons that generates a variety of real-time signals at the surface of solid specimens, which in turn, give important information about the examined sample (e.g., morphological features, crystal structure, composition, etc.).

The method usually offers magnification capabilities between 20X and 300.000X (reaching up to the order of 10^6 X), while its spatial resolution commonly ranges between 50nm and 100nm. In respect to geological samples, the method is usually combined with Energy Dispersive X-ray Spectroscopy (EDS) and is applied on polished and carbon-coated blocks and/or thin sections that have been made of rock samples. EDS operates using the characteristic X-rays that are emitted from the sample during SEM imaging, thus allowing the identification of chemical elements that are present in the sample, as well as their relevant



abundance. The results of EDS analysis are semi-quantitative. The measuring accuracy of chemical element contents varies depending on sample but is usually around 0.3–0.5 weight percent (wt%). Samples with a grain size less than 1–3 μm cannot be analysed reliably. Nor is exact identification of mineral phases from an EDS spectrum always possible. In addition, phases with similar or identical chemical composition cannot be distinguished from each other.

In the frame of the MultiMiner project, the HSGME team will use a JEOL JSM-IT500LV scanning electron microscope coupled with an Ultim Max 100 (OXFORD) EDS detector, in order to acquire the chemical composition of both ore and alteration minerals in ore-bearing samples from the Kallyntiri deposit. This will help us to detect the presence of critical elements, both from a morphological and a semi-quantitative point of view and will allow comparison of the mineral-chemical data to the spectral result, especially in terms of alteration and ore minerals.

The mineralogical composition of tailings samples from Chalkidiki (Greece) will be quantified in the GTK Research Laboratory in Espoo, Finland, to ensure accurate mineralogical information for drone and satellite data calibration and validation. A JEOL JSM 7100F Schottky field emission gun equipped scanning electron microscope (FE-SEM) attached to an Oxford Instruments X-Max 80 mm² EDS detector and INCA / Aztec software will be used. The FE-SEM-EDS modal mineralogical results normalized to 100% will be compared with the mineral composition results obtained by the XRPD method to ensure more accurate composition. The modal mineralogical result shows the mineral phases and their proportions in the tailings samples.

3.1.7 Geochemical analyses of individual minerals (EMPA)

The chemical composition of minerals can be determined by Electron Microprobe Analysis (EMPA) on a micrometer scale. Hence, chemical variations and gradients within individual mineral grains can be examined which reflect changing conditions during crystallization. The method applies an electron beam on the sample (typically a carbon coated polished thin section in geological applications) under vacuum which emits x-rays a wavelengths characteristic to the elements being analyzed. Quantification of intensities of characteristic X-rays received from the sample is achieved by comparison with intensities obtained from a standard with known composition (e.g. Reed, 2010).

With respect to the scope of the MultiMiner project, EMPA results can elucidate the compositional variabilities of certain minerals that are also detectable from spectral analyses. For example, variations in the Al-content of phyllosilicates may be reflected in the characteristics of the Al-OH absorption feature in spectral measurements. Also, absorption features attributed to Fe and Mg hydroxide may display systematic variations due to variations in the occupancy of the cation position. For carbonates, magnesite, dolomite and calcite are known to display distinguishable spectral characteristics (Green and Schodlok, 2016). This is of particular relevance for integration and interpretation of analytical data at the Hochfilzen magnesite deposit.

3.3 UAV data acquisition

Since UAV data acquisition at mine sites entails compliance to additional regulations and specific guidelines, these aspects are relevant to field work and are therefore part of MultiMiner Field guidebook. Furthermore, considerations related to image acquisition and equipment used for on site



calibration are also related to field work activities. Some considerations on UAV data and imagery pre-processing are also included here.

3.3.1 UAV data acquisition in the context of vegetation monitoring (Hochfilzen test site)

The purpose of the multispectral aerial survey (carried out by GeoSphere Austria) is to collect characteristic information of the re-vegetation process at selected areas around the open pit of Weissenstein, representing different states of revegetation as well as naturally developed or with traditional livestock farming, for comparison. The survey is closely coordinated with ground acquisition of LAI (leaf area index) and FVC (fraction of vegetation cover) data (section 3.1.7; In-situ vegetation measurements) in the same areas. From raw UAV-multispectral data, vegetation indices are derived, but raw multispectral data is also prepared for further analysis together with in situ and satellite EO-data by the partner VTT.

Seven survey areas have been selected as defined with the project partners. The data is collected using an Airphen (Hiphen) multispectral UAV sensor with six channels covering the wavelengths 450, 530, 570, 675, 730, 850 nm. Uniform lighting conditions and low-contrast shadows (e.g. overcast weather) are advantageous for multispectral imaging.

The sensor is mounted on an AIR4 drone (MTOW 2 kg, AIR6 Systems). The average flight time is approximately 15 minutes per battery set and area. Flight speed is around 5m/s, which means that around 15 ha can be covered in one flight at a line spacing of 30m and flight altitude between 100 and 120m above ground. In the case of Weissenstein, up to four areas could be covered in one day. Ground control points (GCPs) marked with tags are measured with ground GNSS and used for geo-referencing.

The technical operational safety of UAV equipment is guaranteed by:

- Annual maintenance by the manufacturer
- Preflight check
- Postflight check
- Battery management (controlled charging, discharge-level, storage, fire-safe storage/transport)

The safe execution of the measurement flights is carried out in accordance with the regulations of national aviation authority Austrocontrol and the European aviation authority EASA, which requires registration, flight planning and flight execution in accordance with EASA guidelines.

In detail this includes:

- Registration as a drone operator with the national aviation authority (Austrocontrol)
- Valid remote pilot certificate
- Liability insurance (+ optional fully comprehensive insurance)
- MTOW < 25 kg (maximum take-off weight)
- Flight in VLOS conditions (visual line of site).



- Flight altitude maximum 120 m above ground level.
- Permission / coordination with the property owner (in the case of Weissenstein sufficient - otherwise obtaining approval of the flight plan from Austrocontrol)
- Coordination with other UAV activity (BGR)

3.3.2 UAV data acquisition: in the context of mineral mapping and TSF monitoring

Hyperspectral and Photogrammetry UAV are used in the framework of the project in the context of mineral mapping (Hochfilzen, Chalkidiki and Kallyntiri) and TSF monitoring (Chalkidiki), as well as vegetation monitoring in Hochfilzen.

3.3.2.1 Hyperspectral UAV HySpex Mjöltnir VS620 System

The hyperspectral drones is the BFD XQ – 1400S with the mounted hyperspectral Sensor Mjöltnir VS-620 (https://sphereoptics.de/wp-content/uploads/2015/01/Hyspex_brochure.pdf). The spectral range is from 400 to 2500 nm with a 620 spatial pixel in the SWIR (short wave infrared) range (the VNIR; visible near infrared) range has 1240 spatial pixel. The flight time is approximately 15 min with Gimbal and Mjöltnir payload. We generally work at a flight altitude of 120 m. This means that the hyperspectral drone has a ground resolution of 6.48 cm at a flight speed of 3.6 m/s and a swath width of 42.32 m. The whole system is categorized as “open”.



Figure 4. BFD XQ - 1400S with Gimbal and Mjöltnir.

3.1.7.1 Photogrammetry DJI Mavic 3 RTK System

The BGR UAV's for the photogrammetry Images are the DJI Mavic 3 RTK System with a 4/3 CMOS Sensor and 20 megapixel wide-angle camera and an 1/2" CMOS 12 megapixel tele camera (https://dl.djicdn.com/downloads/DJI_Mavic_3_Enterprise/DJI_Mavic_3E_3T_User_Manual_EN.pdf). The max flight time is up to 45 min (without wind) per battery set. The recommendation is an average flight time to 30 min with the flight speed of 15 m/s. The UAV is connected with the Real Time Kinematic



(RTK) antenna for a higher precise positioning. We generally work at a flight altitude of 120 m. This means that the hyperspectral drone has a ground resolution of 1.23 cm at a flight speed of 15 m/s and a swath width of 65 m. The UAV system categorized as “open”.



Figure 5. DJI Mavic 3E with RTK antenna.

3.1.7.2 Rules and Regulations

The categorisation of the UAV's is written in the European legislation no. EU2019/947. Especially the articles 3 to 6 describe the different usage types of UAV and registrations. In addition, article 11 describes the rules for conducting an operational risk assessment and article 12 describes the authorizing of operations in the 'specific' category.

According to European legislation no. EU2019/947, before a flight of a UAV in the "specific" category can be carried out in a European member state, the UAV operator must submit an application to the competent authority of the Member State, including the following information (Article13 no. 1):

- a) a copy of the operational authorisation granted to the UAS operator in accordance with Article 12; and
- b) the location(s) of the intended operation including the updated mitigation measures, if needed, to address those risks identified under Article 11(2)(b) which are specific to the local airspace, terrain and population characteristics and the climatic conditions

3.1.7.3 Before the flight

It is necessary to prepare every flight. The first consideration should be the location of the flight. With the planning of the flight, the size of the polygon can be determined. It is mandatory to make alignment flights (50 m forwards and backwards) over the white reference target to calibrate the hyperspectral sensor. The flight planning is carried out with the UgCS software (SPH Engineering, Riga, Latvia) for hyperspectral

UAVs. The flight planning for the photogrammetry UAV is carried out with the Software “DJI Pilot 2” (integrated software in the Remote Control). A calibration is not necessary.

Before the flight can start it is necessary to find an open and flat area for the ground station, with chairs and tables to operate. This area should be also free from obstacles and to be secured with pylons (traffic cones) and an emergency landing site has to be defined. After assembling of UAV and control infrastructure/equipment has to be done by using a checklist. All components of the system should be checked for damages and a second person should be going through the steps of the checklist. In addition, reference plates need to be laid out (white reference targets) for hyperspectral data acquisition. These targets have to be overflown during the alignment flights to calibrate the hyperspectral sensor.

Before transmitting the flight plan to the UAV the parameters of the plan have to be double-checked and it needs to be made sure that all spotters are in place and concentrating (a minimum of one spotter is mandatory to secure/monitor air space).

3.1.7.4 During the flight

Once the set up is prepared, all functions need to be checked by the drone operator and a brief test flight needs to be performed to check the flight properties of the UAV system (test following movements: nick pitch, yaw, climb, decline, forward, backwards, flying curves, etc.). The home point (point to return that is automatically detected) has to be defined. Now the flight plan can be transmitted to the UAV and the flight can start.

The UAV has to be flown in a line of sight mode and spotted all the time, to be sure about the air space around the UAV and to interrupt the flight plan in the case something unexpected happens. The sensor has to be checked in the Mjolnir laptop, with the Software HySpex Air (Neo, Oslo, Norway), to make sure that the sensor works perfectly. When the flight plan is finished, the UAV has to be landed manually. Therefore, the UAV has to hover in the altitude of 30 m above ground over the landing site and descent slowly. After landing and during disassembling the UAV, the system must be checked for damages (especially the propeller).

An entry is made in the flight logbook for each individual flight and the field sheet must be filled in so that the recorded data can be accurately investigated later.

For flight planning, validation and calibration tasks protocols are implemented and need to be followed for all UAV flights:

Flight planning:

- The launch site must be a flat and open area.
- Check the launch site and flight area for obstacles.
- Secure launch site with pylons (traffic cones).
- Assembling of UAV and control infrastructure/equipment has to be done using a check list.
- Check all components of the system for damages.



- After assembling the UAV systems, a second person has to check what the first person has done.
- Double check the flight plans.
- Ensure all spotters are in place (a minimum of one spotter is mandatory to secure/monitor the air space).
- Define a home point (an automatic point to return).
- Define an emergency landing site.
- Perform a brief test flight to check the flight properties of the UAV system (test following movements: nick, pitch, yaw, climb, decline, forward, backward, flying curves etc.) before starting the data acquisition flights.

Hyperspectral data acquisition special requirements:

- Lay out reference plates or a reference tarp for calibration purposes if possible – reference plates have to be overflown at the time of the data acquisition (**Error! Reference source not found.**).
- Start the flight plan – planning always N-S/ S-N, data acquisition +/- 2h of solar zenith or minimum 36degrees Azimuth.
- The flight is performed with overlapping line spacing.
- The UAV has to be flown in a line of sight mode.
- After finishing the flight plan, the UAV is landed manually.
- Before landing: briefly hover the UAV in about 30 m altitude above the landing site then descent.
- After disassembling the UAV, check the system for damages (especially, the propeller).



Figure 6. A base station with white reference targets.

3.1.8 UAV data acquisition for water and AMD monitoring

3.3.3.1 Parrot Sequoia multispectral data + RGB photogrammetric products

The Parrot Sequoia is a compact (weight of 72 grams) multispectral camera specifically designed for integration with UAV (Parrot Drone SAS, https://www.parrot.com/assets/s3fs-public/2021-09/sequoia-userguide-en-fr-es-de-it-pt-ar-zn-zh-jp-ko_0.pdf). The camera is equipped with four 1.2 megapixel monochrome sensors capturing data in four spectral bands: green, red, red edge, near infrared (Table 4), and additionally one 16 megapixel RGB sensor. The camera also contains an integrated GPS receiver, ensuring later data georeferencing.

Table 4. Overview of the Parrot Sequoia spectral band setting.

Band Name	Spectral Range (nm)	Central Wavelength (nm)	Bandwidth (nm)
Green	530–570	550	40
Red	640–680	660	40
Red edge (RE)	730–740	735	10
Near infrared (NIR)	770–810	790	40

In addition to the main camera, the Parrot Sequoia camera is complemented by the solar irradiance main sensor (Figure 7). Even though the automatic radiometric calibration provided by the irradiance sensor has been evaluated scientifically (Franzini et al., 2019; Olsson et al., 2021), the reliability of the whole setup has been prove to be sufficient for most applications. Since the whole Parrot Sequoia system comes independently of the UAV platform, the UAV mounting setup has been subject of several studies (Kopačková-Strnadová et al., 2021; Polukhin et al., 2022). CGS team designed and operationally employed mounts tailored for the DJI Phantom 4 Pro UAV using 3D printer, accommodating both camera and the sunshine sensor (Figure 8, Kopačková-Strnadová et al., 2021).



Figure 7. Parrot Sequoia with solar irradiance sensor.

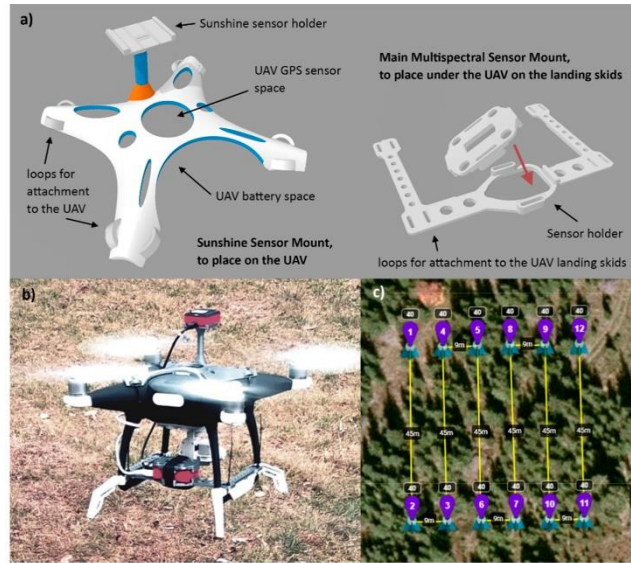


Figure 8. A Parrot Sequoia UAV setup (Kopačková-Strnadová et al., 2021).

The spectral band combination allows for the detailed analysis of vegetation, especially its health status, which has been successfully proved within precision agriculture (Saddik et al., 2022), forestry (González-Jaramillo et al., 2019; Kopačková-Strnadová et al., 2021; Safonova et al., 2021) or environmental monitoring (Song, 2019). Besides the natural field of application, Parrot Sequoia has been previously tested also in geology (Jackisch et al., 2020), archeology (Moriarty et al., 2019) and mine-related applications (Johansen et al., 2019; Padró et al., 2019).

3.1.8.1 Before the flight

Once mounted and connected to the UAV, which serves also as an energy supply, the Parrot Sequoia camera is connected via WIFI with the operators' phone. Here, through a specific setup page various main camera settings and also the multispectral data calibration process is being managed. Multispectral data calibration routine is very easily employed, using the Airinov calibration target (Figure 9). Camera is also equipped with a GPS receiver, which is automatically turned on with the camera. The GPS does not require any specific calibration, however its accuracy has been considered not sufficient for some applications (Paraforos et al., 2022). To ensure correct geographical placement of the final orthomosaic, it is recommended to place a set of GPS-located ground control points (GCP) evenly within the sensed area. Both Sequoia camera and the sunshine sensor are equipped with indicator light which inform operator about the status and correct setup.

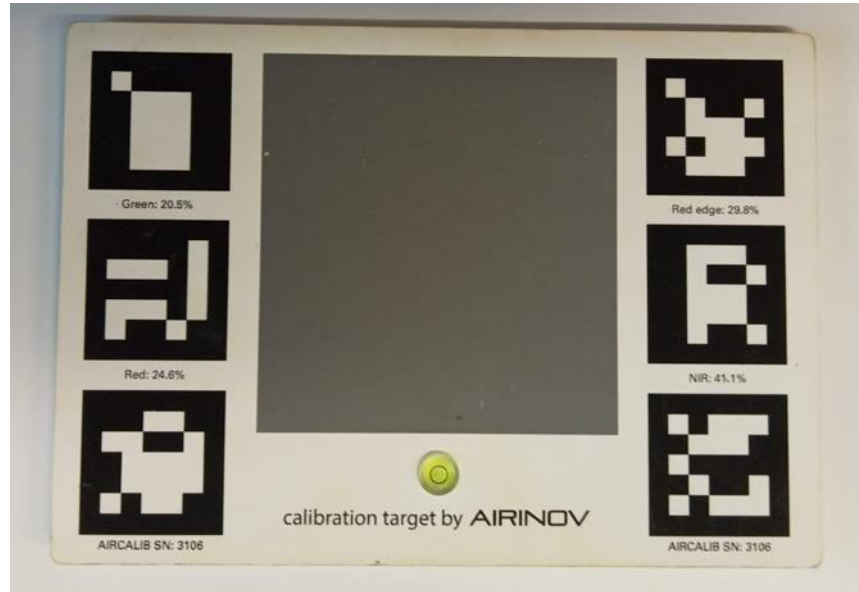


Figure 9. An Airinov calibration target.

3.1.8.2 *Setting up the calibration targets (spectral and geometric)*

The Airinov calibration target is a special panel with different grey intensities, used to calibrate multispectral data. To correctly employ the calibration, exact manufacturer recommendations are being followed using the instructions in the setup page. The camera should be placed approximately 1.5 meters above the target, keeping the sun behind the UAV to ensure no shadow or reflections were affecting the panel. It is recommended that the calibration images are taken both pre- and post-flight. The calibration images are used automatically by the camera for its calibration.

3.1.8.3 *Data acquisition*

The data acquisition routine followed for the Parrot Sequoia camera is similar to other optical sensors. The flight should be planned ideally between 11 am and 3 pm to maximize reflected sunlight and eliminate shadows. The flight parameters (flight height, UAV speed, flight path spacing and shutter speed) should be planned with respect to the planned mission and sensed surface. Ideally, images should be acquired with 70% overlap in the direction perpendicular to the flight and with 95% overlap in the direction of flight, to ensure errorless mosaicking during photogrammetric processing of the data. Depending on the planned spatial resolution, the UAV speed and shutter speed should reflect ideal image overlap.

3.3.4 **Water spectrum acquired by UAV's based microspectrometer OceanOptics STS-VIS**

The Ocean Optics STS-VIS spectrometer is a compact portable spectrometer, manufactured by the Ocean Insight. The Ocean Optics STS-VIS features a spectral range of 337-823 nm, an optical spectral resolution of 1,5 nm, and a field of view (FOV) of 25°. Due to the compact size, the STS-VIS is an ideal solution for unmanned aerial vehicle (UAV) borne missions. In our setup, spectral data are acquired using DJI Phantom

3 quadcopter, equipped with a custom-made 3D-printed holder for the Ocean Optics STS-VIS spectrometer. Ocean Insight provides a development kit that utilizes the STS-VIS spectrometer and is powered by a Linux-based Raspberry Pi 3B microcomputer (Ocean Insight, <https://www.oceaninsight.com/globalassets/catalog-blocks-and-images/manuals--instruction-ocean-optics/spectrometer/sts-dev-kit-api-manual.pdf>). The Raspberry Pi 3B is powered by a small-scale, lithium-ion power bank and contains a Micro-SD card loaded with the necessary WIFI Spectrometer Control software (Figure 10).



Figure 10. STS Development Kit.

3.1.8.4 Before the flight

Prior to data acquisition, the flight altitude of the UAV equipped with the spectrometer requires careful consideration based on the desired spatial resolution of the target measurements. The relationship between flight altitude and spatial resolution is characterized by the following formula:

$$d = 2v \cdot tg\alpha$$

where:



d = final spatial resolution of the measured point

v = height above the surface

α = half of the field of view

In addition to flight altitude, precise geographical coordinates are crucial for data acquisition within the designated area of interest (AOI). This ensures the spectrometer captures measurements from the intended locations. To facilitate precise navigation and data collection, online mission planning software, such as Litchi Mission Hub, offers functionalities to:

- Import or define coordinates: Points of interest within the AOI can be imported from existing geographic information system (GIS) data or manually defined within the software.
- Adjust flight path: The software allows for editing and fine-tuning of the flight path to ensure the drone navigates to each designated location and captures measurements accordingly.
- Autonomous navigation: Upon initiating the pre-programmed flight mission, the UAV autonomously navigates to the specified coordinates, streamlining data acquisition within the AOI.

Employing online mission planning software enhances the efficiency and accuracy of data collection by the UAV-mounted spectrometer.

Due to safety regulations and best practices, operating a UAV equipped with a spectrometer necessitates a two-person team. The first team member serves as the pilot-in-command (PIC), responsible for the safe operation of the UAV through the dedicated remote controller and the Litchi mobile application connected to the Litchi Mission Hub. The second team member, designated as the data operator, focuses on the real-time data acquisition and collection directly from the spectrometer, using a Wi-Fi connection between the spectrometer and the STS-dev-kit. This division of tasks ensures both flight safety and correct data collection during UAV-based spectral mission.

To conclude the field preparation phase, two crucial measurements are acquired for subsequent post-processing involving radiance-to-reflectance transformation: the dark spectrum and the reference spectrum. The dark spectrum measurement (in WIFI Spectrometer Control software: Dark Measurement; **Error! Reference source not found.**) is obtained by closing the spectrometer's lid completely, effectively blocking any external light source (Zeng et al., 2017). This data serves to characterize the inherent noise and signal offset of the instrument itself. The reference spectrum measurement (in WIFI Spectrometer Control software: Reference Measurement; **Error! Reference source not found.**) uses a highly reflective calibrated reflectance panel (Spectralon) provided by the Spectral Evolution (Burkart et al., 2014). The Spectralon should be mounted on the tripod in the horizontal position.

3.1.8.5 Data acquisition

Data collection using Ocean Optics STS-VIS spectrometer utilizes a Wi-Fi connection between the spectrometer and a tablet device. The spectrometer's IP address serves as the connection point for real-



time data transfer. The collected data, comprising radiance intensity measurements, are saved as text files (*.txt) within a designated location on the tablet.

A dedicated software application, WIFI Spectrometer Control, facilitates data acquisition through two primary functionalities: Single Measurement and Acquisition Control.

Single Measurement mode is suitable for capturing individual measurements at user-defined times. Within this mode, the user specifies the output folder and file name for the subsequent data file. Acquisition Control mode enables capturing measurements at pre-defined time intervals, automating data acquisition for specific study designs.

By leveraging the appropriate mode within the WIFI Spectrometer Control software, researchers can efficiently collect radiance intensity data through the Wi-Fi connected spectrometer in accordance with their experimental requirements.

3.3.5 PIKA L hyperspectral data

UAV-based hyperspectral data are acquired using the DJI Matrice 600 Pro hexacopter equipped with a Ronin MX gimbal. The camera used for hyperspectral imaging was the Resonon Pika L (Figure), offering a spectral range of 380-1225 nm with 150 spectral bands. It was fitted with a 17 mm focal length lens, providing a 17.6-degree field of view (FOV) and an instantaneous field of view (IFOV) of 0.71 mrad.



Figure 11. Hyperspectral camera Resonon Pika L. (a) Standalone camera; (b) Camera installed on the Ronin MX on DJI Matrice 600 Pro.

3.1.8.6 Before the flight

Prior to the flight, the Resonon Ground Station software is utilized to configure the hyperspectral camera settings. The GPS/IMU settings are separately adjusted using the SBGcenter software, including magnet calibration of the IMU and camera exposure calibration using a standardized white target. These calibration efforts resulted in a framerate of 36 fps.

3.1.8.7 Setting up the calibration targets

Spectral calibration targets

The reference spectrum measurement utilizes a calibrated, highly reflective reflectance panel (Spectralon™) provided by Spectral Evolution (Haverhill, MA, USA). The Spectralon panel ought to be installed to the tripod in a horizontal orientation. Additionally, within the area of interest (AOI), the calibration canvas (supplied by the camera manufacturer) containing two shades of grey should be positioned (Figure). This canvas is subject to measurement by the Spectral Evolution spectrometer SR2500. The transformation from radiance to reflectance is conducted based on the reflectance of this canvas as measured by the SR2500.



Figure 12. Calibration targets; (a) Spectral Evolution Reflectance Target (spectralon); (b) Resonon Calibration Canvas.

Geometric calibration targets

Geometric calibration is performed using ground control points (GCPs). These GCPs are 50 cm x 50 cm square plastic targets with a checkerboard pattern (Figure) to facilitate their identification in the final orthomosaic image. The GCPs are evenly distributed throughout the area of interest (AOI) at a density of approximately five targets per 100 x 100 m area (depending on the size of the AOI). Their locations are measured using GNSS technology (Nautiz X6 Handheld) and used to georeference the final hyperspectral orthomosaic.



Figure 13. GCP's measured by the GNSS technology.

3.1.8.8 Data acquisition

The data collection is performed at a constant height above the ground (e.g. 120 m resulting in 20x20 cm spatial resolution), utilizing a speed of 1.3 mps (meters per second). To guide the flight path, Litchi for DJI Mission Hub software are employed. The flight paths are designed to run from south to north in order to minimize the bidirectional reflectance distribution function (BRDF) effect. The data collection spanned is conducted between 12:00 and 14:00, to maximize sun light intensity and minimize sun shadows. The flight lines are spaced at 15 m intervals, calculated using the tangent function to ensure a necessary 70% overlap between neighbouring hyperspectral cubes.

4 References

Beckhoff, B., Kanngießer, B., Langhoff, N., Wedell, R., Wolff, H., 2006. Handbook of practical X-ray fluorescence analysis. Springer, 839 p.

Burkart, A., Cogliati, S., Schickling, A., Rascher, U., 2014. A Novel UAV-Based Ultra-Light Weight Spectrometer for Field Spectroscopy. *IEEE Sensors J.* 14, 62–67.

Franzini, M., Ronchetti, G., Sona, G., & Casella, V., 2019. Geometric and radiometric consistency of parrot sequoia multispectral imagery for precision agriculture applications. *Applied Sciences*, 9(24), 5314.

González-Jaramillo, V., Fries, A., & Bendix, J., 2019. AGB estimation in a tropical mountain forest (TMF) by means of RGB and multispectral images using an unmanned aerial vehicle (UAV). *Remote Sensing*, 11(12), 1413.

Green, D. & Schodlok, M., 2016. characterisation of carbonate minerals from hyperspectral TIR scanning using features at 14 000 and 11 3000 nm. *Australian Journal of Earth Sciences*, DOI: 10.1080/08120099.2016.1225601



Jackisch, R., Lorenz, S., Kirsch, M., Zimmermann, R., Tusa, L., Pirttijärvi, M., Saartenoja, A., Hernan, U., Yuleika, M., Savolainen, M. & Gloaguen, R., 2020. Integrated geological and geophysical mapping of a carbonatite-hosting outcrop in Siilinjärvi, Finland, using unmanned aerial systems. *Remote Sensing*, 12(18), 2998.

Johansen, K., Erskine, P. D., & McCabe, M. F., 2019. Using Unmanned Aerial Vehicles to assess the rehabilitation performance of open cut coal mines. *Journal of cleaner production*, 209, 819-833.

Kopačková-Strnadová, V., Koucká, L., Jelének, J., Lhotáková, Z., & Oulehle, F., 2021. Canopy top, height and photosynthetic pigment estimation using Parrot Sequoia multispectral imagery and the Unmanned Aerial Vehicle (UAV). *Remote Sensing*, 13(4), 705.

MacKenzie, W.S., Adams, A.E., Brodie K.H., 2017. Rocks and minerals in thin section. Taylor and Francis, 242 p.

Moriarty, C., Cowley, D. C., Wade, T., & Nichol, C. J., 2019. Deploying multispectral remote sensing for multi-temporal analysis of archaeological crop stress at Ravenshall, Fife, Scotland. *Archaeological Prospection*, 26(1), 33-46.

Nelms, S.M., 2005. Inductively coupled plasma mass spectrometry handbook. Blackwell Publishing, 585 p.

Ocean Insight., 2013. OceanView Installation and Operation Manual. Retrieved from: <https://www.oceaninsight.com/globalassets/catalog-blocks-and-images/manuals--instruction-ocean-optics/software/oceanviewio.pdf>

Ocean Insight., 2014. STS Developer's Kit API Manual. Retrieved from: <https://www.oceaninsight.com/globalassets/catalog-blocks-and-images/manuals--instruction-ocean-optics/spectrometer/sts-dev-kit-api-manual.pdf>

Olsson, P. O., Vivekar, A., Adler, K., Garcia Millan, V. E., Koc, A., Alamrani, M., & Eklundh, L., 2021. Radiometric correction of multispectral UAS images: Evaluating the accuracy of the parrot sequoia camera and sunshine sensor. *Remote Sensing*, 13(4), 577.

Padró, J. C., Carabassa, V., Balagué, J., Brotons, L., Alcañiz, J. M., & Pons, X., 2019. Monitoring opencast mine restorations using Unmanned Aerial System (UAS) imagery. *Science of the total environment*, 657, 1602-1614.

Paraforos, D. S., Sharipov, G. M., Heiß, A., & Griepentrog, H. W., 2022. Position Accuracy Assessment of a UAV-mounted Sequoia+ Multispectral Camera Using a Robotic Total Station. *Agriculture*, 12(6), 885.

Plakk, T., 1994. HF Permittivity measurements by capacitive probe. *Unpublished article*. Adek Ltd, Estonia.

Polukhin, A. A., Litvinov, M. A., Kurbanov, R. K., & Klimova, S. P., 2022. Development of the Parrot Sequoia Multispectral Camera Mount for the DJI Inspire 1 UAV. In *Smart Innovation in Agriculture* (pp. 217-225). Singapore: Springer Nature Singapore.



Reed, S.J.B, 2010. Electron microprobe analysis and scanning electron microscopy in Geology. Cambridge, 212 p.

Saddik, A., Latif, R., Taher, F., El Ouardi, A., & Elhoseny, M., 2022. Mapping agricultural soil in greenhouse using an autonomous low-cost robot and precise monitoring. *Sustainability*, 14(23), 15539.

Safonova, A., Hamad, Y., Dmitriev, E., Georgiev, G., Trenkin, V., Georgieva, M., Dimitrov, S. & Iliev, M., 2021. Individual tree crown delineation for the species classification and assessment of vital status of forest stands from UAV images. *Drones*, 5(3), 77.

Song, W. K., 2019. Application of UAV for Vegetation Monitoring in Urban Green Space. *Journal of the Korean Society of Environmental Restoration Technology*, 22(1), 61-72.

Thompson, M. & Walsh, J.N., 1989. Handbook of inductively coupled plasma spectrometry. Chapman & Hall, 316 p.

Toivanen, T., Koponen, S., Kotovirta, V., Molinier, M. and Chengyuan, P., 2013. Water quality analysis using an inexpensive device and a mobile phone. *Environ Syst Res* 2, 9 (2013). <https://doi.org/10.1186/2193-2697-2-9>

Waseda, Y., Matsubara, E. & Shinoda, K., 2011. X-ray diffraction crystallography: Introduction, examples and solved problems. Springer, 312 p.

Young, K., Evans, C., Hodges, K., Bleacher, J., & Graff, T., 2016. A review of the handheld X-ray fluorescence spectrometer as a tool for field geologic investigations on Earth and in planetary surface exploration. *Applied Geochemistry*, 72. 10.1016/j.apgeochem.2016.07.003.

Young, R.A. [Ed.], 1995. The Rietveld method. International Union of Crystallography, Oxford Science Publication, 308 p.

Zeng, C., Richardson, M. & King, D.J., 2017. The impacts of environmental variables on water reflectance measured using a lightweight unmanned aerial vehicle (UAV)-based spectrometer system. *ISPRS Journal of Photogrammetry and Remote Sensing* 130, 217–230.



Grant agreement	101091374
Project title	Multi-Source and Multi-Scale Earth Observation and Novel Machine Learning for Mineral Exploration and Mine Site Monitoring
Project acronym	MultiMiner
Project coordinator	Dr. Maarit Middleton, GTK
Project start date	Jan 1, 2023
Project duration	42 months
Related work packages	WP 4 – Site Demonstrations
Related task(s)	Task 4.1 In situ data standardization and databases
Lead organization	GeoSphere Austria
Contributing partners	GTK, BGR, VTT, RHI, MUL, EFTAS, HSGME, CGS
Submission date	June 30, 2024
File name	Appendix 1 Data analysis and development of the project database (D4_1_MultiMiner_Field_Guidebook_V1_4.docx)
Organisation responsible for deliverable	GeoSphere Austria
Author name(s)	Piotr Lipiarski, Gerald Schuberth-Hlavac
Date	June 30, 2024
Version	1.0
Status	Complete
Dissemination Level	Public



Table of contents

Table of contents.....	2
Introduction.....	2
Description of the sample field data used for developing the database	4
Development of Database Structure	10
Description of Database Tables	13
Development of the metadata-reporting.....	21
MultiMiner Database - Example queries	26

Introduction

WP4 demonstrates the applicability of different remote sensing data products in real environmental conditions at the five test sites located in Finland, Greece and Austria.

The demonstration is done by utilizing existing *in situ* observations and measurements and by acquiring new ground truth data for accuracy assessments of EO-derived maps.

The first tasks are to develop efficient *in situ* data collection methods, harmonize the data collection procedures and data formats, and develop optimal sampling strategies and appropriate accuracy assessment method

The main tasks of this work package are:

- Determine the type of new *in situ* data needed for ground truth of remote sensing data interpretations
- Collection standards and protocols
- Harmonization of data collecting
- Review the existing standards for field sampling and sample collection and compile them into a field work guidebook
- Determination of the structure of the common project databases used to store e.g., the ground truth spectra collected in the project
- Practical implementation of the associated metadata using the FAIR principles

Field work protocol for in-situ data collection and standardization is a description of workflow for field and laboratory operations.

Collecting terrain data includes the following actions

- Geological mapping
- Spectral analyses of rocks, tailings and acid mine drainage substrates
- Dust emission measurements
- Water quality measurements
- Ground moisture measurements
- Vegetation monitoring measurements

The samples taken in the field can be then analysed using different methods and instruments:

- Spectral analyses of individual rock samples in the laboratory
- X-ray diffraction powder (XRPD) analyses of bulk rock sample powder
- Geochemical analyses of bulk rock sample powder (XRF-analyses; ICP-MS analyses)
- Petrographic description of rock sample thin sections (TS)
- Geochemical analyses of individual minerals (EMPA)

This report will focus on the structure of the project database. This new database should follow the idea and workflow of the field work guide and create standards for the metadata description. The built-in report generator should also be useful when creating standardized project documentation.

This is a beta version and further changes or extensions to the database structure are always possible.

Description of the sample field data used for developing the database

In the course of the field activities in the areas of the Weißenstein and Bürgl magnesite quarries in Hochfilzen, rock samples were taken and spectral measurements were made. Figure 1 shows the location of the sampling points and the measurement points in the field. The red rectangles are the sampling points, the green dots are the in situ measurements with the SM-3500 spot spectrometer, and the violet rectangles are the samples measured with the point spectrometer in the laboratory. Each sample has its own point coordinate, as does each in situ measurement.

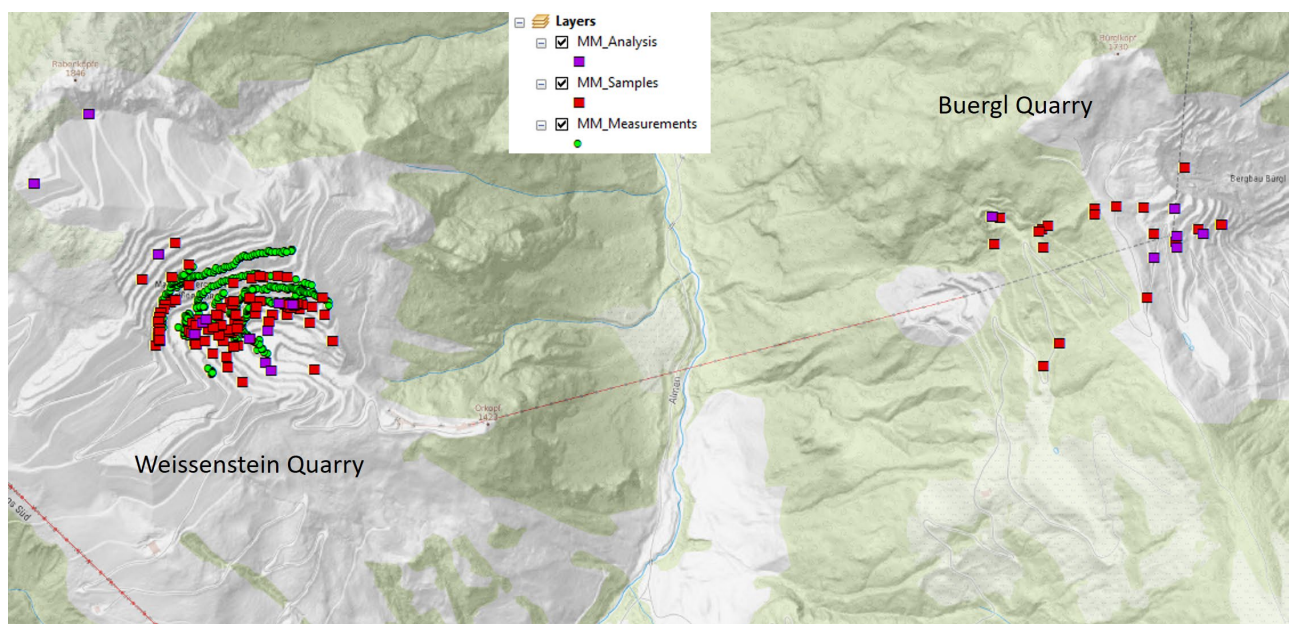


Fig. 1: Location of the sampling points and measuring points in the area of the Weißenstein and Bürgl magnesite quarries in Hochfilzen

The measurement data are stored as SED files (ASCII files), which consist of two parts: metadata and measurement results (wavelength and reflectance). Figure 2 shows an example of metadata of a point spectral measurement.

Project MULTIMINER – Task 4.1 Database

Metadata		
Comment:		
Version: 2.3 [3.0.7870]		
File	Name:	C:\Users\Algiz
8x\Documents\SpectralEvolution\SM-3500_20480S8\2022_Jul_13\WS_E7_00001.sed		
Instrument: SM-3500_20480S8		
Detectors: 512,256,256		
Measurement: REFLECTANCE		
Date: 07/13/2022,07/13/2022		
Time: 02:32:28.76,02:33:27.58		
Temperature (C): 16.87,8.88,-7.52,17.11,8.88,-7.32		
Battery Voltage: 7.90,7.87		
Averages: 10,10		
Integration: 2,4,6,20,50,6		
Dark Mode: AUTO,AUTO		
Foreoptic: PROBE {DN},PROBE {DN}		
Radiometric Calibration: DN		
Units: DN		
Wavelength Range: 350,2500		
Latitude: 47.4258570		
Longitude: 12.5656410		
Altitude: 1547.600m		
GPS Time: 9:31:15 AM		
Satellites: 8		
Calibrated Reference Correction File: none		
Channels: 2151		
Columns [2]:		

Fig. 2: Example of the metadata description of a point spectrometer measurement (file WS_E7_00001.sed)

Project MULTIMINER – Task 4.1 Database

A Microsoft Visual Basic program was written that extracts metadata from individual hyperspectral measurement files and stores them in the database (Fig. 3). The program has a user-friendly interface to extract metadata from all files in a specific directory.

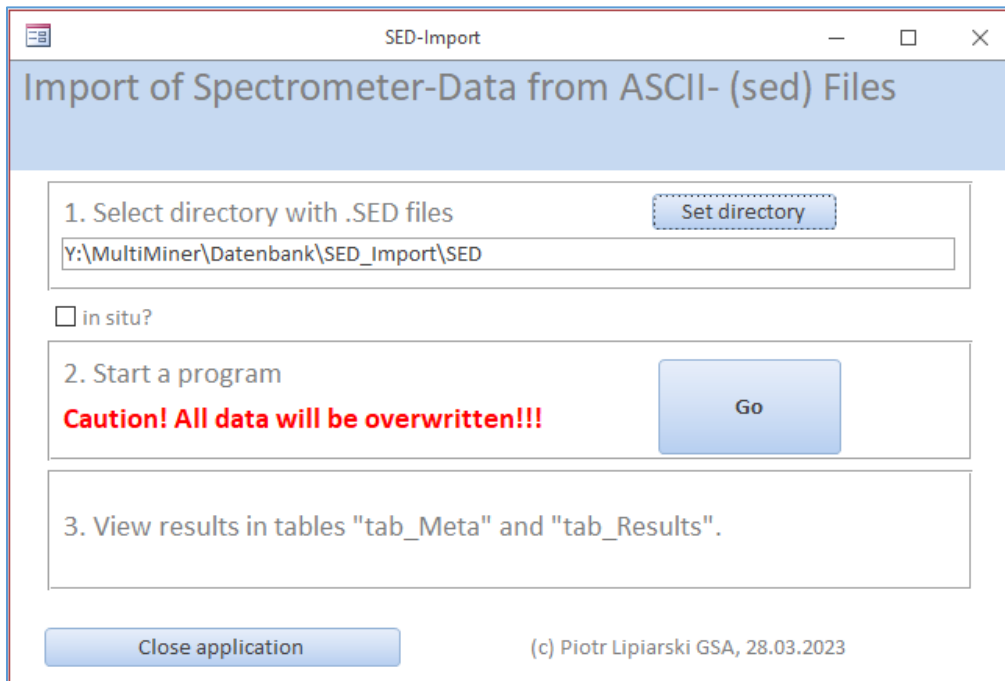


Fig. 3: VBA-Application for importing of Point Spectrometer metadata into a database

Metadata can be exported from the measurement data in a directory to a database table. The following lines are currently exported (Fig. 4):

- File Name (also Name of the Measurement),
- Instrument (SM-3500),
- Date,
- Time,
- Latitude,
- Longitude,
- Altitude.

Project MULTIMINER – Task 4.1 Database



Probenr	Instrument	Datum	Zeit	Latitude	Longitude	Altitude
WS_E8_00002	SM-3500_20480S8	07/13/2022	02:32:28.76	47,4258772	12,5655477	1546,800
WS_E8_00003	SM-3500_20480S8	07/13/2022	02:32:28.76	47,425955	12,56558	1544,600
WS_E8_00004	SM-3500_20480S8	07/13/2022	02:32:28.76	47,4259588	12,5655907	1543,600
WS_E8_00005	SM-3500_20480S8	07/13/2022	02:32:28.76	47,4259563	12,5655843	1541,900
WS_E8_00006	SM-3500_20480S8	07/13/2022	02:44:30.46	47,4259853	12,565661	1559,000
WS_E8_00007	SM-3500_20480S8	07/13/2022	02:44:30.46	47,4259795	12,5656747	1563,500
WS_E8_00008	SM-3500_20480S8	07/13/2022	02:44:30.46	47,4259845	12,5656983	1565,300
WS_E8_00009	SM-3500_20480S8	07/13/2022	02:44:30.46	47,4260272	12,5655847	1549,600
WS_E8_00010	SM-3500_20480S8	07/13/2022	02:44:30.46	47,4259455	12,565603	1535,600
WS_E8_00011	SM-3500_20480S8	07/13/2022	02:44:30.46	47,4259277	12,565553	1529,900
WS_E8_00012	SM-3500_20480S8	07/13/2022	02:44:30.46	47,425976	12,565651	1547,000
WS_E8_00013	SM-3500_20480S8	07/13/2022	02:44:30.46	47,4259905	12,565667	1548,900
WS_E8_00014	SM-3500_20480S8	07/13/2022	02:44:30.46	47,4259947	12,5657028	1556,000
WS_E8_00015	SM-3500_20480S8	07/13/2022	02:56:59.67	47,42601	12,5655523	1557,000

Fig. 4: Extract from the table "Tab_Meta" with the import result

This data is then supplemented with additional attributes, such as

- User (Measurer),
- Data source (for example project),
- Locality,
- Type of measurement,
- Lithology.

Figures 5 to 7 show the structure (with example data set) of three files: 1) an in situ measurement with a point spectrometer, 2) a laboratory measurement and 3) sampling points.

MeasureNr	SM-3500_SN20480S8_00063
File	SM-3500_SN20480S8_00063.SED
Instrument	SM-3500_20480S8
User	Bernhard Neugschwentner, Geosphere Austria
Date_	07/13/2022
Time_	05:42:42.23
Latitude	47,426049
Longitude	12,5653672
Altitude	1527,400
Source	Projekt MRI Magnesit
Type	in situ measurement with spectrometer
Shape	

Fig. 5: Example of the metadata of an in situ measurement imported into the database.

Project MULTIMINER – Task 4.1 Database

SampleNr	JW_2022_HF20
MeasureNr	JW_2022_HF20_B_00007
File	JW_2022_HF20_B_00007.SED
Instrument	SM-3500_20480S8
Datum	06/21/2022
Zeit	14:29:06.66
Latitude	47,42800582
Longitude	12,59686098
Altitude	1463
Sample_Name	Magnesit, Goethit
Location	Hochfilzen, Bürgl
Source	Projekt MRI Magnesit
Type	laboratory measurement with sepectrometer

Fig: 6: Example of the metadata of a laboratory measurement imported into the database. In addition to a MeasureNr, this data also has a Sample Number that connects the measurement to the sample.

SampleNr	JW_2022_HF01
Locality	Hochfilzen, Bürgl
Samplerr	Julia Weilbold
Year	2022
Sample	Probe 1
Remark	Baryt / hydrothermal, Spielbergdolomit
Lithology	Spielbergdolomit
Altitude	1460
Source	Projekt MRI Magnesit
latitude	47,42937844
longitude	12,59631156

Fig: 7: Example of metadata of a sample

In the second step of data processing, all terrain points (sampling points, in situ measuring points) were imported into a GIS feature class (GIS layer). The layer has a WGS84 coordinate system (EPSG number 4326).

Project MULTIMINER – Task 4.1 Database

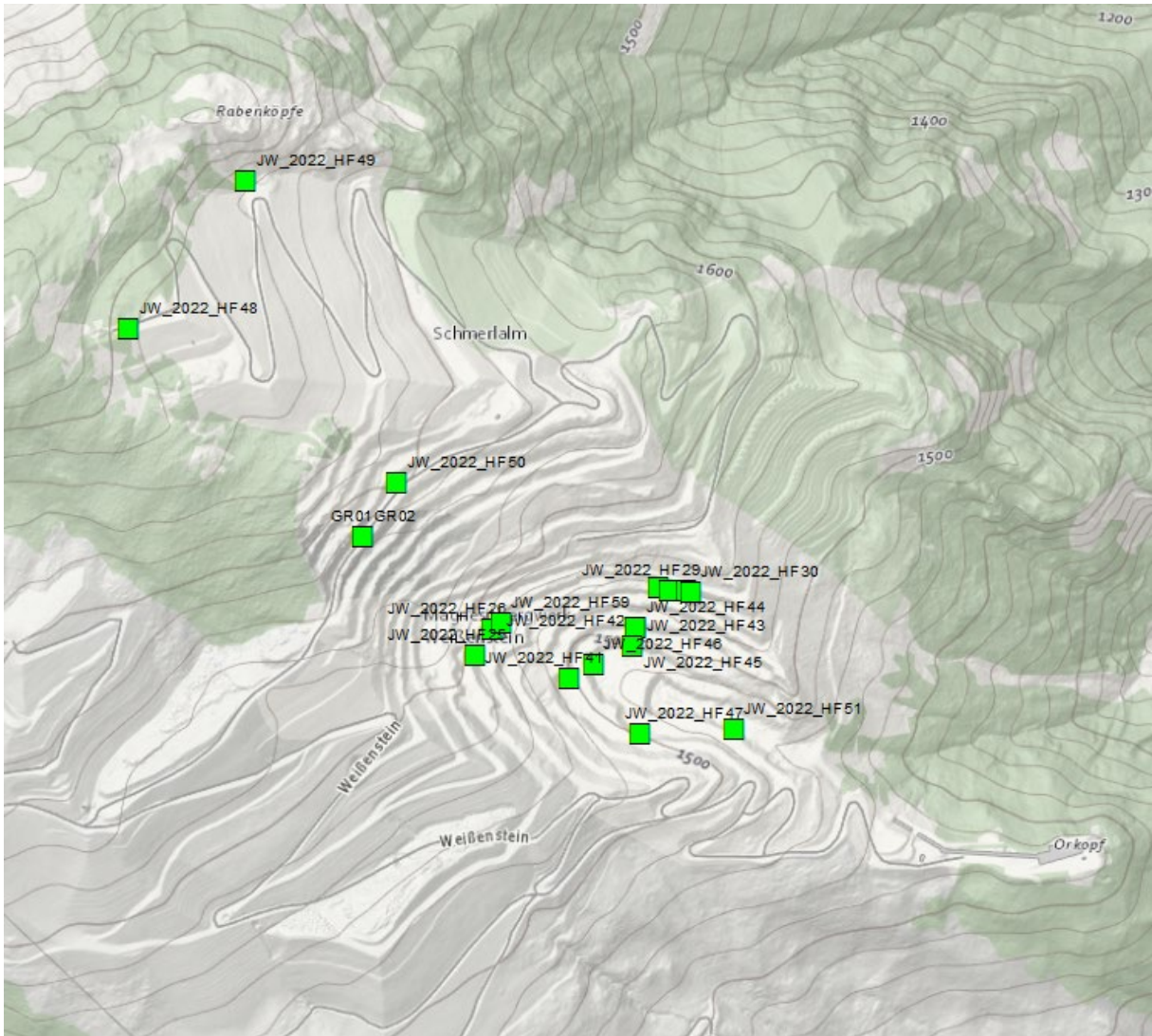


Fig. 8: Samples taken in the Weissenstein quarry (Hochfilzen, Austria).

Development of Database Structure

Further in this report, the following work steps are described that ultimately led to the development of the database:

- Data of Geosphere Austria from Hochfilzen have been taken as an example
- Metadata from spectral measurements have been extracted and imported into a database
- Sample data from different sources have been gathered
- Point coordinates (samples, measurements) have been loaded into a GIS system and transformed into a project coordinate system (1984_Web_Mercator_Auxiliary_Sphere, EPSG 3857)
- Attribute data have been analyzed, database tables have been created
- Relations (constraints) between tables have been defined
- Project data have been imported into a new database structure
- Exemplary result files have been gathered and connected to measurements
- Database has been loaded into GIS system, tables have been joined
- Database Report has been generated

Field observations (geological mapping, dust emissions, water quality, tailings mineralogy, data from rehabilitation sites) are made at a specific point (a location with X,Y,Z coordinates). At this point also a sample and spectral measurement can be taken. Samples can be later measured in a laboratory and analysed with different methods (Fig. 9).

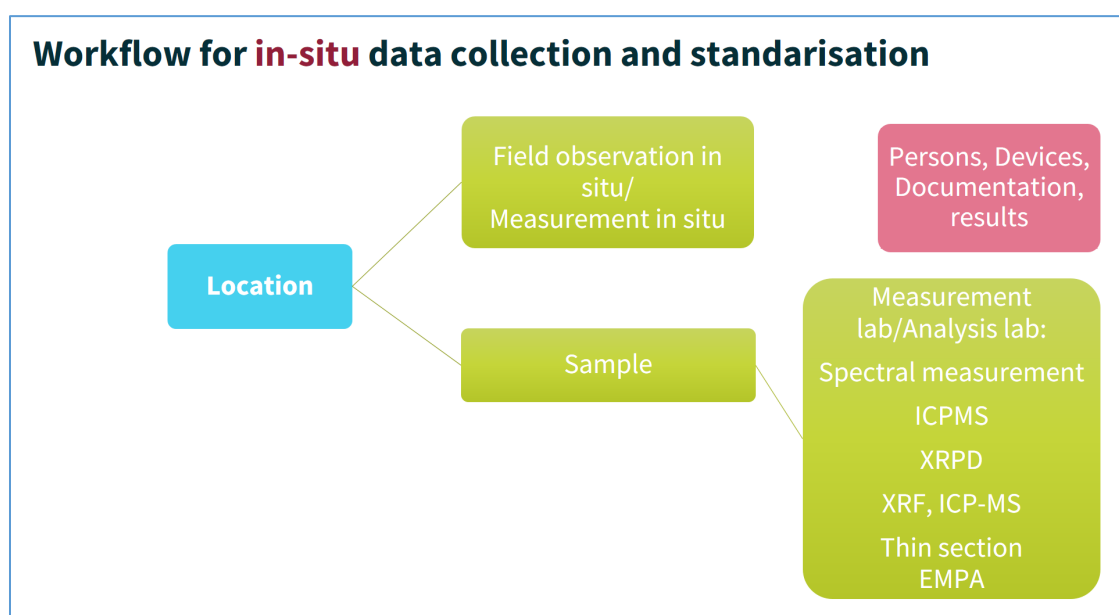


Fig. 9: Diagram showing workflow for in-situ data collection and standardisation

Workflow can be also shown as a relation entity diagram (Fig. 10). 1...∞ connections are one to many relations. For example, one point (A) can have one or more in situ measurements (B) and one or more samples (B). The same relation is between a sample (B) and a spectral measurement or analysis in a laboratory (C).

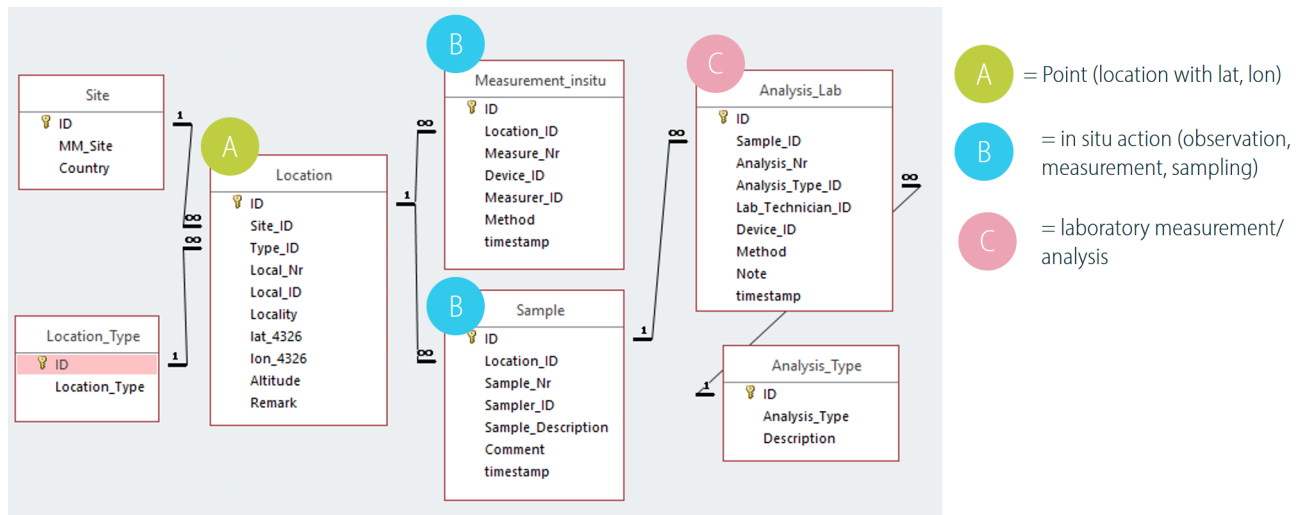


Fig. 10: Relation Entity Diagram of a project database (also see Fig. 9)

The database structure of the MS Access MultiMiner Database is shown in Figure 11. In the figure, blue areas are *in situ* data: location data (X, Y, Z coordinates, location site & type), field observations, samples and spectral *in situ* measurements. Furthermore, in Figure 13, red areas denote laboratory results: spectral measurements in a laboratory or laboratory analysis metadata. In Figure 11, green areas denote documentation (documents, field photos, analysis results in the form of a pdf, xls, doc, jpg etc.), persons and institutions which are involved in this project (sampler, mapper, measurer, operator etc.) and used devices (XRF devices, spectral devices etc). If published in a public repository, the personal data will not be exported.

1...∞ connections are one to many relations (one record is connected to one or more records in the other table).

Each table has a „primary key“ (PK) unique identifier. These PKs are used for relations between the tables because they are unique and cannot be changed. PKs are symbolized by a „key“ and are called „ID“ in each table. Related tables are connected to the PK of the other table through „foreign keys“. Foreign keys (FK) are called as a related table name + „ID“ – for example „Sample_ID“ is a FK in a table „Analysis_Lab“ to connect it to a table „Sample“ (1...n relation)

Project MULTIMINER – Task 4.1 Database

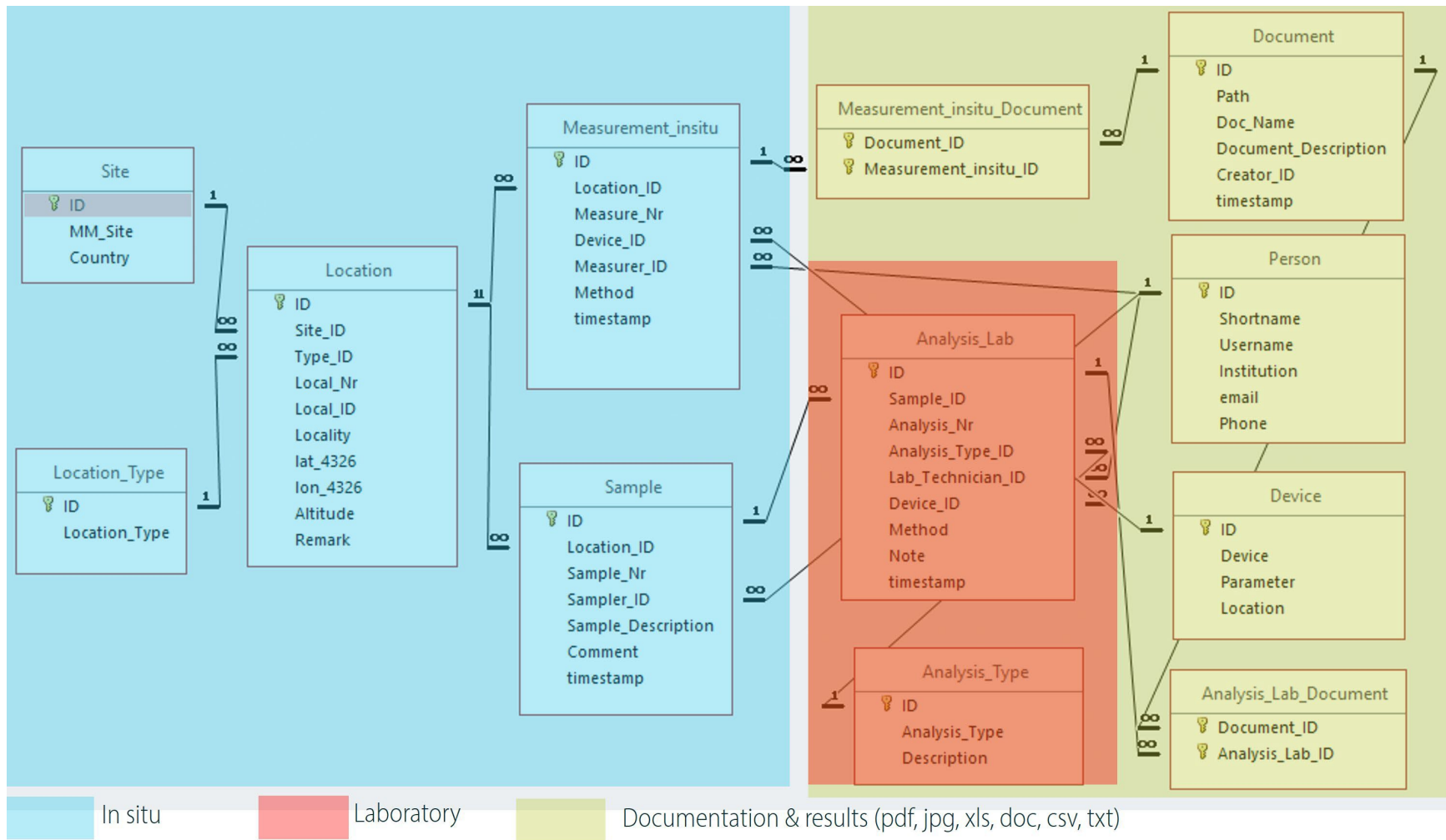


Fig. 11: Database structure of MS Access „MultiMiner“ Database.

Description of Database Tables

Table “Location”

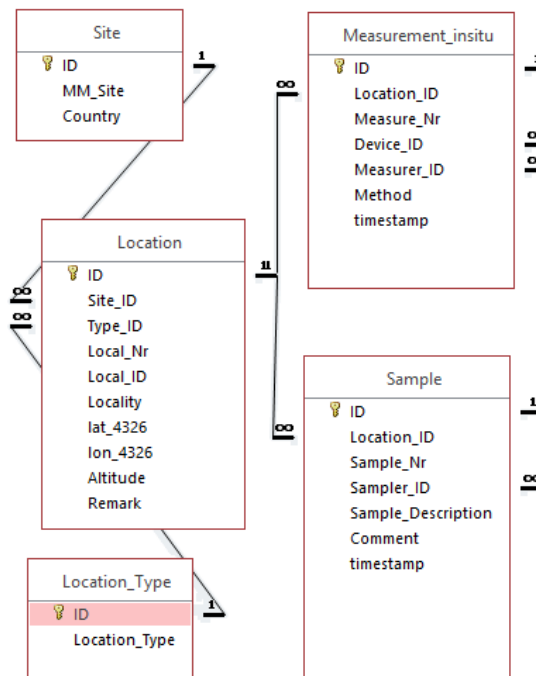


Table “Location” has a position of the measurement(s) or sample(s) as a X,Y,Z coordinate.

Table “Location” has following attributes:

- **ID**: sequence, Primary Key (PK)
- **Site-ID**: ID of the Study area (1=Ihalainen, 2=Hochfilzen, 3=Chalkidiki, 4=Kallyntiri, 5=Kirki)
- **Type_ID**: geographic feature (1=point, 2=line, 3=polygon)
- **Local_Nr**: internal Point Name(optional)
- **Local_ID**: internal Point Number (optional)
- **Locality**: name of the locality
- **Lat_4326**: coordinate in WGS84 EPSG 4326
- **Lon_4326**: coordinate in WGS84 EPSG 4326
- **Altitude**: [m]

Sample records

ID	Site_ID	Type_ID	Local_Nr	Local_ID	Locality	lat_4326	lon_4326	Altitude
1	1	1	JW_2022_HF01		Hochfilzen, Bürgl	47,4293784401335	12,5963115630885	1460
2	1	1	JW_2022_HF02		Hochfilzen, Bürgl	47,428512821163	12,5959790751628	1460
3	1	1	JW_2022_HF03		Hochfilzen, Bürgl	47,428512821163	12,5959790751628	1460
4	1	1	JW_2022_HF04		Hochfilzen, Bürgl	47,4278296425873	12,5960416712503	1460
5	1	1	JW_2022_HF05		Hochfilzen, Bürgl	47,4279376524969	12,5960534114757	1462
6	1	1	JW_2022_HF06		Hochfilzen, Bürgl	47,4277128101004	12,5960565635183	1462
7	1	1	JW_2022_HF07		Hochfilzen, Bürgl	47,4278296425873	12,5960416712503	1460
8	1	1	JW_2022_HF08		Hochfilzen, Bürgl	47,427492510267	12,5953704269183	1461
9	1	1	JW_2022_HF09		Hochfilzen, Bürgl	47,4279962428033	12,5953766130492	1459
10	1	1	JW_2022_HF10		Hochfilzen, Bürgl	47,4285732048624	12,594188857951	1503
12	1	1	JW_2022_HF12		Hochfilzen, Bürgl	47,4285061300017	12,5935535808002	1500
13	1	1	JW_2022_HF13		Hochfilzen, Bürgl	47,4283982057242	12,5935550989255	1501
14	1	1	JW_2022_HF14		Hochfilzen, Bürgl	47,428542802323	12,5950508335609	1503
15	1	1	JW_2022_HF15		Hochfilzen, Bürgl	47,4277132801884	12,5919609530999	1460
16	1	1	JW_2022_HF16		Hochfilzen, Bürgl	47,427793399341	12,5904488218604	1462

Table “Measurement_insitu”

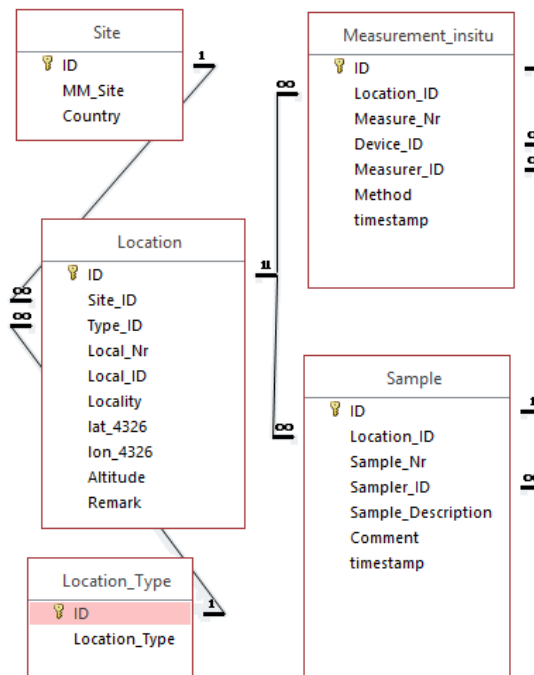


Table „Measurement_insitu“ contains metadata of the spectral in situ measurement(s) and field observation.

Table „Measurement_insitu“ has following attributes:

- **ID**: sequence, Primary Key (PK)
- **Location_ID**: FK, relation to the table „Location“
- **Measure_Nr**: measurement number
- **Device_ID**: instrument used by measurement (see Table “Device”)
- **Measurer_ID**: ID of a person (see Table „Person“)
- **Method**: description of method used
- **Timestamp** (Date, time)

Sample records

ID	Location_ID	Measure_Nr	Device_ID	Measurer_ID	Method	timestamp
1	66	WS_E8_00063	2	2	Point measurement	13.07.2022 05:43:25
2	67	WS_E8_00064	2	2	Point measurement	13.07.2022 05:44:53
3	68	WS_E8_00065	2	2	Point measurement	13.07.2022 05:46:16
4	69	WS_E8_00066	2	2	Point measurement	13.07.2022 05:48:59
5	70	WS_E8_00000	2	2	Point measurement	13.07.2022 02:33:12
6	71	WS_E8_00001	2	2	Point measurement	13.07.2022 02:33:27
7	72	WS_E8_00002	2	2	Point measurement	13.07.2022 02:33:38
8	73	WS_E8_00003	2	2	Point measurement	13.07.2022 02:37:41
9	74	WS_E8_00004	2	2	Point measurement	13.07.2022 02:38:05
10	75	WS_E8_00005	2	2	Point measurement	13.07.2022 02:38:17
11	76	WS_E8_00006	2	2	Point measurement	13.07.2022 02:45:34
12	77	WS_E8_00007	2	2	Point measurement	13.07.2022 02:45:54
13	78	WS_E8_00008	2	2	Point measurement	13.07.2022 02:46:05
14	79	WS_E8_00009	2	2	Point measurement	13.07.2022 02:50:53

Table “Sample”

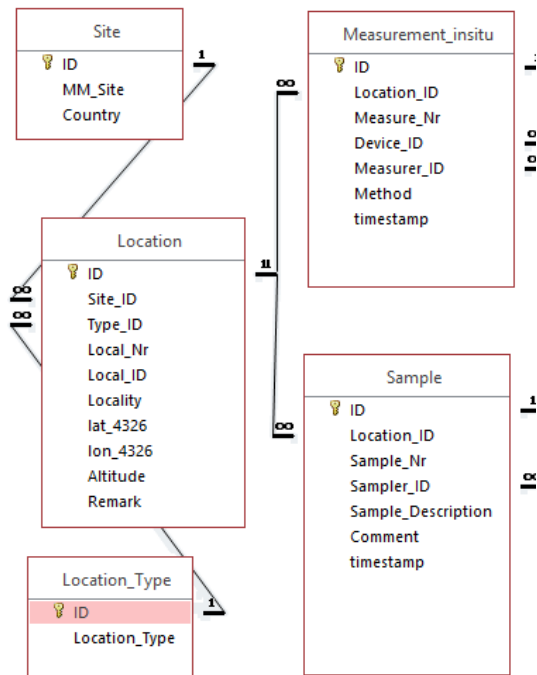


Table “Sample” contains information of sample taking in the field. Point information is obligatory.

Table “Sample” has following attributes:

- ID: sequence, Primary Key (PK)
- Location_ID: FK, relation to the table „Location“
- Sample_Nr: sample number
- Sampler_ID: ID of a person (see Table „Person“)
- comment: remarks
- timestamp (Date, time)

Sample records

ID	Location_ID	Sample_Nr	Sampler_ID	Sample_Description	Comment	timestamp
1	1	JW_2022_HF01	1	Dolomit	Baryt / hydrothermal, Spielbergdolomit	13.07.2022
2	2	JW_2022_HF02	1	Dolomit	Dolomit mit Schichtsilikate, Winde, Liege	13.07.2022
3	3	JW_2022_HF03	1	Magnetit	Magnetit mit Aragonit, Winde, Liegendk	13.07.2022
4	4	JW_2022_HF04	1	Magnetit	Magnetit, braun, Bürgl Körper	13.07.2022
5	5	JW_2022_HF05	1	Porphyroidmylonit	Porphyroidmylonitzone, Schichtsilikate, E	13.07.2022
6	6	JW_2022_HF06	1	Porphyroidmylonit	Hangengrenze, mylonitisch, rot, Bürgl, S	13.07.2022
7	7	JW_2022_HF07	1		2 Proben für Christian (Aragonitkristalle),	13.07.2022
8	8	JW_2022_HF08	1	Dolomit schwarz	schwarzer Dolomit mit Schichtsilikaten, R	13.07.2022
9	9	JW_2022_HF09	1	Magnetit	Magnetit, schwarz, Hangenschicht, AF 1,	13.07.2022
10	10	JW_2022_HF10	1	Magnetit	Magnetit rot und gelbe Magnetitklüfte, A	13.07.2022
12	12	JW_2022_HF12	1	Dolomit	rekristallisierter Dolomit, streichende Ve	13.07.2022
13	13	JW_2022_HF13	1	Mangan	Mangan, da waren wir nie ;)	13.07.2022
14	14	JW_2022_HF14	1	Goethit. Mangan	Goethit. Mangan. AF1. 2. Abbauhorizont.	13.07.2022

Table “Analysis_Lab”

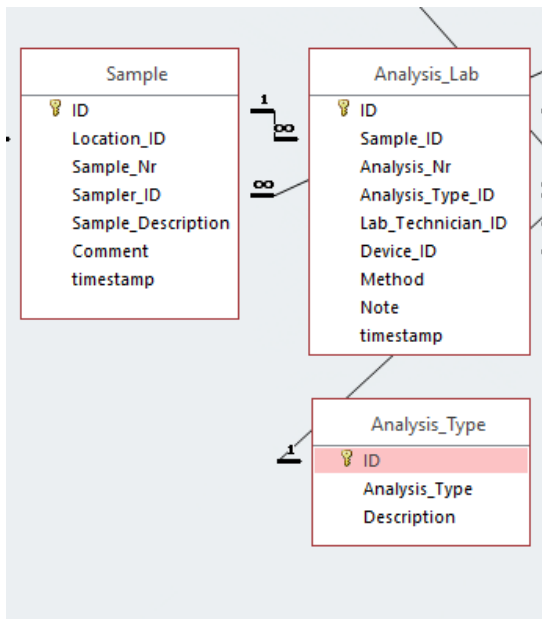


Table “Analysis_Lab” contains information about laboratory analysis. Sample input is obligatory. Information about the type of analysis (Spectral measurement lab, XRF, ICP-MS, electron microscopy and so on) and a used device must also be available.

Table “Analysis_Lab” has following attributes:

- ID: sequence, Primary Key (PK)
- Sample_ID: FK, relation to the table „Sample“
- Analysis_Type_ID: type of measurement
- Lab_Technician_ID: ID of a technician (see Table „Person“)
- Device_ID: type of device (see Table „Device“)
- Method: Method used
- Note: Remarks
- Timestamp (Date, time)

Sample records

ID	Sample_ID	Analysis_Nr	Analysis_Type_ID	Analyst_ID	Device_ID	Method	Note	timestamp
51	24	JW_2022_HF24_F1_00002	6	2	2	Point measurement	Messung Hannover	17.04.2023
52	24	JW_2022_HF24_F1_00003	6	2	2	Point measurement	Messung Hannover	17.04.2023
53	24	JW_2022_HF24_F1_00004	6	2	2	Point measurement	Messung Hannover	17.04.2023
54	24	JW_2022_HF24_F2_00005	6	2	2	Point measurement	Messung Hannover	17.04.2023
55	24	JW_2022_HF24_F2_00006	6	2	2	Point measurement	Messung Hannover	17.04.2023
56	24	JW_2022_HF24_F2_00007	6	2	2	Point measurement	Messung Hannover	17.04.2023
57	24	JW_2022_HF24_F3_00008	6	2	2	Point measurement	Messung Hannover	17.04.2023
58	24	JW_2022_HF24_F3_00009	6	2	2	Point measurement	Messung Hannover	17.04.2023
59	24	JW_2022_HF24_F3_00010	6	2	2	Point measurement	Messung Hannover	17.04.2023
60	24	JW_2022_HF24_F3_00011	6	2	2	Point measurement	Messung Hannover	17.04.2023
61	24	JW_2022_HF24_F4_00012	6	2	2	Point measurement	Messung Hannover	17.04.2023
62	24	JW_2022_HF24_F4_00013	6	2	2	Point measurement	Messung Hannover	17.04.2023
63	25	JW_2022_HF25_1_F1_00001	6	2	2	Point measurement	Messung Hannover	17.04.2023
64	25	JW_2022_HF25_1_F1_00002	6	2	2	Point measurement	Messung Hannover	17.04.2023
65	25	JW_2022_HF25_1_F1_00003	6	2	2	Point measurement	Messung Hannover	17.04.2023
66	25	JW_2022_HF25_1_F2_00004	6	2	2	Point measurement	Messung Hannover	17.04.2023

Table “Analysis_Type”

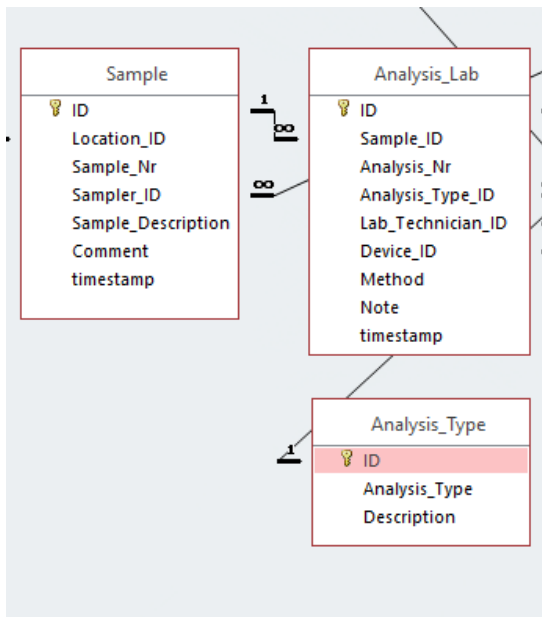


Table “Analysis_Type” is a list of analysis methods used during the project. The “ID” is then used in the Table “Analysis_Lab” (Analysis_Type_ID).

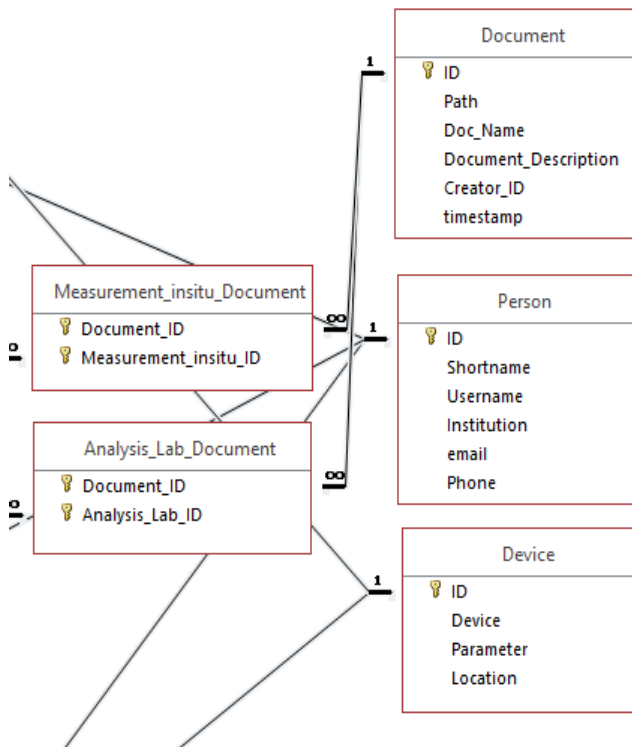
Table “Analysis_Type” has following attributes:

- ID: sequence, Primary Key (PK)
- Analysis_Type: type of measurement
- Description of the method

Sample records

ID	Analysis_Type	Description
1	XRPD	X-ray powder diffraction analyses of bulk rock sample powder
2	XRF	X-ray fluorescence analysis for the major elements as oxides
3	ICP-MS	rock sample analysis with inductively coupled plasma-mass spectrometry
4	EMPA	Geochemical analyses of individual minerals by Electron Microprobe Analysis
5	Thin Section	A section of rock specimen prepared on an mounting glass typically 26x46mm in size
6	Spectral measurement	Spectral measurement of a sample taken in the field
7	RAMAN	Raman Spectroscopy

Table “Document”



The "Document" table contains various document types (.doc, .xls, .pdf, .jpg...) that were created in the course of the workflow of sampling, measurement and analysis. This can be a photo in the field, or an analysis result of a spectral measurement. The documents are then linked to the different tables at various points. For example the Table “Analysis_Lab_Document” is a connection between a Document (Document_ID) and an Analysis (Analysis_Lab_ID).

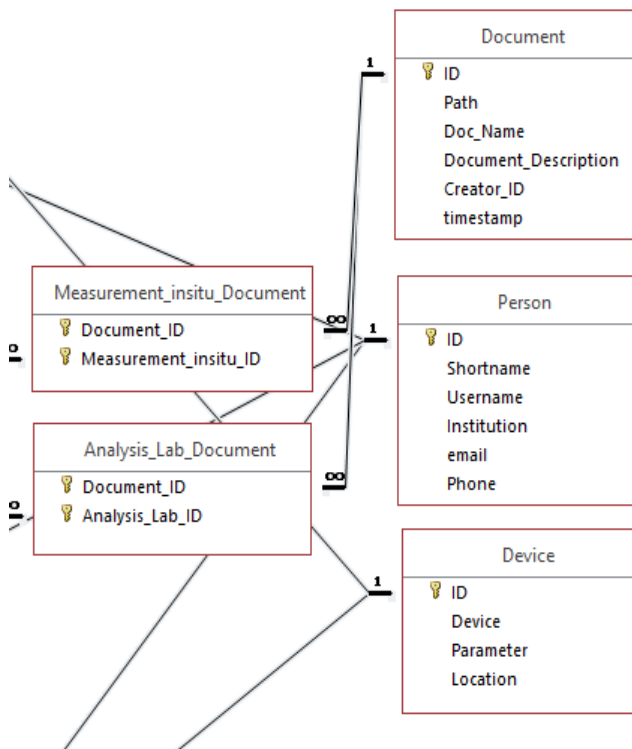
Table “Document” has following attributes:

- ID: sequence, Primary Key (PK)
- Path: path for document
- Doc_name: Filename of the Document
- Creator_ID: Author (see Table “Person”)
- Timestamp (Date, Time)

Sample records

ID	Path	Doc_Name	Document_Description	Creator_ID	timestamp
9	AT\Hochfilzen\ORE_PRO_Measurements\AT_HF_WS_ORE_E8	WS_E8_00065.SED	Hochfilzen, Weißenstein; Point measurement	2	13.07.2022 05:46:16
10	AT\Hochfilzen\ORE_PRO_Measurements\AT_HF_WS_ORE_E8	WS_E8_00066.SED	Hochfilzen, Weißenstein; Point measurement	2	13.07.2022 05:48:59
11	AT\Hochfilzen\ORE_PRO_Measurements\AT_HF_WS_ORE_E8	WS_E8_00000.SED	Hochfilzen, Weißenstein; Point measurement	2	13.07.2022 02:33:12
12	AT\Hochfilzen\ORE_PRO_Measurements\AT_HF_WS_ORE_E8	WS_E8_00001.SED	Hochfilzen, Weißenstein; Point measurement	2	13.07.2022 02:33:27
13	AT\Hochfilzen\ORE_PRO_Measurements\AT_HF_WS_ORE_E8	WS_E8_00002.SED	Hochfilzen, Weißenstein; Point measurement	2	13.07.2022 02:33:38
14	AT\Hochfilzen\ORE_PRO_Measurements\AT_HF_WS_ORE_E8	WS_E8_00003.SED	Hochfilzen, Weißenstein; Point measurement	2	13.07.2022 02:37:41
15	AT\Hochfilzen\ORE_PRO_Measurements\AT_HF_WS_ORE_E8	WS_E8_00004.SED	Hochfilzen, Weißenstein; Point measurement	2	13.07.2022 02:38:05
16	AT\Hochfilzen\ORE_PRO_Measurements\AT_HF_WS_ORE_E8	WS_E8_00005.SED	Hochfilzen, Weißenstein; Point measurement	2	13.07.2022 02:38:17
17	AT\Hochfilzen\ORE_PRO_Measurements\AT_HF_WS_ORE_E8	WS_E8_00006.SED	Hochfilzen, Weißenstein; Point measurement	2	13.07.2022 02:45:34
18	AT\Hochfilzen\ORE_PRO_Measurements\AT_HF_WS_ORE_E8	WS_E8_00007.SED	Hochfilzen, Weißenstein; Point measurement	2	13.07.2022 02:45:54
19	AT\Hochfilzen\ORE_PRO_Measurements\AT_HF_WS_ORE_E8	WS_E8_00008.SED	Hochfilzen, Weißenstein; Point measurement	2	13.07.2022 02:46:05
20	AT\Hochfilzen\ORE_PRO_Measurements\AT_HF_WS_ORE_E8	WS_E8_00009.SED	Hochfilzen, Weißenstein; Point measurement	2	13.07.2022 02:46:16

Table “Person”



The "Person" table contains a list of all for measuring, sampling and analytics responsible persons with a link to the institution.

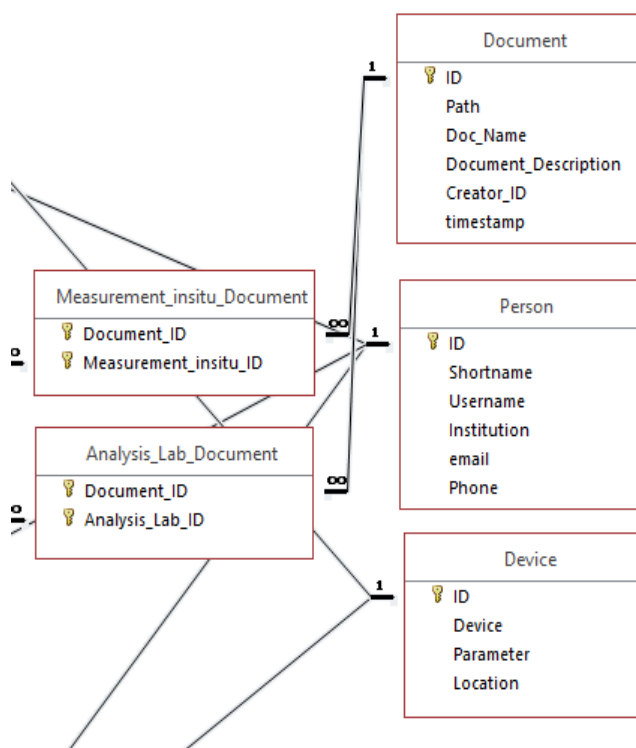
Table "Person" has following attributes:

- ID: sequence, Primary Key (PK)
- Shortname (first 3 letters of a family name + first 3 letters of the first name).
- Username: Name of the person
- Institution: Name of Institution
- Email (optional)
- Phone (optional)

Sample records

ID	Shortname	Username	Institution	email
1	WEIJUL	Julia Weibold	Geosphere Austria	julia.weibold@geosphere.at
2	NEUBER	Bernhard Neugschwentner	Geosphere Austria	Bernhard.Neugschwentner@geosphere.at
3		Christoph Stranzl	RHI Magnesita	
4		Johann Raith	Montanuniversität Leoben	
5	PERMAN	Mandana Peresson	Geosphere Austria	Mandana.Peresson@geosphere.at
6	LIPPPIO	Piotr Lipiarski	Geosphere Austria	Piotr.Lipiarski@geosphere.at
7		Michaela Frei	BGR Hannover	Michaela.Frei@bgr.de
8	LASKON	Konstantinos Laskaridis	Hellenic Survey of Geology and Min	laskaridis@igme.gr
9	WERMAN	Manuel Werdenich	Geosphere Austria	manuel.werdenich@geosphere.at
10	HAMFER	Ferdinand Hampl	Montanuniversität Leoben	
11	SCHGER	Gerald Schubert-Hlavac	Geosphere Austria	Gerald.Schubert-Hlavac@geosphere.at
12		Gerd Rantitsch	Montanuniversität Leoben	
13	FEIMON	Monika Feichter	Montanuniversität Leoben	
14		Maarit Middleton	Geological Survey of Finland	

Table “Device”



The “Device” table contains a list of all used devices (measure, analytics).

Table “Device” has following attributes:

- **ID**: sequence, Primary Key (PK)
- **Device**: Name of the device
- **Parameter**: device parameters
- **Location**: Institution, Partner, University...

Sample records

ID	Device	Parameter	Location
1	Röntgendiffraktometer PANalytical X’Pert Pro Powder	Messbedingungen im Bereich von 3° 2 Theta bis 70° 2 Theta	Geosphere Austria
2	OreXpress™ Portable Spectrometer	Punktspektrometer SM-3500_20480S8	Geosphere Austria
3	XRD PANALYTICAL X’Pert MRD PRO		Hellenic Survey of Geology and Mineral Exploration
4	XRF S4 PIONEER, BRUCKER AXS		Hellenic Survey of Geology and Mineral Exploration
5	Thermo Scientific Niton XL5 Plus handheld XRF analyzer		Hellenic Survey of Geology and Mineral Exploration
6	ICPMS- τύπου SCIEX-ELAN 6100		Hellenic Survey of Geology and Mineral Exploration
7	JEOL JSM-IT500LV scanning electron microscope coupled with an Ultim Max 100 (OXFORD) EDS		Hellenic Survey of Geology and Mineral Exploration
8	optical Microscope		
9	Field Observation	Field observation during mapping progress	
10	geological Compass	Structural measurements in the field	
11	Horiba LabRAM HR Evolution	Equipped with a 100mW Nd:Yag (532nm) laser, a confocal microscope (100x objective, hole	Montanuniversität Leoben
12	Percometer	Percometer is an instrument for measurements of dielectric value, electrical	GTK, Finland

Development of the metadata-reporting

In order to be able to display the database contents clearly, a Project Report was created. It can be started for each Point-ID (Fig. 12).



Fig. 12: MultiMiner Report Generator (MS Access Report)

Either point-ID can be entered directly, or the Sample-nr (Measure-Nr) can be selected from the list (Fig. 13).

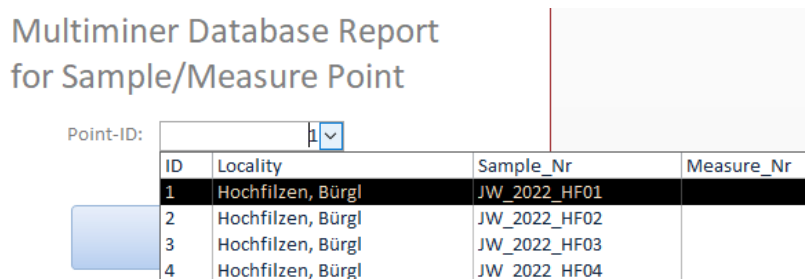


Fig. 13: MultiMiner Report Generator – search for Sample-Nr or Measure-Nr

Project MULTIMINER – Task 4.1 Database

Figures 14-17 show some examples of reports for different situations: only sampling, sample with analysis result, only field measurement, sampling and measurement in the laboratory.

The screenshot displays a web-based report generator interface titled "Point". The main content area is divided into several sections:

- Multiminer Database:** A blue header section containing:
 - ID: Localit:
 - Remark:
 - Coordinates table:

latitude	longitude	Altitude
<input type="text" value="47,429"/>	<input type="text" value="12,596"/>	<input type="text" value="1460"/>
- MULTIMINER Logos:** A collection of logos for partner institutions including GTK, VTI, BGR, SCIENCE CONNECT, TUM, Helias GOLD, and Geosphere Austria. A note at the bottom states: "The MultiMiner project is funded by the European Union's Horizon 2020 research and innovation programme under the Marie Skłodowska Curie Grant Agreement." (with a partially visible URL).
- Sample Information:** A grey bar containing:
 - Sample ID: Sample_Nr: timestamp:
- Metadata:** Text fields for:
 - Sampler:
 - Institution:
 - Comment:

Fig. 14: MultiMiner Report Generator – Example for a Point-ID=1 – sample only (without measurement and analysis)

Project MULTIMINER – Task 4.1 Database

Point

Multiminer Database

ID: Localit

Remark:

latitude	longitude	Altitude
<input type="text" value="47,427"/>	<input type="text" value="12,568"/>	<input type="text" value="1530"/>



MULTIMINER

The MultiMiner project is funded by the European Union

Sample ID: Sample_Nr: timestamp:

Sampler:

Institution:

Comment:

Sample Analysis ID: Analysis_Type

Description

Analyst Institution

Device

Document(s)

Document:

Description:

Fig. 15: MultiMiner Report Generator – Example for a Point-ID=27 – sample + analysis + linked document with analysis results

Project MULTIMINER – Task 4.1 Database

Multiminer Database

ID: Localit

Remark:

latitude	longitude	Altitude
47,426	12,566	1545















The MultiMiner project is funded by the Austrian Government through the Austrian Research Promotion Agency (FFG) and the European Union through the Horizon 2020 research and innovation programme under the Marie Skłodowska Curie grant agreement.

Measurement(s) insitu

Measurement-ID	4	Measure_Nr	WS_E8_00066	timestamp:	13.07.2022 05:48:59
Device:	OreXpress™ Portable Spectrometer				
Username:	Bernhard Neugschwentner	Institution:	Geosphere Austria		
Method:	Point measurement				

Document(s)

2022_07_13_Weissenstein_350-2500nm_all.png (Auswertung der insitu Messungen vom Weissenstein, gemessen mit Punktspektrometer). Creator: Bernhard Neugschwentner

2022_07_13_Weissenstein_350-2500nm_all_stacked.png (Auswertung der insitu Messungen vom Weissenstein, gemessen mit Punktspektrometer). Creator: Bernhard Neugschwentner

WS_E8_00066.SED (Hochfilzen, Weißenstein; Point measurement). Creator: Bernhard Neugschwentner

Fig. 16: MultiMiner Report Generator – Example for a Point-ID=69 – spectral measurement in situ + linked documents with measurement results

Project MULTIMINER – Task 4.1 Database

Multiminer Database

ID: Localit

Remark:

latitude	longitude	Altitude
<input type="text" value="47,428"/>	<input type="text" value="12,590"/>	<input type="text" value="1495"/>


















MULTIMINER

The MultiMiner project is funded by the European Union under the Horizon 2020 research and innovation programme (grant agreement No. 101019719).

Sample ID: Sample_Nr: timestamp:

Sampler:

Institution:

Comment:

Sample Analysis ID: Analysis_Type

Description

Analyst Institution

Device

Document(s)

Sample Analysis ID: Analysis_Type

Description

Analyst Institution

Device

Document(s)

Sample Analysis ID: Analysis_Type

Description

Analyst Institution

Device

Document(s)

Fig. 17: MultiMiner Report Generator – Example for a Point-ID=24 – sample + spectral measurement in laboratory

25

MultiMiner Database - Example queries

In this chapter some query examples will be shown. Queries can be defined as “inner join” or “outer join” queries. “Inner join” queries show as a result only these records, which are available in all tables of this query. Figure 18 shows an example of a “inner join” query which shows no results – because we do not have any data in a database which have a sample and a spectral measurement in situ for the same point.

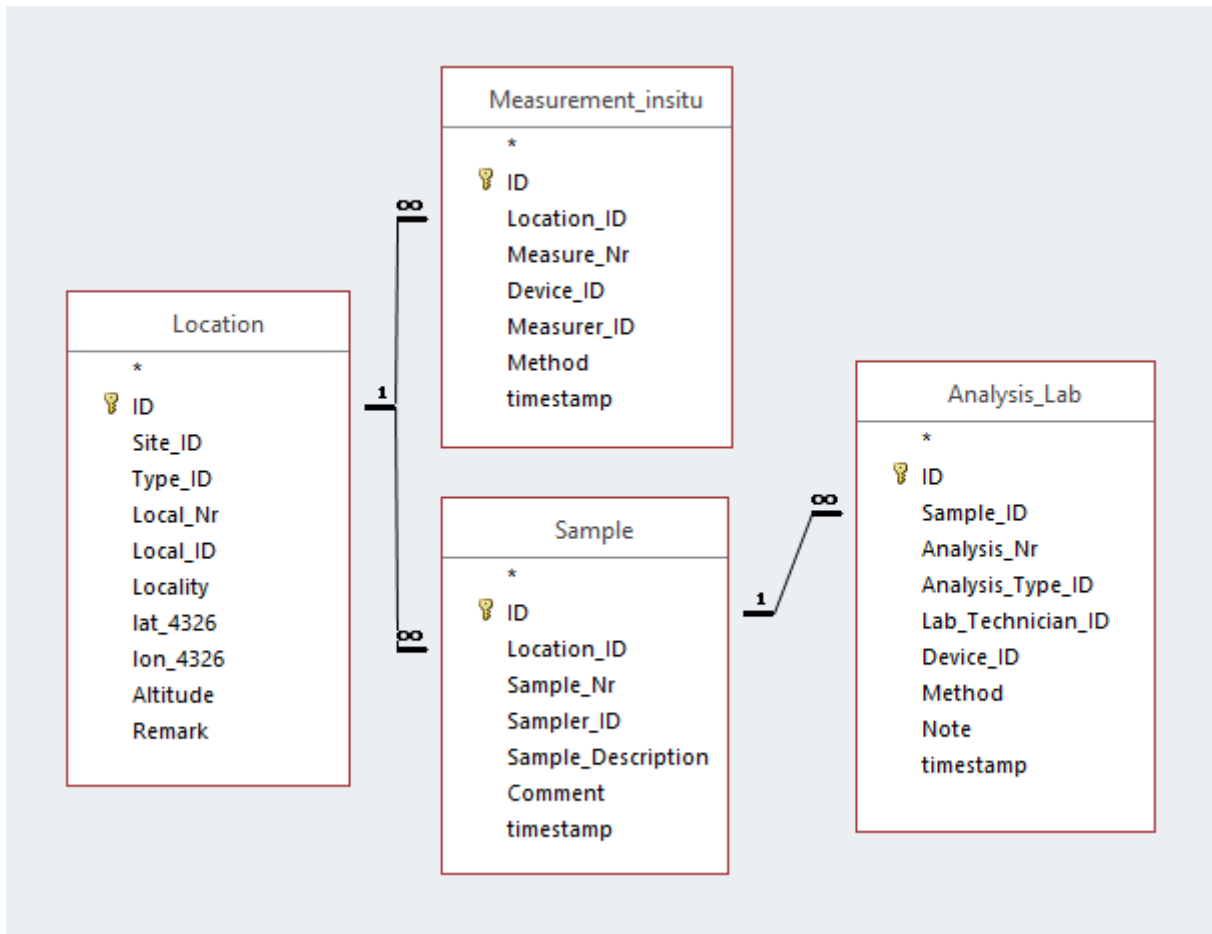


Fig. 18: Example of a database query with inner joins only (“qryMultiMiner_innerjoin”). This query shows no results. Inner joins are shown in a query as “lines”

In this case, we should use a so-called “outer join”. Outer join connects a table with the other one in that way, that not only matched records, but also unmatched records can be shown (Fig. 19 and 20).

Project MULTIMINER – Task 4.1 Database

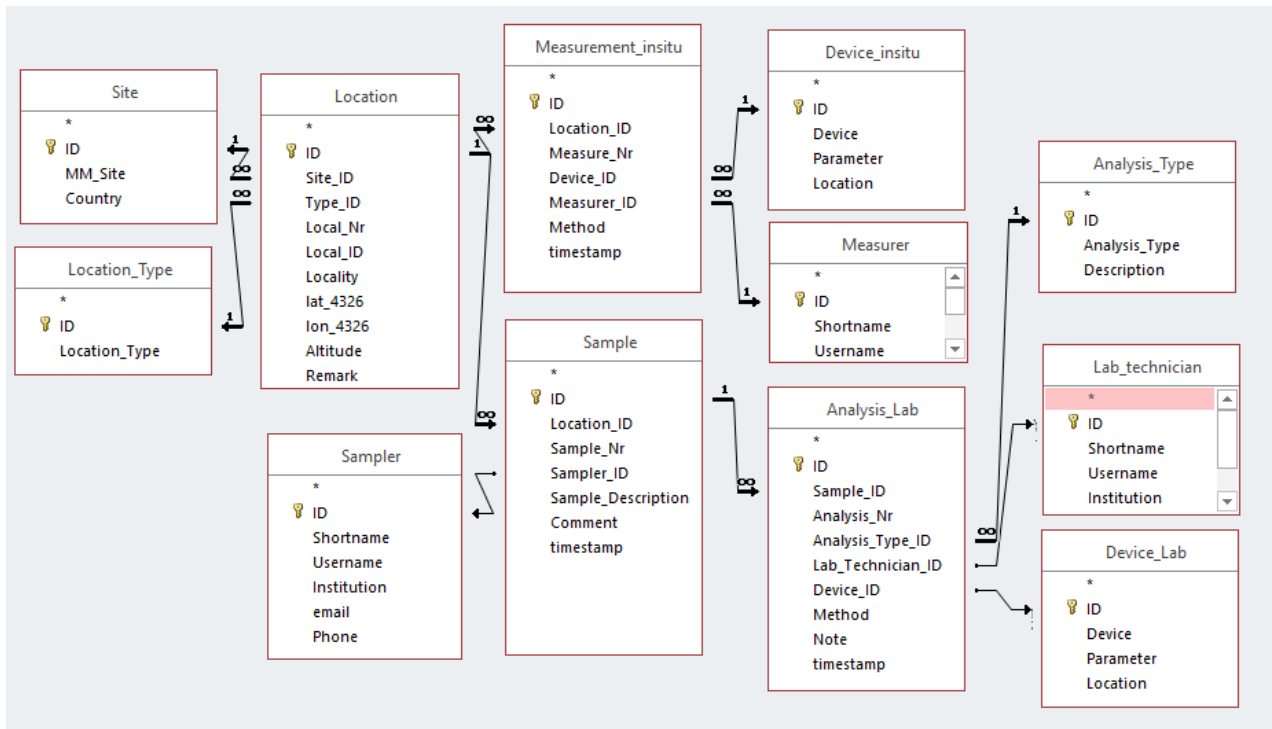


Fig. 19: Example of a database query with outer joins (“qryMultiMiner_outerjoin”). This query shows all records from a database. Outer joins are shown in a query as “arrows”. Outer joins return values that both match and do not match the SQL query from tables.

ID	Locality	lat_4326	lon_4326	Sample_Nr	Measure_Nr
62	Hochfilzen, Hochfilzen, Bürgl	47,4266800033189	12,5951400036705	GR03	
63	Hochfilzen, Rettenwand	47,4257100033184	12,5924600036679	GR04	
64	Hochfilzen, Rettenwand	47,4257100033184	12,5924600036679	GR05	
65	Hochfilzen, Rettenwand	47,425250003318	12,5919500036674	HF8	
66	Hochfilzen, Weißenstein	47,426049	12,5653672		WS_E8_00063
67	Hochfilzen, Weißenstein	47,4259917	12,5655435		WS_E8_00064
68	Hochfilzen, Weißenstein	47,4259595	12,5655627		WS_E8_00065
69	Hochfilzen, Weißenstein	47,425979	12,5657202		WS_E8_00066
70	Hochfilzen, Weißenstein	47,4258912	12,565616		WS_E8_00000
71	Hochfilzen, Weißenstein	47,425857	12,565641		WS_E8_00001
72	Hochfilzen, Weißenstein	47,4258772	12,5655477		WS_E8_00002
73	Hochfilzen, Weißenstein	47,425955	12,56558		WS_E8_00003
74	Hochfilzen, Weißenstein	47,4259588	12,5655907		WS FR 00004

Fig. 20: Part of the result of the query shown in Fig. 20 (outer join). By the points with a sample a Measure_nr is empty, by the points with in situ measurement there is no sampling.

Figure 21 shows an example of using subqueries (small help-queries) to make a query easier to read and more efficient.

Project MULTIMINER – Task 4.1 Database

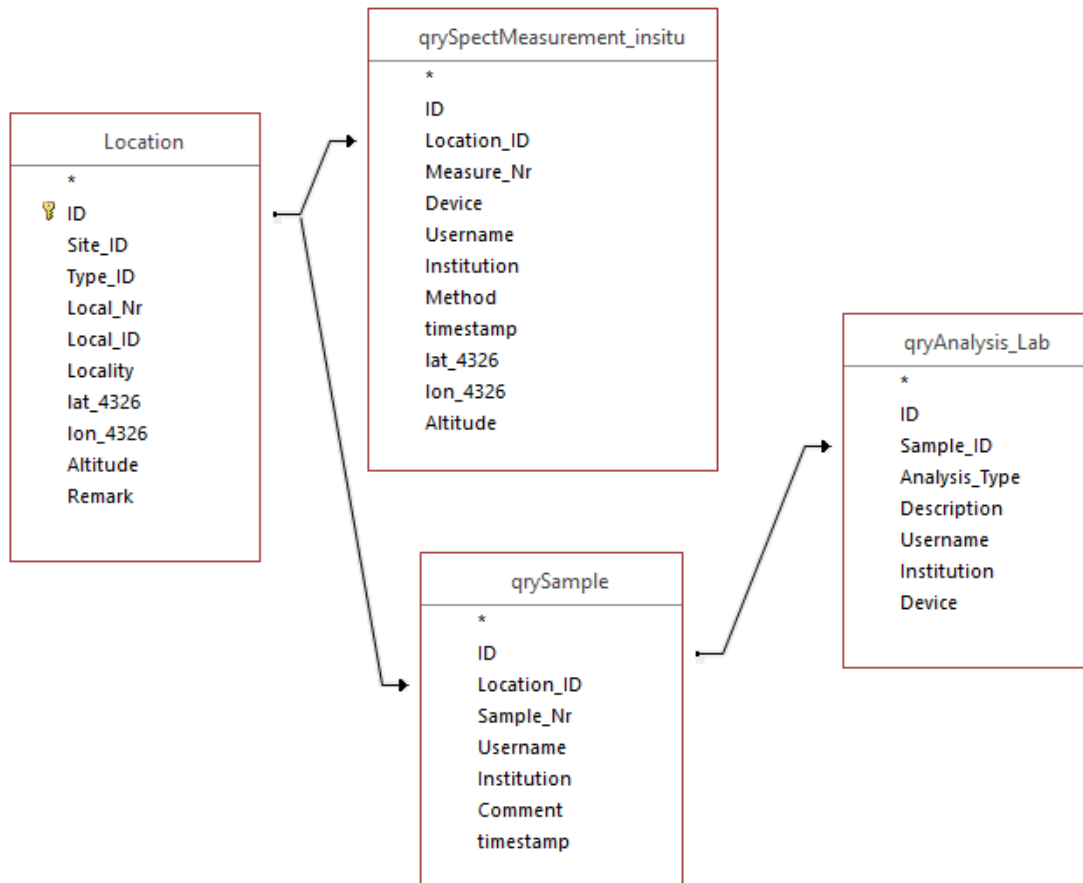


Fig. 21: Example of a database query with outer joins (“qryAllData”) which uses another queries. This query shows all records from a database. All IDs (Person, Device, Analysis) has been “translated” into expressions inside subqueries.

Grant agreement	101091374
Project title	Multi-Source and Multi-Scale Earth Observation and Novel Machine Learning for Mineral Exploration and Mine Site Monitoring
Project acronym	MultiMiner
Project coordinator	Dr. Maarit Middleton, GTK
Project start date	Jan 1, 2023
Project duration	42 months
Related work packages	WP 4 – Site Demonstrations
Related task(s)	Task 4.1 In situ data standardization and databases
Lead organization	GeoSphere Austria
Contributing partners	GTK, BGR, VTT, RHI, MUL, EFTAS, HSGME, CGS
Submission date	June 30, 2024
File name	Appendix 2 MultiMiner Austria – Mapping Hochfilzen (D4_1_MultiMiner_Field_Guidebook_V1_4.docx)
Organisation responsible for deliverable	GeoSphere Austria
Author name(s)	Gerald Schuberth-Hlavac, Christoph Stranzl, Johann Raith, Benjamin Huet, Holger Paulick
Date	October 10, 2024
Version	1.1
Status	Complete
Dissemination Level	Public





MultiMiner
Earth Observation for Smart Mining

MultiMiner Austria – Mapping Hochfilzen

Overview for geological mapping

GERALD SCHUBERTH-HLAVAČ¹, CHRISTOPH STRANZL², JOHANN RAITH³, BENJAMIN HUET¹,
HOLGER PAULICK¹

1. GeoSphere Austria
2. RHI Magnesita
3. Montanuniversität Leoben

2024-10-03

Version 4

Table of contents

1	Introduction	2
1.1	Location of the study area	2
1.2	Map sheets	2
1.3	Questions	2
1.4	Issues	3
2	Regions and areas	5
2.1	East Region	5
2.2	Central Region	5
2.3	West Region	8
3	Geological framework	9
4	Rock types and lithological units	14
4.1	Blasseneck porphyroid	14
4.2	Spielberg dolomite group	15
4.3	Slate	16
4.4	Radiolarite	16
4.5	Metabasites of the Glemmtal complex	16
5	Magnesite deposits in the Hochfilzen area, Eastern Alps: Genetic considerations	22
6	Rock descriptions	24
6.1	Blasseneck porphyroid	24
6.2	Spielberg dolomite group	24
6.3	Slate combined with Spielberg dolomite	25
6.4	Dolomite-radiolarite complex	25
6.5	Metabasalts of the Glemmtal complex	26
6.6	Magnesite	28
	References	29

1 Introduction

This is intended to serve as an introduction for the preparation of the geological mapping at Hochfilzen site for MultiMiner project. The areas to be mapped are defined and a brief geological overview is presented. The study area is placed in a modern regional geological framework and the rocks most relevant for the mapping work are presented.

As a base for a more in-depth familiarization, the explanations for sheet 122 Kitzbühl ([Heinisch et al., 2015](#)) and especially the rich literature list there should be mentioned. A geological overview of the magnesite deposits near Hochfilzen is given by e.g. Vavtar ([1976](#)).

Magnesite mineralizations are currently known in the Spielberg dolomite group and in the dolomite-radiolarite complex (see below). The known deposits, such as Weißenstein and Bürgl, are located in the Hochhörndler complex ([Heinisch et al., 2015](#)). Regarding the magnesite deposits in the study area, it should be mentioned that there is a discussion about their age and their genesis going back to the 19th century with significant differences of opinion. The inferred age of mineralization ranges from middle Silurian over Variscan to Alpidic and the spectrum of genesis models include primary-sedimentary, synsedimentary to early diagenetic to metasomatic. Also, there are different ideas about the origin of magnesium intake ([Tollmann, 1977](#)). See also Section 5 on this topic.

1.1 Location of the study area

Geographically, the study area is located about five to seven kilometers southwest of Hochfilzen – see Figure 1.1. It is mostly located in the province of Tyrol and a small part is located in the province of Salzburg.

1.2 Map sheets

The areas to be mapped concern sheets 122 Kitzbühl ([Heinisch et al., 2003](#)) and 123 Zell am See ([Heinisch et al., 1995](#)). Explanatory notes ([Heinisch et al., 2015](#)) are available for the former map sheet. The boundary of the two map sheets in the study area is the, here approximately north-south oriented, Fieberbrunner Ache. The majority of the areas to be investigated are located on sheet 122.. Mentionable “sheet edge faults” between these sheets are not known in the study area and are not of major importance here because no mapping area overlaps the sheets. Important lithologies have different numbers on the map sheets, but are named roughly the same.

1.3 Questions

The basic concern of the mapping work is the magnesite mineralization. Accordingly, the focus is on geological parameters that can be assumed to be relevant as evidence for magnesite mineralization processes. Important geological features include contacts to the adjacent rocks, differences in grain sizes, faults, . . .

It must be kept in mind that in the course of the MultiMiner project, the study area will be

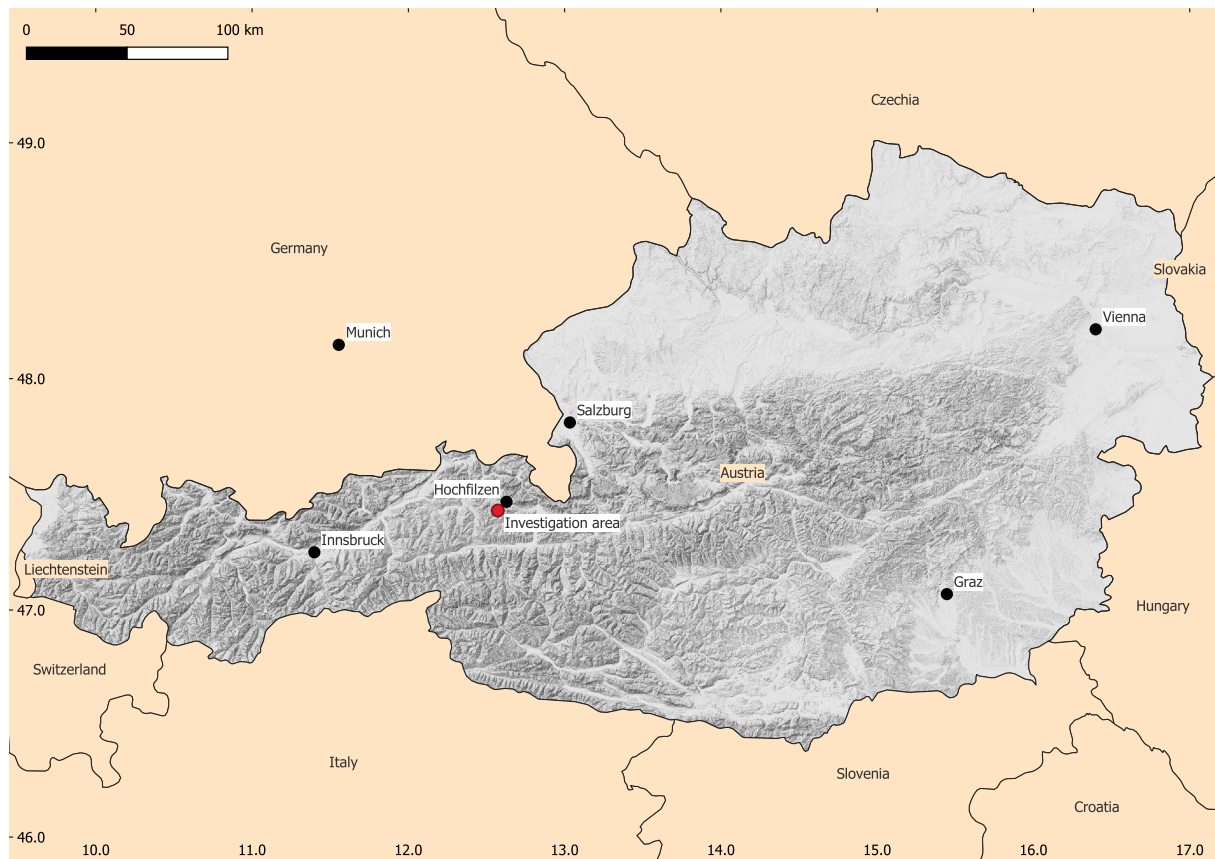


Figure 1.1: Location of the study area – marked in red (base map: basemap.at)

surveyed using spaceborne and drone-based Earth Observation (EO) methods, and the results of the mapping work will be linked to the results of these methods. In this respect, the field work should also take into account what a satellite or drone “sees” and thus, for example, not only nice outcrops should be examined, but also weathered rock.

1.4 Issues

At this point a few words about the practical field work and its preparation:

- Online, the regions and areas are shown with different map material at <https://ardigeos.geologie.ac.at/mumimap>.
- The mapping areas can be obtained as GeoPackage through the link <https://rhea.geologie.ac.at/index.php/s/rUqqImMIXdzGAUI>.
- The two map sheets can be obtained through the Tethys Research Data Repository, of Geosphere Austria, through the following links as PDFs and as GeoPackages:
 - GK 122 Kitzbühl: <https://doi.tethys.at/10.24341/tethys.53>
 - GK 123 Zell am See: <https://doi.tethys.at/10.24341/tethys.54>
- The Geological Maps of the Republic of Austria 1:50,000 can be integrated into GIS programs as raster layers via the following WMS/WMTS link: https://gisgba.geologie.ac.at/arcgis/services/image/AT_GBA_GK50/ImageServer/WMSServer?request=GetCapabilities
- WGS84, EPSG:4326, is to be used as the coordinate system for marking field points. This is the same coordinate system used by GPS devices.
- The positions of points recorded by GPS must be checked with a GIS program and satellite images (e.g. the orthophoto layer of basemap.at) and corrected if necessary prior to further use.

- Structural measurements are to be reported in (dipDirection, dip)-value pairs – as they are provided by structure compasses after Clar – and not in (strike, dip)-value pairs as it is still common in the Anglo-American area.
- The use of 10% of hydrochloric acid to distinguish magnesite from dolomite has not proved successful. This can be deceptive, as aragonite may also be present in part. Macroscopic identification of carbonates is more appropriate.
- Sample labeling should not be done on the sample with a permanent or paint marker, rather the sample should be placed in a bag and the bag should be labeled. The reason is a possible spectral analysis on the sample in the laboratory and colors added by markers could make this analysis difficult or impossible.
- For field work, the period June-July seems to be ideal, because here mostly a stable weather situation (especially July) prevails and the days are long. In August, precipitation is traditionally expected. In September, however, favorable weather conditions could arise again, although the days are already shorter at this time.

2 Regions and areas

The areas to be mapped are located in a roughly west-east oriented strip south of Fieberbrunn and Hochfilzen with the active open pit Weißenstein roughly in the middle – see Figure 2.1 and Figure 2.2. For (preliminary) structuring, the study area is divided into three regions and associated areas. These are now briefly described here – from east to west and with decreasing priority.

2.1 East Region

Lies to the east of the active Weißenstein open pit and is the only one of the regions on map sheet 123. It is bounded by the former Bürgl open pit, to the west, and Inschlagalpe underground mine, to the east. Two varieties of magnesite can be identified in this region: One fine-grained and one coarse-grained.

2.1.1 Area 1

East of the former Bürgl open pit resp. the eastern side of the Spielberggraben. This area should be easily accessible: Access via Burgeralm and parking there and on. After consultation with the landowners, it may also be possible to use the alpine path to the Kleberkopf saddle. For parts of this area there is a detailed description and mapping by Riedler (2010).

2.1.2 Area 2

The area around the former mine site Inschlagalpe. Here, a well exposed area to the west of the former mine site is of great interest. (South)East of this, the terrain is quite steep and forested – however mapping information exists from when the mine was in operation. A relatively coarse-grained magnesite with zero porosity is found here.

Access via the Schwarzleotal with parking at the show mine Leogang. Possibly, the private road behind the gate can be used after consultation with the landowner.

2.1.3 Area 3

This is still vaguely defined. Here, laser scans should be consulted in order to identify potential outcrops. If none of them could be identified the southern border of the Spielberg dolomite should be followed.

Access via the Schwarzleotal with parking possibility at the Leogang show mine. Possibly, the private road behind the barrier can be used after consultation with the landowner.

2.2 Central Region

This region is on the eastern edge of map sheet 122. It is the area to the west and north around the Weißenstein open pit.

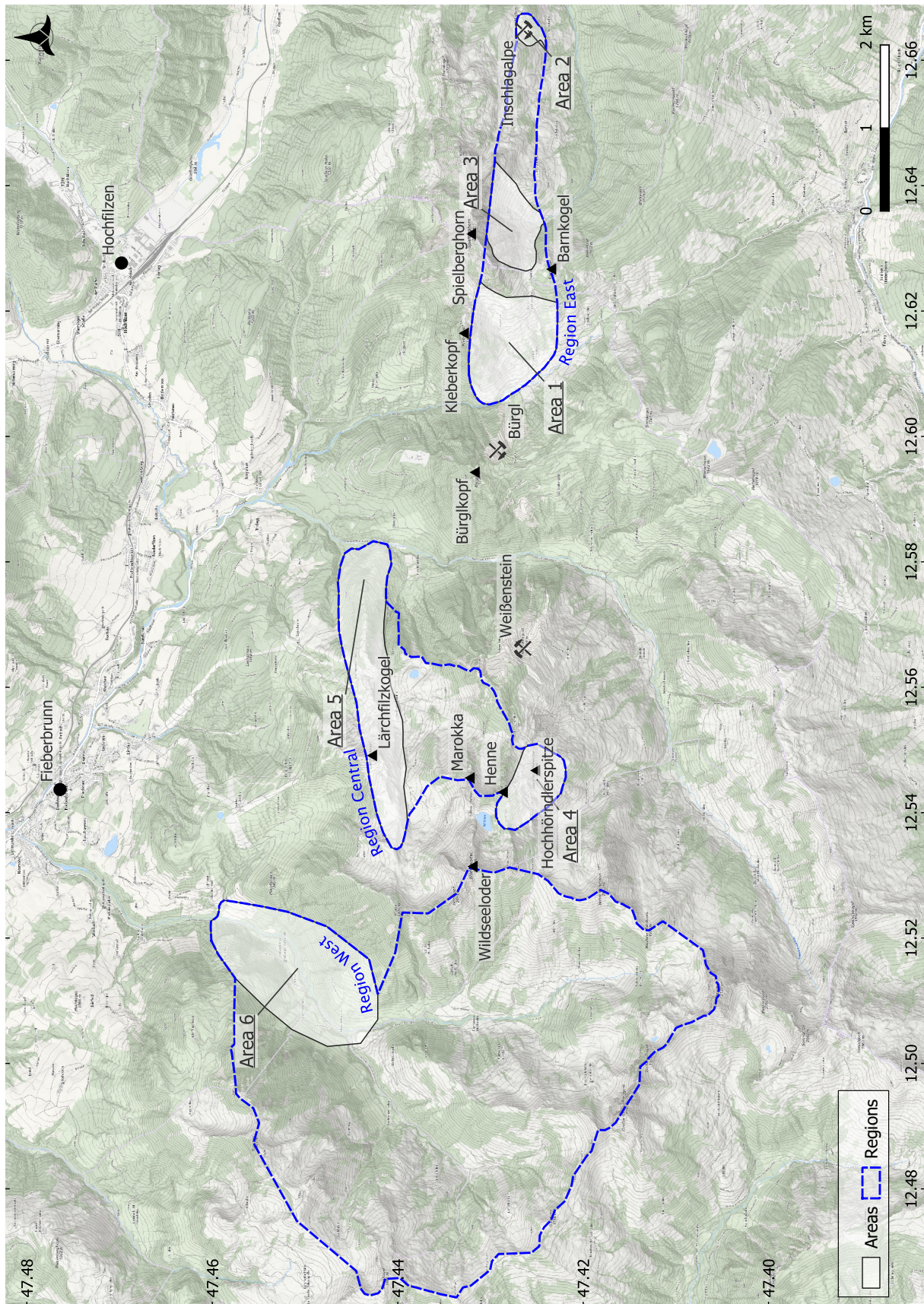


Figure 2.1: Overview of the mapping areas (base map: basemap.at)

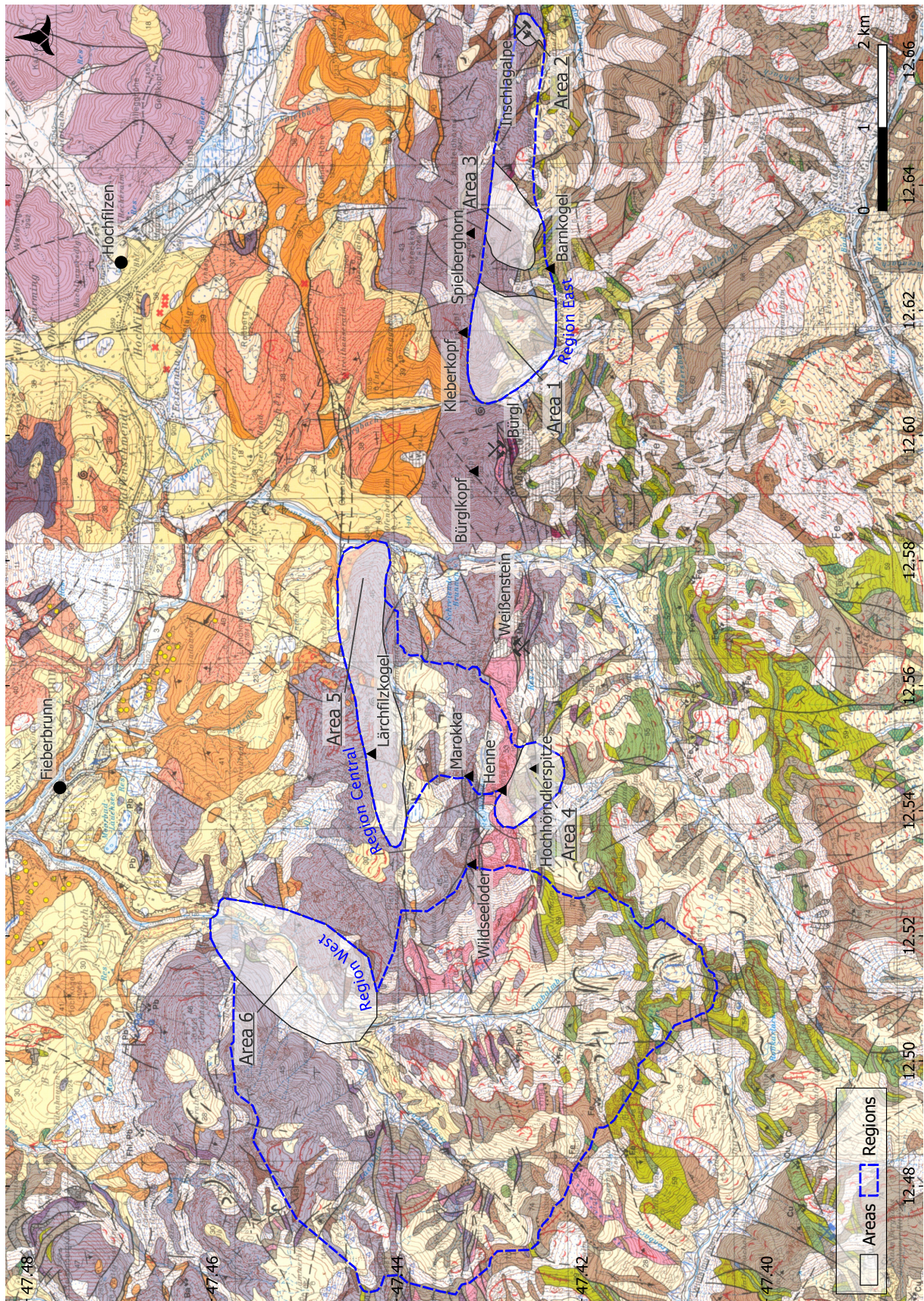


Figure 2.2: Overview of mapping areas (base map: Geological Map Austria)

2.2.1 Region 4

This is a hiking area including the Blumenweg track and some via ferrata near the ridge in the north. Of great interest here is an outcrop of black dolomite and especially its contacts with the neighbouring rock. Furthermore, this is an area where the Glemmtal complex and the Hochhörndler complex are exposed and therefore more metabasites could be found here.

2.2.2 Area 5

Along the roughly west-east oriented “ridge” at the Lärchfilzkogel down to the Hörndlingergraben. Parking is possible at the Lärchfilzhochalm and in the Hörndlingergraben.

2.3 West Region

The region is located directly at the western connection to Central Region and on map sheet 122. This region is intended for model verification of spaceborne and drone-based Earth Observation (EO). The EO shall first provide indications of possible magnesite mineralization, which will subsequently be searched for.

This region is characterized by the Pletzerbach and its tributaries, the Lengfilzenbach and Grubalm with Sulztalbach.

2.3.1 Area 6

In this area Magnesite is known as rolled pieces in the bedload of the Pletzerbach creek. Their origin in the form of outcrops is not known and should be clarified if possible. In the north of the Pletzergraben mighty Spielberg dolomites are exposed. Especially their boundaries to the south are to be localized and worked on. The area is part of the Pletzergraben and should be mapped on both sides of the Pletzenbach.

This area has the lowest priority and should be mapped depending on possibilities.

3 Geological framework

On the map sheets mentioned above, the study area is located in the Wildseeloder unit \subset Grauwackenzone \subset Upper Austroalpine. Small-scale contacts with the Glemmtal unit – also graywacke zone – and the Northern Calcareous Alps \subset Upper Austroalpine occur.

This traditional nomenclature of geological units no longer corresponds to the current state of knowledge. According to modern tectonic nomenclature, the area under investigation is part of the Staufen-Höllengebirge nappe, which is assigned to the Tyrolian-Noric nappe system (Schmid et al., 2004; Heinisch et al., 2015; Huet et al., 2019).

An overview tectonic map of the Eastern Alps is given in Figure 3.1 and Figure 3.2 shows a schematic diagram of the major tectonic units of the Eastern Alps and the incorporation of the Tyrolian-Noric nappe system into these units (Schuster et al., 2013; Schuster and Stüwe, 2022). The palaeogeographic position of the Austroalpine from Cambrian to Devonian is outlined in Figure 3.3.

The lithostratigraphic division of Paleozoic rocks within the Staufen-Höllengebirge nappe (Huet et al., 2019, 2022) was based on the explanations of GK 122 Kitzbühl (Heinisch et al., 2015). Four complexes are distinguished, which correspond to Variscan tectonic units. From the footwall to the hanging wall, these are the following lithodemic units: Uttendorf complex, Glemmtal complex, Hochhörndler complex and Wildseeloder complex. These are unconformably overlain by Permomesozoic lithostratigraphic units.

The metamorphic history of the Staufen-Höllengebirge nappe is poorly studied. In general, it is assumed that there is an increase in the degree of metamorphism from north to south (e.g. Schlaegel-Blaut, 1990; Rantitsch and Judik, 2009; Heinisch et al., 2015). In general maximum greenschist facies pressure-temperature conditions can be assumed for the study area: Approximately in the range of 350 °C–400 °C and pressures greater than 3 kbar and less than 4,5 kbar–8 kbar (Schlaegel-Blaut, 1990 and references therein). In detail, however, it seems difficult to assign the deformations and metamorphism to the Variscan or the Eoalpin event (Huet et al., 2019).

Based on data from illite crystallinity, the degree of graphitization, the presence of chloritoid and the Conodont Alteration Index (CAI), metamorphism in the (lower) greenschist facies is assumed to have occurred during the (Cretaceous) Eoalpidian event. $^{40}\text{Ar}/^{39}\text{Ar}$ ages, from white mica fine fractions, in the 115 Ma–95 Ma range indicate cooling of the rocks of the Staufen-Höllengebirge nappe and their exhumation during this event (Schuster et al., 2004; Heinisch et al., 2015 and references therein). This metamorphism was again weakly overprinted by advective heat transport and circulating fluids during the course of the Alpine orogeny, in the Oligocene to Miocene (Rantitsch and Judik, 2009). Variscan metamorphism is not documented in the study area; however, weak (lowermost greenschist facies) prealpine deformation and metamorphism is assumed (Heinisch et al., 2015). This is consistent with $^{40}\text{Ar}/^{39}\text{Ar}$ dating (Panwitz, 2006) of detrital muscovites indicating Neoproterozoic ages (in the range 600 Ma–800 Ma). The closure temperature of muscovite in the Ar/Ar system, 390 ± 50 °C (Schaen et al., 2020), has thus not been (significantly) exceeded since that time.

Note

Regarding the terms “Greywacke Zone” and “Northern Calcareous Alps”, it should be mentioned that these historical terms date from a time before today’s understanding of the tectonic nappe structure of the Alps ([Schuster, 2015](#)). One can probably understand these terms as geological units in the sense that they refer to rocks characteristic for them. However, they are not tectonic or lithostratigraphic units in the strict sense ([Huet et al., 2019](#)).

The term graywacke zone describes a geographic unit ([Schuster, 2015](#)) which represents an east-west oriented strip of Paleozoic rocks. This is several hundreds of kilometers long, extends roughly from Schwaz in Tyrol to Lower Austria at the margin of the Vienna Basin, and has a maximum width of about 25 km ([Heinisch et al., 2015](#)). Based on the spatial allocation, the Western and Eastern Grauwackenzone can be distinguished.

Thus, the term graywacke zone – and the accompanying subgroups such as northern, southern, western and eastern – should be seen as an informal term without stratigraphic and tectonic implications.

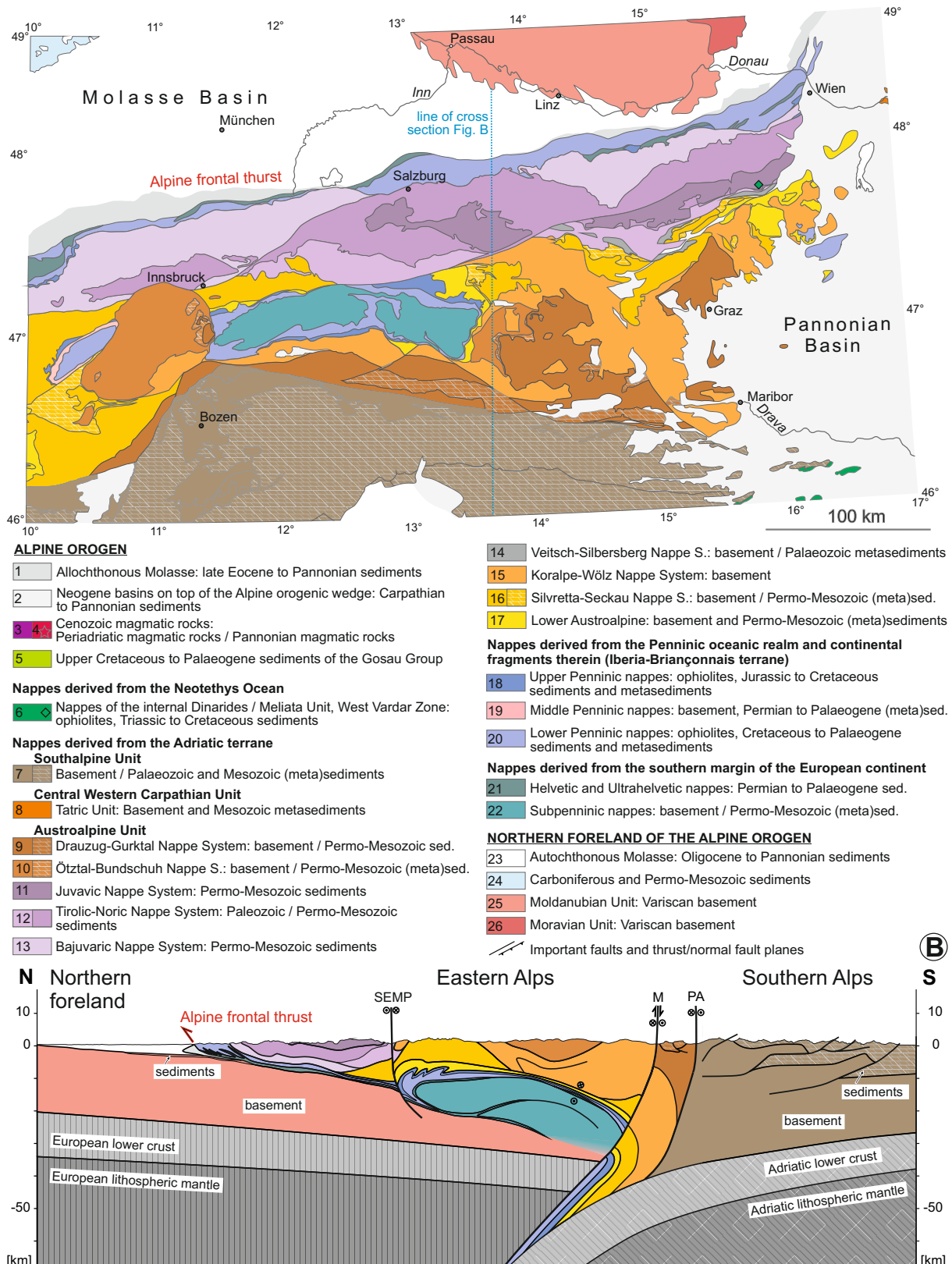


Figure 3.1: Tectonic map of the eastern Alps and the northern foreland, nomenclature after Schmid et al. (2004), Modified after Schuster et al. (2013) and Schuster and Stüwe (2022). Numbers reference to tectonic units in Figure 3.2.

SEMP: Salzach-Ennstal-Mariazell-Puchberg-, M: Mölltal-, PA: Periadriatic fault system

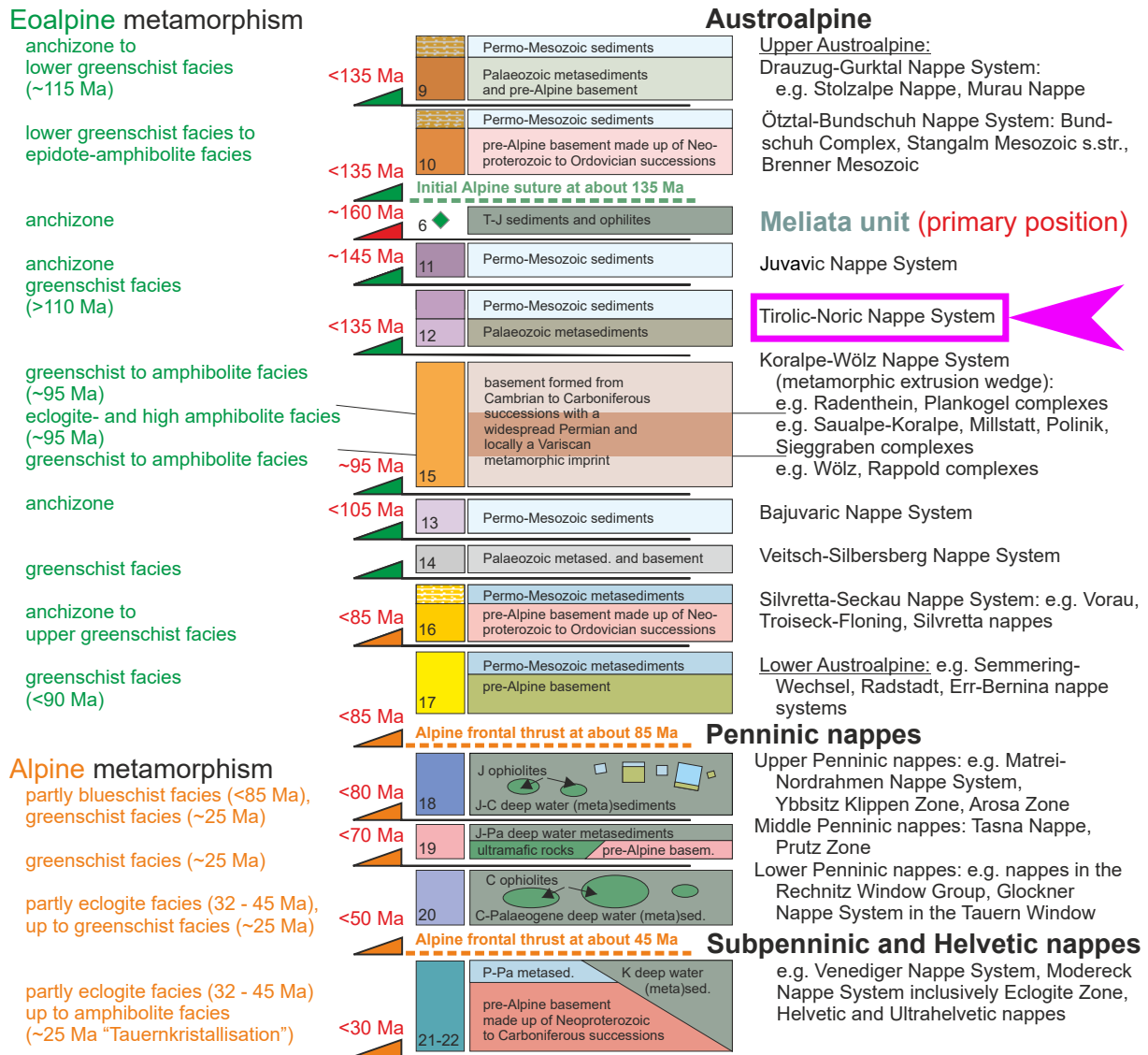


Figure 3.2: Schematic diagram of the major tectonic units of the Eastern Alps, after Schuster et al. (2013) and Schuster and Stüwe (2022). Highlighted is the Tyrolian-Noric nappe system in which the mapping area is located.

- Left: Degree of metamorphism during the Eoalpine (Cretaceous) and Alpine (Cenozoic) events and the time of peak metamorphism;
 - Middle: Major lithologic content of tectonic units, red numbers indicate time of emplacement in Alpine orogen wedge, numbers in colored boxes reference tectonic units on map in Figure 3.1.;
 - Right: tectonic and lithostratigraphic units.
- T: Triassic, J: Jurassic, C: Cretaceous, Pa: Paleogene.



Spätes
Kambrium

Spätes
Silur



Spätes
Devon

Krustenstücke Österreichs

- **Ostalpin**, Südalpin
- Moldanubikum, Subpenninikum
- △ Moravikum

Figure 3.3: Palaeogeographic position of the Austroalpine (red ellipse) from Cambrian to Devonian. Pieces of crust split off at the northern edge of Gondwana and drift north towards Laurentia or Baltica. From an initial position near the South Pole it drifts to a position near the equator with changed climatic conditions. From Schuster et al. (2015)

4 Rock types and lithological units

Lithologically particularly relevant for the investigations here is the Wildseeloder complex, which is made up of Middle Ordovician metaignimbrite (Blasseneck porphyroid), Upper Devonian siliciclastics and various Silurian to Upper Devonian carbonate rocks – including the Spielberg dolomite group (Heinisch et al., 2015; Huet et al., 2019).

Rocks of the Glemmtal complex and the Hochhörndler complex can occur primarily on the southern edges of the areas to be examined. The Glemmtal complex comprises mostly Early Paleozoic to Lower Carboniferous mudstone, siltstone, sandstone and conglomerate with a turbiditic origin with subordinate inclusions of Ordovician and Devonian metabasites and also locally occurrences of Blasseneck porphyroid and carbonate rocks (Huet et al., 2019). The Hochhörndler complex consists of a siliciclastic matrix with isolated carbonate and magmatic elements from the Wildseeloder complex and the Glemmtal complex and it probably represents a sequence with olistoliths and/or a tectonic zone (Huet et al., 2019). Hence, rock types of the neighboring complexes are present in the Hochhörndler complex as reworked components.

In the map sheets, only the Wildseeloder and Glemmtal complexes are distinguished. These represent different facies with their specific lithologies. The Hochhörndler complex is implicitly to be understood as a “transition zone” – in which the lithologies of the other two complexes are mixed.

For practical fieldwork, the rocks can be assigned to the complexes as follows:

Wildseeloder Complex Thick carbonates and metaignimbrite, almost no basites, almost no pelites

Hochhörndler Complex Isolated, small-scale bodies of basites, carbonates, porphyroids in a matrix of siliciclastics such as slates, quartzites, . . .

In the geological maps, the Hochhörndler Complex can be recognized by the fact that units of the Wildseeloder Complex lie next to units of the Glemmtal Complex without faults in between.

Glemmtal Complex Basites in carbonates and siliciclastics

Important lithologies are briefly described here and are summarized in stratigraphic divisions in Figure 4.1 and Figure 4.2.

4.1 Blasseneck porphyroid

In the study area, this porphyroid can be found, for example, at the Wildseeloder with a succession of up to 600 m thickness (Heinisch et al., 2015). It has been correlated with the Blasseneck porphyroid, named after the Styrian type locality, on the basis of lithological criteria and its stratigraphic location under the Llandovery¹ limestones (Hubmann et al., 2014).

This porphyroid is interpreted as a subaerial pumice-rich deposit, resulting from a pyroclastic density current that was washed into shallow sea basins. The volcanism is considered to be SiO₂-rich, alkaline rhyolitic to rhyolitic. Hence, the chemistry suggests an extensional regime based on the alkaline rhyolitic character. Therefore, it could have been rift-related magmatism, which led to a partial melting of the continental crust due to an increased heat flow (Heinisch,

¹Llandovery: Lower Silurian stratigraphic series: rounded 444 Ma–433 Ma; named after the town of Llandovery in Wales

1981; Heinisch et al., 2015).

More recent investigations which include U-Pb dating from zircons and studies on zircon systematics by Blatt (2013) show ages in the range of 471 Ma–461 Ma and also suggest an interpretation of continental rifting. The paleogeographical position is assumed to be the northern edge of Gondwana.

4.2 Spielberg dolomite group

This group forms the host rock of some deposits such as siderite, baryte, fahlore and - here of particular importance - magnesite.

These dolomites represent the most important summits in the study area and form a coherent mountain range from the Kitzbühlerhorn via the Wildseeloder, the Spielbergerhorn to the Inschlagalpe. The type locality of these dolomites, the Spielbergerhorn (Hubmann et al., 2014), is one of the study area boundaries (Region 2, Figure 2.1 and Figure 2.2).

This rock group is interpreted as a Silurian-Devonian carbonate platform (Blatt, 2013) - which is now dolomitized. An age classification based on macrofossil remains, albeit sparse and weakly metamorphic, of corals, crinoids, and occasional conodonts indicates a Lower to Upper Devonian age (Heinisch et al., 2015 and references there).

The typical formation of a carbonate platform with reef complexes and a lagoon can be inferred from the rock and the fossil remains. The transition to the mainland can be seen from the inputs of clayey-sandy clastics, influences of which can be found in the upper part. The different facies manifest themselves in different forms in the dolomite rock. According to Heinisch et al. (2015), a distinction can be made between:

“Massenfazies” – massive dolomite Occasional coral relics indicate that this massive dolomite represents the reef facies of the carbonate platform

“Bankfazies” – banked dolomite The transition from the “Massenfazies” to the “Bankfazies” is diffuse and thus the bank thickness varies from two meters (rarely) to decimeters (more often).

This facies or this dolomite outweighs the other dolomites of this group in terms of frequency of occurrence. Due to the thickness and extent of these rocks, an extensive (Devonian) carbonate platform is assumed.

Sedimentary structures are occasionally preserved as laminites seen as remnants of algal mats from the stillwater area of a lagoon facies. Furthermore, crinoid remains can occasionally be seen, which could represent a transition from reef debris facies to reef areas.

“Flaserdolomit-Fazies” – red “Flaserdolomit” In the facies transition to the “Bankfazies”, thinly banked colored zones occur and layers of argillaceous slate up to centimeters thick can be observed. The red color of the “Flaserdolomit” can be seen as an aeolian input of desert dust.

“Dolomit-Sandstein-Folge” Banked dolomites alternate with quartz sandstone banks and clay slates. Quartz clasts have also been found within the dolomites. Together with the “Flaserdolomit”, this sequence is interpreted as a terrigenous sedimentary input from an adjacent continent. In terms of facies, these two dolomites could represent the transition from the lagoon facies to the beach area.

Overall, the Spielberg dolomite group represents a shallow water facies close to the coast on the northern edge of Gondwana (e.g. Blatt, 2013; Heinisch et al., 2015 and references there). For sketches and more information about such a possible deposition space, see e.g. Nichols (2009), Boggs (2009), McCann and Manchego (2015) or Wikipedia.

4.2.1 Südfazies

A term that appears in the (older) literature is the so-called “Südfazies”, which goes back to Mavridis (1969). He divides the carbonate rocks, in the area between Wörgl in the west and Bischofshofen in the east (Haditsch and Mostler, 1970), into two facies for the first time: the “northern facies” and the “southern facies”. These two facies were described as both lithologically and stratigraphically distinct and separated by a somewhat west-east oriented fault. Mostler (1970) also saw a “dolomite barrier” between the northern Spielberg dolomite and the Südfazies. The term Spielberg dolomite was introduced for the northern facies and its stratigraphic range was defined as Emsian to Eifelian (upper Lower Devonian to lower Middle Devonian). The southern facies has been defined as an association of distinct dolomites (stratigraphically ranging from footwall to hanging wall): black dolomite, light gray dolomite and red “Flaserdolomit”, and light to dark gray coarse sparry dolomite. The stratigraphic range of these dolomites extends from the Younger Silurian (Ludlow) to the Upper Devonian (Mavridis, 1969).

In the classification of the current map sheets (Heinisch et al., 1995, 2003) and the explanations (Heinisch et al., 2015) the term “Südfazies” is no longer in use. Rather, parts of the “southern facies” were included in the Spielberg dolomite group and the black dolomite mentioned was assigned to the Dolomit-Kieselschiefer complex. The term “Südfazies” is also not found in the current (revised) stratigraphic table (Hubmann et al., 2014), but is mentioned there as a synonym for some lithologies.

Consequently, the term “Südfazies” should also be avoided when working on the MultiMiner project. However, what can be relevant for the work here is the distinction of the different dolomites as reef and basin sediments (SiO₂-bearing dolomites, siliceous slate layers, ...).

4.3 Slate

In association with the Spielberg dolomite, alternating layers of slate occur occasionally. In the hanging wall of the platform dolomite, a smooth transition into these very fine clastic sediments can be observed. Due to the macroflora residues contained in this slate, its age can be narrowed down to the Upper Devonian or younger (Heinisch et al., 2015).

4.4 Radiolarite

Associated with the banked and massive dolomite sequences of the Spielberg dolomite group, alternating sequences of black, banked dolomite, radiolarite (lydite), black slate and gray clay slate can occasionally occur. These occurrences can be assigned stratigraphically at the base of the carbonate platform, but also represent décollements and are found along faults or as small rock bodies (Heinisch et al., 2015). Chronostratigraphically, this alternation sequence is assumed to belong to the middle to younger Silurian – middle Wenlock to lower Ludlow – and its origin is considered to be a deep marine environment with euxinic conditions (Hubmann et al., 2014). The black dolomite mentioned above should be particularly emphasized here, as it is the (main) carrier rock of the magnesite mineralization at the Weißenstein.

4.5 Metabasites of the Glemmtal complex

The metabasites are marked in the maps as metabasalt, metatuff, metatuffite, and gabbroic and dioritic dykes. This suggests some diversity in terms of volcanic genesis. Compared to recent volcanic provinces, analogies to pillow and sheet lava stacks, different variants of basaltic pyroclastics, epiclastic rearrangements and subaquatic eruptions with different production rates

can be identified. These volcanics are variously intruded by gabbroic rocks. Here, sills and vertical dykes as well as stock-like intrusions occur (Heinisch et al., 2015).

To sum it up, these metabasites can be interpreted as a product of multiphase basic volcanism with subvolcanic intrusives. Detailed geochemical investigations by Schlaegel-Blaut (1990) were able to rule out connections between volcanism and active plate boundaries – both oceanic ridges and subduction zones. Rather, they suggest a basic intraplate volcanism, which represents volcanic high zones (seamounts, island volcanoes) in a shallow marginal sea.

In summary, these metabasites are interpreted by Heinisch et al. (2015) as mostly shallow marine seamounts. Biostratigraphically, this event can be assigned to the Lower Devonian based on conodonts. Furthermore, the Glemmtal complex is described as basin facies.

Geochronological dating of these rocks using the U/Pb and Sm/Nd methods yielded ages in the range of 492 Ma–454 Ma (Heinisch et al., 2015 and references there). This covers a broad period from the late Cambrian to the middle Upper Ordovician and is in contradiction to the conodont stratigraphic classification given above. According to Heinisch et al. (2015), this contradiction must be considered open.

Note on geological vocabulary

Regarding the subvolcanic intrusives mentioned above, it should be noted that in the literature they are partly summarized as basaltic-gabbroid material and also as diabase (schist). The former is supposed to express the transitional character of the fabric of subvolcanics. Subvolcanites are intrusive rocks formed by cooling and crystallization below the surface of the earth – but at shallower depths and usually with smaller volumes than typical plutonites. Their fine-grainedness is often not as pronounced as that of the volcanic rocks and they represent transition from the volcanic rocks to the plutonic rocks. These relatively coarse-grained basaltic rocks, often with an intergranular to ophitic texture (Vinx, 2015), are called dolerites or microgabbros (grain size over three millimeters). The term diabase, which is often used synonymously, should be avoided due to its ambiguity (Le Maitre et al., 2002).

Staufen-Höllengebirge Nappe

Wildseeloder **Group** Hochhörndler **Complex** **Hinterglemm** **Complex**

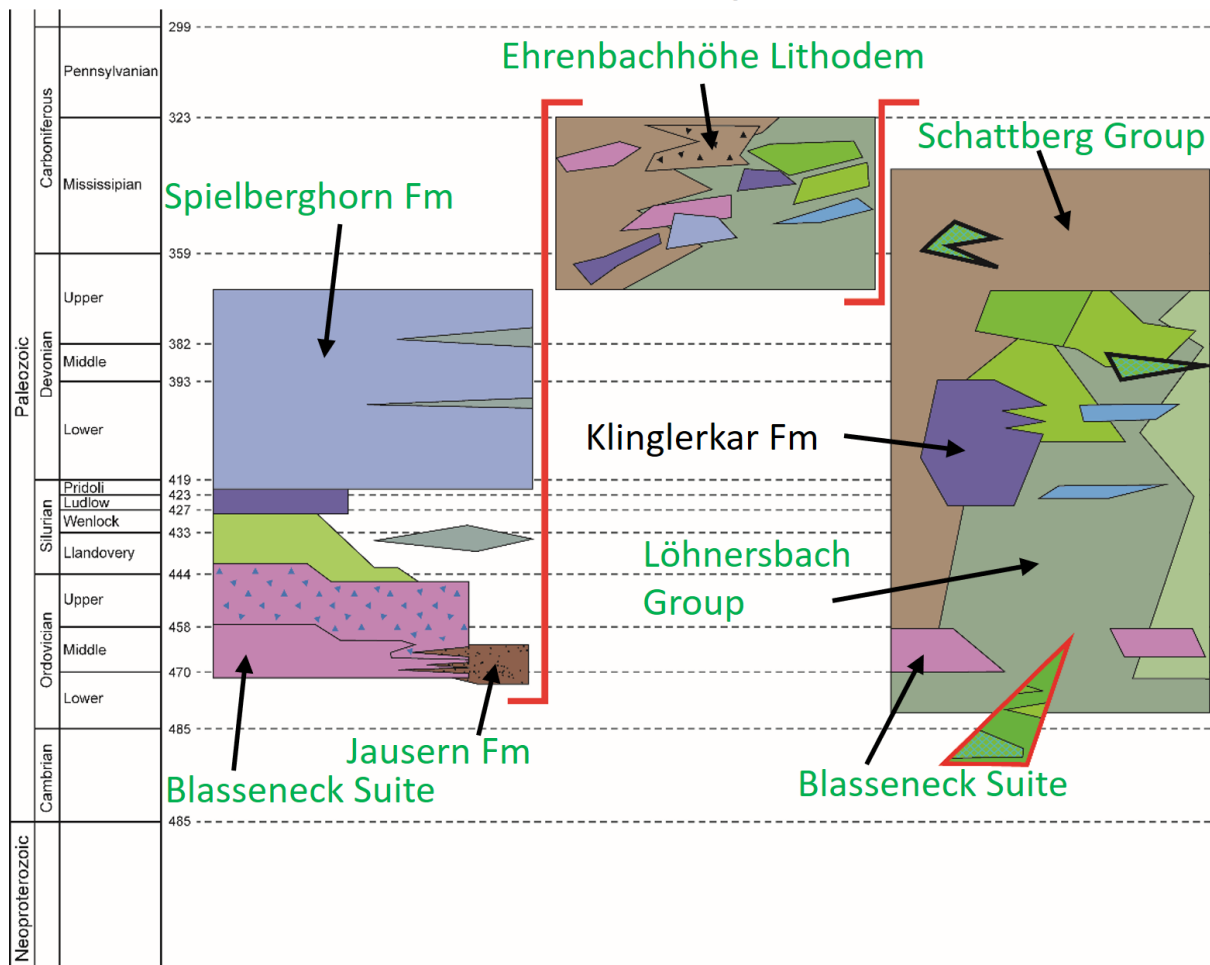


Figure 4.2: Modern lithostratigraphic model of the Staufen-Höllengebirge nappe, modified after (Huet et al., 2019, 2022); Green: proposed new denotations, for the units according to Heinisch et al. (2015) (see Figure 4.1), following a modern lithostratigraphic resp. lithodemic nomenclature (North American Commission on Stratigraphic Nomenclature, 2005). Detailed lithostratigraphy of each complex in Figure 4.3, Figure 4.4, Figure 4.5

Wildseeloder Complex

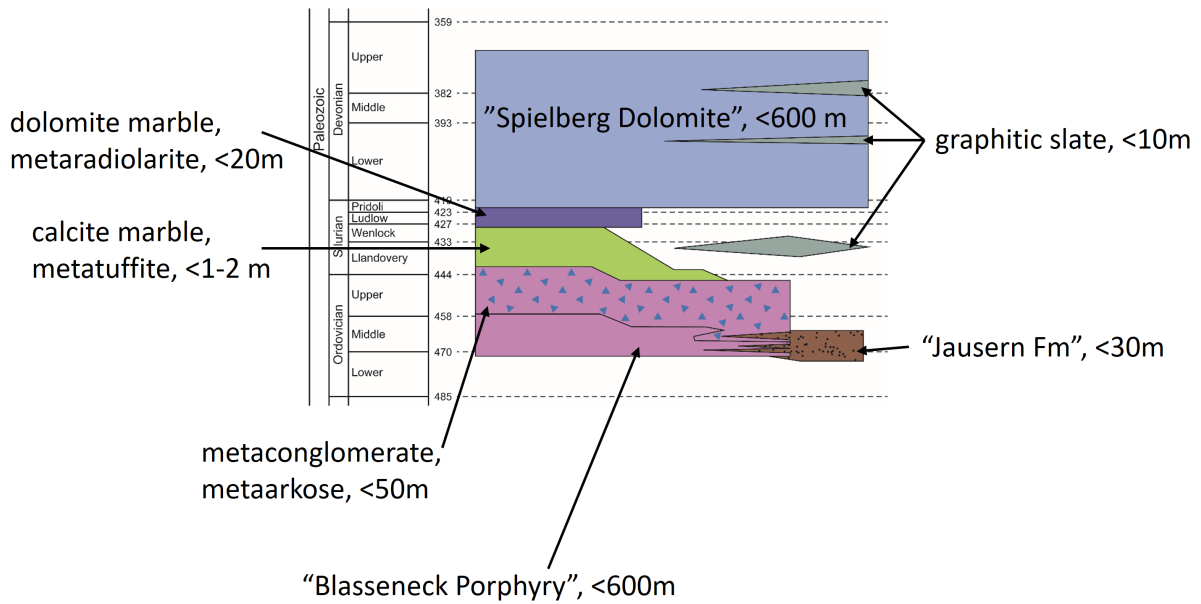


Figure 4.3: Lithostratigraphy of the Wildseeloder complex, modified after (Huet et al., 2019, 2022)

Glemmtal Complex

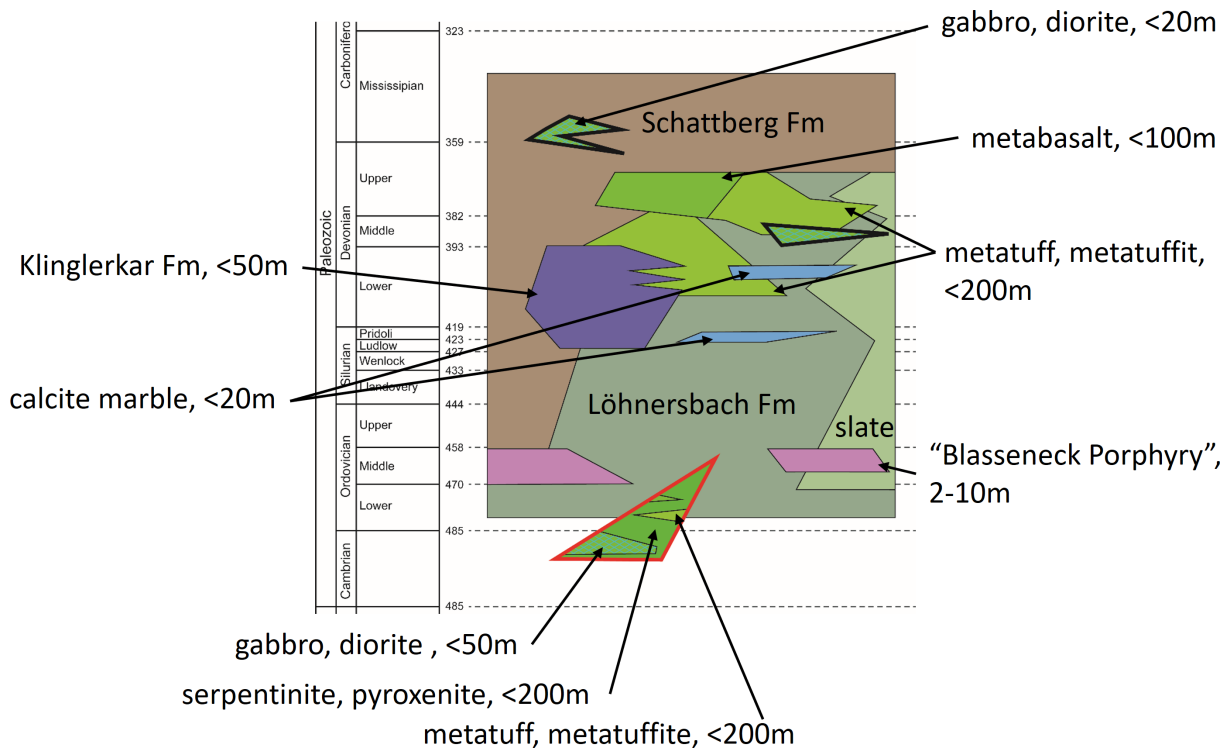


Figure 4.4: Lithostratigraphy Glemmtal complex, modified after (Huet et al., 2019, 2022)

Hochhörndler Complex

from the Wildseloder Complex

from the Glemmtal Complex

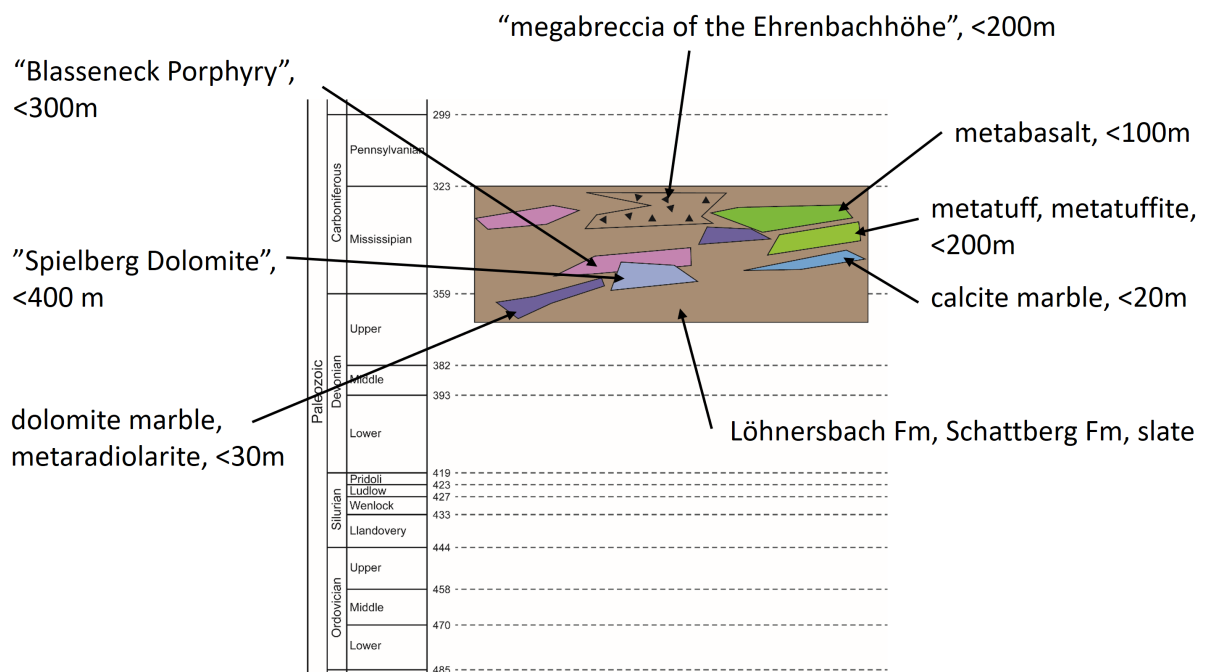


Figure 4.5: Lithostratigraphy of the Hochhörndler complex, modified after (Huet et al., 2019, 2022)

5 Magnesite deposits in the Hochfilzen area, Eastern Alps: Genetic considerations

Worldwide, most economic magnesite deposits are either of the cryptocrystalline Kraubath type or the sparry Veitsch type. Magnesite formed in sedimentary lacustrine environments only plays a subordinate role (Pohl, 2020).

Cryptocrystalline magnesite of the Kraubath type (named after an occurrence in Styria, Austria) occurs as white and very fine-grained masses (bone magnesite) in veins, stockworks and massive bodies within (meta)ultramafic rocks. It is the product of low- to moderate-temperature reactions between Mg-rich rocks and CO₂-rich aqueous fluids of hypogene or supergene origin (e.g. Pohl, 1990). Sparry magnesite of the Veitsch type (named after an abandoned mine in Styria, Austria) forms irregular to strata-bound bodies that are preferentially hosted in carbonate-dominated sequences. Deposits of this magnesite type are massive, commonly coarse-grained and often show a sparry to pinolitic texture. Marine clastic to carbonate shelf sediments are the most common precursor rocks which are transformed by Mg-rich fluids in a process known as Mg-metasomatism. Metasomatic replacement textures are widely documented in these deposits, but the timing, the nature of the fluids, the source of magnesium and the exact pressure, temperature and chemical (pTX) conditions of magnesite formation are a matter of debate since more than 150 years. Historically, two schools evolved that either propagated epigenetic (metasomatic-hydrothermal) or syngenetic (sedimentary to early diagenetic) models – for a review see Deelman (2020).

Most magnesite deposits in the Eastern Alps are of the sparry Veitsch type and occur in carbonate-dominated Paleozoic formations within the tectonic highest Austroalpine geological, i.e., the Veitsch-Silbersberg nappe system, Tirolian-Noric nappe system (geographically “Greywacke Zone”), or the Graz Paleozoic nappe complex. The magnesite deposits and their country rocks commonly record low-grade to rarely medium grade pre-Alpine and Alpine regional metamorphism.

The main deposits currently mined by RHI Magnesita in Austria are located at Breitenau (Styria), in the Hochfilzen area (Tyrol) and at Radenthein (Carinthia). Smaller active mining operations of other companies are located at Oberdorf an der Laming and Hohentauern in Styria. The total annual Austrian magnesite production in 2022 was about 844 000 t (Mayer-Jauck and Schatz, 2023).

Magnesite deposits in the Hochfilzen area are situated in the Tirolian-Noric nappe system (geographically “Northern greywacke zone”) and include several active and abandoned mines at Weißenstein, Bürgl, and Inschlagalpe. These mines stretch along a ca. 6 km long corridor that is associated to the tectonically complex Hochhörndler complex (see Section 4). The carbonate host rocks are mainly dolostones and limestones of Silurian to Early Devonian age. Previous studies distinguished a northern reef-dominated dolomitic facies (Early to Middle Devonian Spielberg Dolomite) and a southern facies (“Südfazies”) of Silurian fossiliferous limestones to Early Devonian dolostones (Mavridis and Mostler, 1971) – see also Section 4.2.1. According to Mostler (1970), the magnesite deposits are restricted to the southern facies.

It is to be noted that the magnesite deposits in the western “Greywacke Zone” formed in different lithologies and in carbonate sequences of different stratigraphic age (Mostler, 1973). Hence, they are not strictly stratiform but strata-bound, at best. The magnesite deposits have been affected by low-grade greenschist facies metamorphism as indicated by chloritoid, pyrophyllite

and paragonite in the surrounding metapelites (Morteani, 1989; Morteani and Neugebauer, 1990).

The spatial vicinity of the magnesite deposits in the western “Greywacke Zone” to tectonic nappe boundaries was pointed out in previous studies (Mostler, 1973; Morteani, 1989). Variscan thrust planes were thought to be possible fluid pathways for the Mg-rich mineralizing fluids in a metamorphic-metasomatic model. In this metamorphic-metasomatic model the replacement of dolomite by magnesite is controlled by inversion of the temperature gradient due to tectonic overthrusting and influx of Mg²⁺-rich fluids from the overthrust unit (Morteani, 1989; Morteani and Neugebauer, 1990). The rare earth element (REE) contents and patterns of magnesite compared to those of the meta-sedimentary carbonate host rocks support this interpretation (Morteani et al., 1982).

Magnesite from the Weißenstein quarry is macrocrystalline but it lacks the cm-sized sparry magnesite texture that is typical for many other deposits. Banding is rarely preserved in finer grained magnesite. It has been interpreted as relict of an older sedimentary fabric whereby indicating an initial stage of sedimentary magnesite formation prior to subsequent metamorphic recrystallization (Vavtar, 1976; Schulz and Vavtar, 1989).

Magnesite was also reported from the Permian Gröden Formation (redbed sediments), which unconformably overlie the Early Paleozoic strata hosting the sparry magnesite deposits in Hochfilzen area. These Permian magnesites occur as nodules, in discrete layers within mudstones as well as intergranular cement (Spötl and Burns, 1994). Magnesite in these redbed sediments formed diagenetically in a playa-lake system and the magnesium was derived from weathering of Devonian dolostones and associated magnesite deposits (Spötl and Burns, 1994). Magnesite was also documented in the Permian basal breccia – Brunnsink breccia – (Siegl, 1953; Angel and Trojer, 1955). This breccia contains magnesite-bearing clasts, which were interpreted as sedimentary components and provided a key argument for supporting the pre-Permian (Variscan) age of the magnesite formation in the Alps (Angel and Trojer, 1955). However, detailed textural observations indicate that magnesite formation in this breccia is in fact post-depositional (Siegl, 1964; Mostler, 1970).

It remains an interesting question if and how the processes forming the sparry magnesite deposits in the Hochfilzen area and those in the Permian formations are genetically linked.

Some progress in our understanding of the fluids involved in the formation of sparry magnesite deposits comes from crush-leach analyses (Prochaska, 2001). Na/Br vs. Cl/Br plots generated by this method reveal that sparry magnesites plot at the end of the seawater evaporation trend indicating that the saline fluids (“bittern brines”) derived from strongly evaporated seawater (Prochaska, 2016). The few conventional fluid inclusion studies done on magnesite deposits in the Eastern Alps confirm that the mineralizing fluids are saline aqueous brines belonging to the H₂O-NaCl system (Azim Zadeh et al., 2011). The temperatures obtained from microthermometry seem to reflect the metamorphic grade of the deposits (i.e., the fluid inclusions have undergone at least partial metamorphic re-equilibration).

Establishing a correct genetic model for sparry magnesite deposits in the Eastern Alps strongly depends on availability of reliable age data. So far only a very limited number of age data is available. The most precise age was determined in the Breitenau deposit where magnesite formation was dated at $229,3 \pm 2,4$ Ma with the Sm-Nd method (Henjes-Kunst et al., 2014). This Middle to Upper Triassic age invalidates models of orogenic (Variscan, Alpine) magnesite formation as repeatedly proposed in the historic metasomatic models. Instead, the formation of sparry magnesite deposits must be seen in the larger geodynamic context of lithospheric extension with enhanced crustal heat flow due to the break-up of Pangea and formation of the Neotethys.

It must be stressed that neither modern fluid inclusion studies nor age data are yet available for the Hochfilzen deposits. Both would be required to establish a sound genetic model that could be the basis of future exploration and help in interpretation of airborne data.

6 Rock descriptions

To give an impression of the main rock types in the study area, the descriptions given by Heinisch et al. (2015) were extracted and translated. Further detailed rock descriptions are given, for example, by Vavtar (1976) and Schlaegel-Blaut (1990).

6.1 Blasseneck porphyroid

Lithology numbers (53 | 49) in sheet (122 | 123)

“In the field, the light-colored, rather coarse-banded to massive protrude rocks can be mapped well. A pastel green to yellowish color is characteristic. The porphyry structure is perfectly preserved or also heavily overprinted depending on the degree of alteration and deformation. The macroscopically recognizable, mm-sized porphyroclasts are recognized in the thin section as quartz and alkali feldspar. Idiomorphic forms (high quartz), some with magmatic corrosion bays, are common. Alkaline feldspar generally shows perthite texture, with individual domains being sericitized to varying degrees. Plagioclase occurs only subordinately and is always strongly altered. The matrix is composed of a fine felt of quartz, albite, sericite and possibly chlorite. Idiomorphic zircons demonstrate the primarily magmatic character. [...]

The variable content of xenolith fragments compared to phenocrystals can be used for a first field differentiation (of the lithotypes). Almost crystal-free, dense porphyroid layers, yellow-green in appearance, can also be distinguished. These, as well as thinner layers, are usually heavily foliated and have conspicuously shiny silvery discontinuities, some of which appear as soapy separation surfaces.

In the ideal case, however, the rocks crumble in a coarse-blocky and gneiss-like manner and then form detrital material for local moraines (Wildseeloder). They can be traced to the foothills of the alps as the main drift. [...]

Especially on the Wildseeloder, volcanological details can still be recognized in the field today.”

6.2 Spielberg dolomite group

Lithology numbers (44-47 | 42-44) in sheet (122 | 123)

“These are dolomite rocks of different characteristics in their facies with a thickness of up to 600 m. This creates a typical weathered dolomite landscape, which is initially rounded off by glaciers, tends to form debris and only supports sparse vegetation. The karstification that occurs throughout leads to corresponding dry vegetation. [...]

The rocks are greyish when weathered, but mostly rust-brown in colour, and are occasionally covered with map lichen. Freshly broken, they appear pure white to pale pink, occasionally also light grey. Primary sedimentary structures are extremely rare due to diagenetic recrystallization and metamorphic overprinting.

Mineralogically, it consists predominantly of dolomite with admixtures of ankerite or iron-rich dolomites. This causes the weathering color, which is often rusty brown. Calcite rarely occurs. The grain size ranges from 0,1 mm to 1 mm. The rocks can therefore be described as dolomite marble. Gritted decay and sanding are common secondary effects within this grain size.”

Dolomit-Sandstein-Folge #44: “Well bedded dolomite alternates in layers with quartz sandstone beds and slates. Microscopic quartz clasts can also be found within the dolomite beds.”

Banked Dolomite (#45): Shows “[...] bank thicknesses from 2 m to decimeter bank thickness. The latter case is the more common. [...] In favorable cases there are relict sedimentary structures preserved in the form of laminites [...]. In other cases, fragments of crinoid calyxes and crinoid stalk segments are found [...]”.

Massive Dolomite (#46): This dolomite “[...] segregates in coarse blocky. Karst vents are common, as is striation. Irregular fracturing is common. Occasional relics of coral [...]” may occur.

Red Flaserdolomit, Flasermarmor with violet slate (#47): These “[...] stand out because of their intense play of colors (white-violet), their cm-thick banks and their mostly wavy, flaky structure. [...] The content of clayey material varies greatly, there can even be cm-thick slate interlayers. [...] Occasionally, the violet slates are also secondarily bleached, giving the rock assemblage a green-grey colour.”

Note: According to Heinisch et al. (1995), the massive dolomite can be a carrier of magnesite mineralization – e.g. deposits Bürgelkopf and Inschlagalpe – and is therefore of particular importance.

6.3 Slate combined with Spielberg dolomite

Lithology numbers (43 | 41) in sheet (122 | 123)

“Gray argillaceous slate occasionally occurs in alternating layers with Spielberg dolomite (43) (to the west of”Platte” (mountain) in the direction of Pletzergraben, Malernalm near Kitzbühel). However, they also develop in the hangingwall with a sedimentary transition from the platform dolomites. A corresponding profile can be found on the Wildseeloder, to the south of the Griessenbodenalm. Here it can be shown that these are the youngest preserved sedimentary sequences of the Wildseeloder unit below the Variscan angular unconformity.”

6.4 Dolomite-radiolarite complex

Lithology numbers (49 | 46) in sheet (122 | 123)

“Alternating sequences of dolomites, radiolarite (lydite), black shale and gray slate, which are summarized as the Dolomit-Kieselschiefer complex (49). [...] They often function [...] as décollement and can be found along faults (e.g. Lämmerbichlalm) or in rock slices (e.g. Lachtalbach, Römerweg-Barmleiten, Brunnalm, Jufenkamm). The common characteristic of the alternation is the black colour, due to the high proportion of organic carbon. Banked up to decimeters, dark, sugar-grained dolomite alternates in layers in the cm to dm range with lydites and black shales. Gray slates are also intercalated. In view of the peculiar colouration, the usually thin sequence forms a well mappable guiding horizon. Maximum thicknesses of up to 80 m are

known. However, given the tendency for internal small folding, thrust tectonics and décollement, stratigraphically undisturbed profiles are very rare. This is due to the high contrast in consistency to the often neighboring banded and massive dolomite sequences.”

6.5 Metabasalts of the Glemmtal complex

Lithology numbers (55, 57, 58, 59 | 50, 51, 52, 55) in sheet (122 | 123)

6.5.1 Metabasalt, massive or with a pillow structure

Lithology numbers (55 | 50) in sheet (122 | 123)

“Metabasalts (55) can be found in the entire Glemmtal unit, with primary structures and fabrics (pillows, bubbles, glass edges) commonly preserved. Connected metamorphic lava sequences reach a maximum thickness of 300 m. [...]

The pillows show sizes of maximum 1.5 x 1 m and minimum 0.3 x 0.1 m. A clear variation of the pillow size from the footwall to the hanging wall was not detectable in any of the sequences, however, multiple shifts between layered and pillow lavas can be observed. Due to the concave top, convex bottom and adaptation to the predefined morphology at the base of well-preserved pillows stratigraphically direction in some places can be shown. This agrees with the results from the biostratigraphically datable profiles. In other cases, the tectonic reshaping of the pillow structures made interpretation difficult. Occasionally relict glass fragments are preserved in the metabasalts. These appear dense, dark gray to black and are 1–3 cm across. The former glass is fully devitrified and transformed into a fine fringe of chlorite and ore pigment.

Two types of metabasalt can be distinguished macroscopically. Both occur as metamorphic pillow lavas and layered lavas. Dark gray to dark green, irregularly breaking rocks are partly developed as “Diabasmandelstein” (“amygdaloidal diabase”); they have numerous filled bladder shaped cavities averaging around 0.3 cm in diameter. Light grey, very hard, splintery and sharp-edged types, on the other hand, occur in the lower Saalachtal (sheet 123 Zell am See). The latter show a lower proportion of bubbles.[...]

The thin section investigations show pyroxene and plagioclase as well as pseudomorphoses after clinopyroxene, orthopyroxene, olivine and plagioclase as phenocrystals. Plagioclase, hornblende, chlorite, epidote, sericite, calcite, leucoxene, stilpnomelane, clinozoisite and quartz can be observed in the matrix. The content of phenocrysts and their grain size vary greatly, with phenocryst-rich and aphanitic textures present. The phenocrysts are a maximum of 7 mm long. They are often completely replaced by secondary minerals.”

6.5.2 Metatuff (pyroclastic volcanic rock)

Lithology numbers (59 | 55) in sheet (122 | 123)

“Vulcaniclastic rocks can occur both in association with the metabasalts and in layers in the metasediments. These are volcanic slate, which often still contain identifiable components. For example, the primarily pyroclastic nature of the components can

be demonstrated, e.g. as lapilli or scoria. In other cases the volcanic fragments are clearly epiclastic.

[...]

The lion's share of pyroclastics is found in the fine fraction (coarse ash to fine ash tuff). These occur today as dull green to blue-green appearing volcanic slates. They make up the main part of the outcrop area, for example at the end of the Glemmtal valley or along the Pass-Thurn-Straße south of Jochberg. As a rule, they show clear foliation; parts that occasionally appear more massive represent former coarse ash tuffs and are easily confused with layered lava flows. Microscopically, the mineral composition is poorly resolvable. It is a fine felt of chlorite, epidote, albite and occasionally calcite. Fine pigmentation by opaque minerals is the rule. Phenocrystal relics are almost always metamorphically altered."

6.5.3 Gabbroid dykes

Lithology numbers (57 | 51) in sheet (122 | 123)

"Metamorphic gabbroid rocks (57) occur unconformably as dykes or stock-like masses and concordantly as sills throughout the Glemmtal unit (thicknesses often in the meter range, rarely more than 10 m up to a maximum thickness of about 100 m). In the front part of Glemmtal a close association of gabbroid sills and metamorphic basaltic lavas is characteristic [...]. In the remaining areas, metamorphic basalts and metagabbros are found less frequently together. Concordant and discordant dykes or stocky gabbroic intrusive rocks were mapped within the metamorphic volcanoclastic rocks or within the siliciclastic metasediments[...] Some dykes are only dm thick, in which case they can easily be mistaken for greywacke beds.

[...] The macroscopic and microscopic appearance of the metamorphic gabbroid intrusives is very different. In outcrop, these rocks appear massive, dark green to grey. Grain size and structure vary from uniform (coarse, medium to fine-grained) to porphyry-grained with maximum 1.5 cm long pyroxene crystals. A wide range of variations in the content of pyroxene and feldspar is noticeable even in the hand sample. The microscopically determined mineral composition consists mainly of clinopyroxene, plagioclase, hornblende, epidote/clinozoisite, leucoxene and stilpnomelane. Alkali feldspar, apatite, titanite and zircon could be observed as accessories. The most common are subophitic texture (rocks with predominantly pyroxene) and intersertal texture (rocks with predominantly plagioclase, pyroxene then as gusset filling, [...])."

6.5.4 Dioritic dykes

Lithology numbers (58 | 52) in sheet (122 | 123)

"The term dioritic dykes (58) summarizes variants with a tendency towards intermediate chemistry. These metadiorites are especially significant as sills. [...]

In hand sample, the rocks appear massive, mostly fine-grained to dense. The rock color shows a medium grey. Occasionally, small feldspar-slats are identified on the fresh fractured rock surface. As a result, they are usually confused with greywacke beds. However, the leather-brown weathering color and occasional pyrite leads to a correct assignment in the field, which often had to be confirmed by thin sections.

The microscopically determined mineral composition consists mainly of plagioclase, hornblende, sericite, chlorite, pyroxene and epidote. Quartz and opaque minerals

are subordinate in appearance. Apatite and zircon can be observed on accessories. The main components of the rock are hypidiomorphic, twinned, zonal plagioclase strips (about 1 mm long). They form a bulky irregular intersertal or intergranular structure. The interstices are filled with opaque minerals, sericite and chlorite; in addition, small hypidiomorphic hornblendes and isolated pyroxenes occur. Quartz is also part of the gusset fillings. It is not clear to decide whether it is primarily igneous quartz or metamorphic recrystallisation.

Due to the proximity to gabbros, the rocks are interpreted as product of differentiation.”

6.6 Magnesite

Magnesite is not shown as a distinctive rock unit on the geological maps. Due to its major importance for this mapping project, the description of the magnesite occurring in the investigation area is taken from (Vavtar, 1976):

“Magnesite occurs in a wide variety of color variations. There are all possible transitions from [...] red-colored to orange to yellow to dark brown and gray-colored magnesite. Three more distinctive types can be distinguished:

1. Yellow to grey-yellow magnesite with pyrite, goethite and lepidocrocite.
2. Red [...] magnesite with hematite and minor pyrite.
3. Gray to black magnesite with pyrite. [...]

The magnesites differ not only in color but also in hardness. Bulky, relatively hard as well as porous, softer types coexist.

Various factors are responsible for the different appearance of the magnesite:

Colouring pigment: Sericite layers rich in hematite or the finest hematite-scales color the magnesite red. Locally, the hematite can be enriched to nodules parallel to the lamination. Pyrite-rich layers of sericite cause the magnesite to have a dark gray color. [...]

Weathering: The magnesite is colored brown by weathering of the pyrite via lepidocrocite to goethite.

Recent magnesium mobilization: Yellow magnesite can often be observed along joints, which partly extends into the bedding from such fine cracks and gives the magnesite a “cloudy” appearance. This is a more recent magnesium mobilization since the layered change in grain size that is otherwise often observed is absent and these magnesites are completely pigment-free even where they penetrate pigmented magnesite or extend parallel into layers.

Grain size change: The rhythmic change in grain size can also cause grey-yellow layering of the magnesite. [...] In the rhythmic change in grain size, however, no polar or geopetal structure in the form of vertical grain sorting can be determined.”

Note: According to the current state of knowledge, the black coloring is due to a high proportion of organic carbon.

References

- Angel, F., and Trojer, F., 1955, Zur Frage des Alters und der Genesis alpiner Spatmagnesite, *in* Radex-rundschau, Radenthein, Radex Austria A.G., v. 2, p. 374–392, https://opac.geologie.ac.at/ais312/dokumente/Radex-Rundschau_1955_374-392.pdf.
- Azim Zadeh, A.M., Bakker, R.J., and Ebner, F., 2011, P-T conditions of fluid trapping at Hohentauern/Sunk sparry magnesite deposit (Eastern Alps, Austria), *in* Bakker, R.J., Baumgartner, M., and Doppler, G. eds., 21st biennial conference - european current research on fluid inclusions: ECROFI XXI: 9 - 11 august 2011 leoben austria: abstracts, Wien, Geologische Bundesanstalt, Berichte der geologischen bundesanstalt 87, p. 28–29, https://opac.geologie.ac.at/ais312/dokumente/BR0087_028_A.pdf.
- Blatt, A., 2013, Geochronologische Datierung des Kellerjochgneises und der Porphyroide in der Nördlichen Grauwackenzone (Tirol, Österreich), *in* Mertmann, D., Degen, T., and Stöber, S. eds., Hallesches jahrbuch für geowissenschaften / beiheft, Institut für Geowissenschaften und Geographie der Martin-Luther-Universität Halle-Wittenberg, v. 29, doi:10.25673/90997.
- Boggs, S., Jr., 2009, Petrology of Sedimentary Rocks: Cambridge University Press, 607 p., <https://www.cambridge.org/9780521897167>.
- Deelman, J.C.C., 2020, Investigating magnesite from Austria: Research Report, <https://hal.science/hal-02899916>.
- Haditsch, J.G., and Mostler, H., 1970, Die Kupfer-Nickel-Kobalt-Vererzung im Bereich Leogang (Inschlagalm, Schwarzleo, Nöckelberg), *in* Archiv für lagerstättenforschung in den ostalpen, Montanistische Hochschule Leoben, Institut für Mineralogie und Gesteinskunde, v. 11, p. 161–209, https://opac.geologie.ac.at/ais312/dokumente/ALO11_161_209.pdf.
- Heinisch, H., 1981, Zum ordovizischen "Porphyroid" – Vulkanismus der Ost- und Südalpen, Stratigraphie, Petrographie, Geochemie, *in* Jahrbuch der geologischen bundesanstalt, Geologische Bundesanstalt (GBA), Wien, 1, v. 124, p. 1–109, https://opac.geologie.ac.at/ais312/dokumente/JB1241_001_A.pdf.
- Heinisch, H., Pestal, G., and Reitner, J.M., 2015, Erläuterungen zu Blatt 122 Kitzbühl, *in* Geologische Karte der Republik Österreich 1:50.000: Erläuterung, Geologische Bundesanstalt (GBA), Wien, https://opac.geologie.ac.at/ais312/dokumente/122_Kitzbuehel.pdf.
- Heinisch, H., Pestal, G., Reitner, J., and Stingl, V., 2003, Blatt 122 Kitzbühl, *in* Geologische karte der republik Österreich 1:50.000, Geologische Bundesanstalt (GBA), Wien, https://opac.geologie.ac.at/ais312/dokumente/GK0122_000_A.pdf.
- Heinisch, H., Pestal, G., Stingl, V., and Hellerschmidt-Alber, J., 1995, Blatt 123 Zell am See, *in* Geologische karte der republik Österreich 1:50.000, Geologische Bundesanstalt (GBA), Wien, https://opac.geologie.ac.at/ais312/dokumente/GK0123_000_A.pdf.
- Henjes-Kunst, F., Prochaska, W., Niedermayr, A., Sullivan, N., and Baxter, E., 2014, Sm-Nd dating of hydrothermal carbonate formation: An example from the Breitenau magnesite deposit

- (Styria, Austria): *Chemical Geology*, v. 387, p. 184–201, doi:[10.1016/j.chemgeo.2014.07.025](https://doi.org/10.1016/j.chemgeo.2014.07.025).
- Hubmann, B., Ebner, F., Ferretti, A., Kido, E., Krainer, K., Neubauer, F., Schönlaub, H.-P., and Suttner, T.J., 2014, The Paleozoic Era(them), *in* Piller, W. ed., The lithostratigraphic units of the austrian stratigraphic chart 2004 (sedimentary successions), Geologische Bundesanstalt (GBA), Wien, *Abhandlungen der geologischen bundesanstalt*, v. 66, https://opac.geologie.ac.at/ais312/dokumente/AB0066_001_A.pdf.
- Huet, B., Iglseder, C., and Schuster, R., 2022, A lithostratigraphic model for the Western Greywacke Zone and the Innsbruck Quarzphyllite Zone (Eastern Alps, Tirol, Salzburg, Austria) (G. Rantitsch & J. G. Raith, Eds.): https://opac.geologie.ac.at/ais312/dokumente/Pangeo_Austria_2022_078.pdf.
- Huet, B., Iglseder, C., and Schuster, R., 2019, Eine neue tektonische und lithostratigrafische Gliederung im Ostalpin auf der Geologischen Karte der Republik Österreich 1:50.000, Blatt 121 Neukirchen am Großvenediger:, https://opac.geologie.ac.at/ais312/dokumente/ATA-2019_221.pdf.
- Le Maitre, R.W. et al., 2002, *Igneous Rocks: A Classification and Glossary of Terms: Recommendations of the International Union of Geological Sciences Subcommission on the Systematics of Igneous Rocks* (R. W. Le Maitre, Ed.): Cambridge, Cambridge University Press, doi:[10.1017/CBO9780511535581](https://doi.org/10.1017/CBO9780511535581).
- Mavridis, A., 1969, Geologie der Umgebung des Spielberghornes (Nördliche Grauwackenzone, Tirol - Salzburg), *in* Kurzfassungen von in innsbruck fertiggestellten dissertationen (1965-1977); teil 1, Geologisch-Paläontologische Mitteilungen Innsbruck, p. 28–30, https://opac.geologie.ac.at/ais312/dokumente/GPM_06_10_028-030.pdf.
- Mavridis, A., and Mostler, H., 1971, Zur Geologie der Umgebung des Spielberghorns mit einem Beitrag über die Magnesitvererzung (Nördliche Grauwackenzone, Tirol-Salzburg), *in* Mostler, H. ed., Beiträge zur mikrofazies und stratigraphie von tirol und vorarlberg 1971, Innsbruck, Universitätsverlag Wagner, p. 523–546.
- Mayer-Jauck, H., and Schatz, M., 2023, Österreichisches Montan-Handbuch: Wien, Bundesministerium für Finanzen, v. 96, https://www.bmf.gv.at/dam/jcr:4abaabea-0c4b-4600-9415-939756f0a79a/MHB_2022_barrierefrei_V1.pdf.
- McCann, T., and Manchego, M.V., 2015, *Geologie im Gelände*: Springer Berlin Heidelberg, doi:[10.1007/978-3-8274-2383-2](https://doi.org/10.1007/978-3-8274-2383-2).
- Morteani, G., 1989, Mg-metasomatic type sparry magnesites of Entachen Alm, Hochfilzen/Bürglkopf and Spiessnägel (Austria) (P. Möller, Ed.): Berlin, Borntraeger, Monograph series on mineral deposits 28, p. 105–113.
- Morteani, G., Moeller, P., and Schley, F., 1982, The rare earth element contents and the origin of the sparry magnesite mineralizations of Tux-Lanersbach, Entachen Alm, Spiessnaegel, and Hochfilzen, Austria, and the lacustrine magnesite deposits of Aiani-Kozani, Greece, and Bela Stena, Yugoslavia: *Economic Geology*, v. 77, p. 617–631, doi:[10.2113/gsecongeo.77.3.617](https://doi.org/10.2113/gsecongeo.77.3.617).
- Morteani, G., and Neugebauer, H., 1990, Chemical and tectonic controls on the formation of sparry magnesite deposits - the deposits of the northern Greywacke Zone (Austria): *Geologische Rundschau*, v. 79, p. 337–344, doi:[10.1007/bf01830630](https://doi.org/10.1007/bf01830630).

- Mostler, H., 1973, Alter und Genese ostalpiner Spatmagnesite unter besonderer Berücksichtigung der Magnesitlagerstätten im Westabschnitt der Nördlichen Grauwackenzone (Tirol, Salzburg), *in* Festschrift werner heißel zum 65. geburtstag, Universität Innsbruck, p. 237–266, https://op.ac.geologie.ac.at/ais312/dokumente/Mostler_1973_Spatmagnesite_Grauwackenzone.pdf.
- Mostler, H., 1970, Ein Beitrag zu den Magnesitvorkommen im Westabschnitt der nördlichen Grauwackenzone (Tirol und Salzburg), *in* Archiv für lagerstättenforschung in den ostalpen, Montanistische Hochschule Leoben, Institut für Mineralogie und Gesteinskunde, v. 11, p. 113–125, https://opac.geologie.ac.at/ais312/dokumente/ALO11_113_125.pdf.
- Nichols, G., 2009, Sedimentology and stratigraphy: Chichester [u.a.], Wiley-Blackwell, 419 p.
- North American Commission on Stratigraphic Nomenclature, 2005, North American Stratigraphic Code: AAPG Bulletin, v. 89, p. 1547–1591, doi:[10.1306/07050504129](https://doi.org/10.1306/07050504129).
- Panwitz, C., 2006, Provenienzanalyse an paläozoischen Metasedimenten der Ostalpen mit Schwerpunkt in der Nördlichen Grauwackenzone [PhD thesis]: Martin-Luther-Universität Halle-Wittenberg, doi:[10.23689/FIDGEO-198](https://doi.org/10.23689/FIDGEO-198).
- Pohl, W.L., 2020, Economic Geology: Principles and Practice. Metals, Minerals, Coal and Hydrocarbons - Introduction to Formation and Sustainable Exploitation of Mineral Deposits: Stuttgart, Germany, Schweizerbart Science Publishers, 755 p., http://www.schweizerbart.de/publications/detail/isbn/9783510654413/Pohl/_Economic/_Geology/_2/_Auf1/_geb.
- Pohl, W., 1990, Genesis of magnesite deposits – models and trends: Geologische Rundschau, v. 79, p. 291–299, doi:[10.1007/bf01830626](https://doi.org/10.1007/bf01830626).
- Prochaska, W., 2016, Genetic concepts on the formation of the Austrian magnesite and siderite mineralizations in the Eastern Alps of Austria: Geologia Croatica, v. 69, p. 31–38, doi:[10.4154/gc.2016.03](https://doi.org/10.4154/gc.2016.03).
- Prochaska, W., 2001, Magnesite mineralization of the Eastern Alps and the Carpathians, *in* Piestrzyński, A. ed., Mineral deposits at the beginning of the 21st century, London, CRC Press, p. 1017–1019, doi:[10.1201/9781003077503-260](https://doi.org/10.1201/9781003077503-260).
- Rantitsch, G., and Judik, K., 2009, Alpine metamorphism in the central segment of the Western Greywacke Zone (Eastern Alps): Geologica Carpathica, v. 60, p. 319–329, doi:[10.2478/v10096-009-0023-2](https://doi.org/10.2478/v10096-009-0023-2).
- Riedler, E., 2010, Geologische Charakterisierung und 3D-Modellierung des Magnesitvorkommens Bürglkopf (Hochfilzen/Tirol; westliche Grauwackenzone) [Master's thesis]: Montanuniversität Leoben, <https://puretest.unileoben.ac.at/files/1909816/AC08216179n01vt.pdf>.
- Schaen, A.J. et al., 2020, Interpreting and reporting 40Ar/39Ar geochronologic data: GSA Bulletin, doi:[10.1130/B35560.1](https://doi.org/10.1130/B35560.1).
- Schlaegel-Blaut, P., 1990, Der basische Magmatismus der Nördlichen Grauwackenzone, Oberostalpinen Paläozoikum: Geologische Bundesanstalt (GBA), Wien, Abhandlungen der geologischen bundesanstalt, v. 43, https://opac.geologie.ac.at/ais312/dokumente/AB0043_001_A.pdf.
- Schmid, S.M., Fügenschuh, B., Kissling, E., and Schuster, R., 2004, Tectonic map and overall architecture of the Alpine orogen: Eclogae Geologicae Helvetiae, v. 97, p. 93–117,

doi:10.1007/s00015-004-1113-x.

- Schulz, O., and Vavtar, F., 1989, Genetic fabric interpretation of the magnesite deposit of Weißenstein (Hochfilzen, Tyrol) (P. Möller, Ed.): Berlin, Borntraeger, Monograph series on mineral deposits 28, p. 115–134.
- Schuster, R., 2015, Grauwackenzone und Veitsch-Silbersberg-Deckensystem:, p. 38–43, https://opac.geologie.ac.at/ais312/dokumente/ATA2015_Auflage_2_038.pdf.
- Schuster, R., Daurer, A., Krenmayr, H.G., Linner, M., Mandl, G.W., Pestal, G., and Reitner, J.M., 2015, Rocky Austria: Geologie von Österreich-kurz und bunt: Geologische Bundesanstalt (GBA), Wien.
- Schuster, R., Koller, F., Hoeck, V., Hoinkes, G., and Bousquet, R., 2004, Explanatory notes to the map: Metamorphic structure of the Alps – Metamorphic evolution of the Eastern Alps: Mitteilungen der Österreichischen Mineralogischen Gesellschaft, v. 149, p. 175–199, https://opac.geologie.ac.at/ais312/dokumente/Mitt_OEMinGes_149_175-199.pdf.
- Schuster, R., Kurz, W., Krenn, K., and Fritz, H., 2013, Introduction to the Geology of the Eastern Alps, *in* Schuster, R. ed., 11th workshop on alpine geological studies & 7th european symposium on fossil algae: Abstracts & field guides, Wien, Geologische Bundesanstalt (GBA), Berichte der geologischen bundesanstalt 99, p. 121–133, https://opac.geologie.ac.at/ais312/dokumente/BR0099_121_A.pdf.
- Schuster, R., and Stüwe, K., 2022, Geological and Tectonic Setting of Austria, *in* Embleton-Hamann, C. ed., Landscapes and landforms of Austria, Springer International Publishing, World geomorphological landscapes, p. 3–26, doi:10.1007/978-3-030-92815-5_1.
- Siegl, W., 1964, Die Magnesite der Werfener Schichten im Raume Leogang bis Hochfilzen sowie Ellmau in Tirol, *in* Radex-rundschau, Radenthein, Radex Austria A.G., v. 3, p. 178–191, https://opac.geologie.ac.at/ais312/dokumente/Radex-Rundschau_1964_178-191.pdf.
- Siegl, W., 1953, Magnesit in den Werfener Schichten bei Leogang, *in* Österreichische akademie der wissenschaften mathematisch-naturwissenschaftliche klasse anzeiger, Wien, Springer, v. 90, p. 178–180.
- Spötl, C., and Burns, S.J., 1994, Magnesite diagenesis in redbeds: a case study from the Permian of the Northern Calcareous Alps (Tyrol, Austria): Sedimentology, v. 41, p. 543–565, doi:10.1111/j.1365-3091.1994.tb02010.x.
- Tollmann, A., 1977, Geologie von Österreich: Band I: Die Zentralalpen: Deuticke, Wien.
- Vavtar, F., 1976, Gefügeanalytische Untersuchungen der Magnesitlagerstätte Bürglkopf – Weißenstein bei Hochfilzen, Tirol, *in* Verhandlungen der geologischen bundesanstalt, Wien, Geologische Bundesanstalt (GBA), Verhandlungen der geologischen bundesanstalt 2, p. 147–182, https://opac.geologie.ac.at/ais312/dokumente/VH1976_147_A.pdf.
- Vinx, R., 2015, Gesteinsbestimmung im Gelände: Springer Spektrum, doi:10.1007/978-3-642-55418-6.



INTERNATIONAL CHRONOSTRATIGRAPHIC CHART

www.stratigraphy.org

International Commission on Stratigraphy

v 2023/09



Enthem / Era	System / Period	Series / Epoch	Stage / Age	numerical age (Ma)	GSSP
Cenozoic	Quaternary	Holocene	Meghalayan M UL	Present	
			Northern UL	0.0082	
		Upper UL	0.0117		
		Chibanian M	0.129		
	Pleistocene	Calabrian		0.774	
		Gelasian		1.80	
	Pliocene	Placenzian		2.58	
		Zanclean		3.600	
	Neogene	Messinian		5.333	
				7.246	
Tortonian			11.63		
Miocene	Serravallian		13.82		
	Langhian		15.98		
	Burdigalian		20.44		
Oligocene	Aquitanian		23.03		
	Chattian		27.82		
	Rupelian		33.9		
Eocene	Priabonian		37.71		
	Bartonian		41.2		
	Lutetian		47.8		
Paleocene	Ypresian		56.0		
	Thanetian		59.2		
	Selandian		61.6		
Mesozoic	Upper	Danian		66.0	
		Maastrichtian		72.1 ± 0.2	
	Cenomanian	Campanian		83.6 ± 0.2	
		Santonian		86.3 ± 0.5	
		Coniacian		89.8 ± 0.3	
	Albian	Turonian		93.9	
		Cenomanian		100.5	
	Lower	Albian		~ 113.0	
		Aptian		~ 121.4	
		Barremian		125.77	
Berriasian	Hauterivian		~ 132.6		
	Valanginian		~ 139.8		
	Berriasian		~ 145.0		

Enthem / Era	System / Period	Series / Epoch	Stage / Age	numerical age (Ma)	GSSP
Phanerozoic	Paleozoic	Mississippian	Lower	Tournaisian	358.9 ± 0.4
			Middle	Visean	346.7 ± 0.4
		Upper	Serpukhovian	330.9 ± 0.2	
	Permian	Guadalupian	Lower	Bashkirian	323.2 ± 0.4
			Middle	Moscovian	315.2 ± 0.2
		Upper	Kasimovian	303.7 ± 0.1	
	Carboniferous	Pennsylvanian	Upper	Asselian	307.0 ± 0.1
			Lower	Gzhelian	298.9 ± 0.15
		Cisuralian	Sakmarian	290.1 ± 0.26	
	Permian	Guadalupian	Lower	Artinskian	283.5 ± 0.6
Middle			Kungurian	273.01 ± 0.14	
Upper		Wuchiapingian	266.9 ± 0.4		
Triassic	Lopingian	Lower	Changhsingian	251.902 ± 0.024	
		Upper	Induan	251.2	
	Induan	Wuchiapingian	254.14 ± 0.07		
Triassic	Upper	Lower	Capitanian	259.51 ± 0.21	
		Middle	Wardian	264.28 ± 0.16	
	Upper	Roadian	269.9 ± 0.4		
Jurassic	Upper	Lower	Capitanian	269.51 ± 0.21	
		Middle	Wardian	264.28 ± 0.16	
	Upper	Roadian	269.9 ± 0.4		
Mesozoic	Triassic	Upper	Lower	Wuchiapingian	259.51 ± 0.21
			Middle	Wardian	264.28 ± 0.16
		Upper	Roadian	269.9 ± 0.4	
	Jurassic	Upper	Lower	Wuchiapingian	259.51 ± 0.21
			Middle	Wardian	264.28 ± 0.16
		Upper	Roadian	269.9 ± 0.4	
	Cretaceous	Upper	Lower	Wuchiapingian	259.51 ± 0.21
			Middle	Wardian	264.28 ± 0.16
		Upper	Roadian	269.9 ± 0.4	

Enthem / Era	System / Period	Series / Epoch	Stage / Age	numerical age (Ma)	GSSP
Phanerozoic	Paleozoic	Furongian	Lower	Tremadocian	477.7 ± 1.4
			Middle	Dapingian	470.0 ± 1.4
		Upper	Stage 10	485.4 ± 1.9	
	Ordovician	Middle	Stage 9	Jiangshanian	~ 489.5
			Stage 8	Palbian	~ 494
		Lower	Guzhangian	~ 497	
	Silurian	Upper	Stage 7	Drumian	~ 500.5
			Stage 6	Wuliuan	~ 504.5
		Lower	Stage 5	Stage 4	~ 509
	Devonian	Upper	Stage 4	Stage 3	~ 514
Stage 3			Stage 2	~ 521	
Lower		Fortunian	~ 529		
Phanerozoic	Paleozoic	Furongian	Lower	Tremadocian	477.7 ± 1.4
			Middle	Dapingian	470.0 ± 1.4
		Upper	Stage 10	485.4 ± 1.9	
	Ordovician	Middle	Stage 9	Jiangshanian	~ 489.5
			Stage 8	Palbian	~ 494
		Lower	Guzhangian	~ 497	
	Silurian	Upper	Stage 7	Drumian	~ 500.5
			Stage 6	Wuliuan	~ 504.5
		Lower	Stage 5	Stage 4	~ 509
	Devonian	Upper	Stage 4	Stage 3	~ 514
Stage 3			Stage 2	~ 521	
Lower		Fortunian	~ 529		

Enthem / Era	System / Period	Series / Epoch	Stage / Age	numerical age (Ma)	GSSP
Phanerozoic	Paleozoic	Furongian	Lower	Tremadocian	477.7 ± 1.4
			Middle	Dapingian	470.0 ± 1.4
		Upper	Stage 10	485.4 ± 1.9	
	Ordovician	Middle	Stage 9	Jiangshanian	~ 489.5
			Stage 8	Palbian	~ 494
		Lower	Guzhangian	~ 497	
	Silurian	Upper	Stage 7	Drumian	~ 500.5
			Stage 6	Wuliuan	~ 504.5
		Lower	Stage 5	Stage 4	~ 509
	Devonian	Upper	Stage 4	Stage 3	~ 514
Stage 3			Stage 2	~ 521	
Lower		Fortunian	~ 529		

Units of all ranks are in the process of being defined by Global Boundary Stratotype Section and Points (GSSP) for their lower boundaries, including those of the Archean and Proterozoic, long defined by Global Standard Stratigraphic Ages (GSSA). Italic fonts indicate informal units and placeholders for unnamed units. Versioned charts and detailed information on ratified GSSPs are available at the website <http://www.stratigraphy.org>. The URL to this chart is found below.

Numerical ages are subject to revision and do not define units in the Phanerozoic and the Ediacaran; only GSSPs do. For boundaries in the Phanerozoic without ratified GSSPs or without constrained numerical ages, an approximate numerical age (±) is provided.

Ratified Subseries/Subepochs are abbreviated as UL (Upper/Late), M (Middle) and LE (Lower/Early). Numerical ages for all systems except Quaternary upper Paleogene, Cretaceous, Jurassic, Triassic, Permian, Cambrian and Precambrian are taken from 'A Geologic Time Scale 2012' by Gradstein et al. (2012), those for the Quaternary, upper Paleogene, Cretaceous, Jurassic, Triassic, Permian, Cambrian and Precambrian were provided by the relevant ICS subcommissions.



Colouring follows the Commission for the Geological Map of the World (www.cgmw.org)

Chart drafted by K.M. Cohen, D.A.T. Harper, P.L. Gibbard, N. Car (c) International Commission on Stratigraphy, September 2023

To cite: Cohen, K.M., Finney, S.C., Gibbard, P.L. & Fan, J.-X. (2013; updated) The ICS International Chronostratigraphic Chart. Episodes 36: 199-204.

URL: <http://www.stratigraphy.org/ICSchart/ChronostratChart2023-09.pdf>

Grant agreement	101091374
Project title	Multi-Source and Multi-Scale Earth Observation and Novel Machine Learning for Mineral Exploration and Mine Site Monitoring
Project acronym	MultiMiner
Project coordinator	Dr. Maarit Middleton, GTK
Project start date	Jan 1, 2023
Project duration	42 months
Related work packages	WP 4 – Site Demonstrations
Related task(s)	Task 4.1 In situ data standardization and databases
Lead organization	GeoSphere Austria
Contributing partners	GTK, BGR, VTT, RHI, MUL, EFTAS, HSGME, CGS
Submission date	June 30, 2024
File name	Appendix 3 A field guide to the Kallyntiri Sb-deposit, NE Greece (D4_1_MultiMiner_Field_Guidebook_V1_4.docx)
Organisation responsible for deliverable	GeoSphere Austria
Author name(s)	Constantinos Mavrogonatos, Marianthi Anastasatou, Konstantinos Laskaridis
Date	June 30, 2024
Version	1.0
Status	Complete
Dissemination Level	Public





**Hellenic Survey of Geology and
Mineral Exploration
(HSGME)**



**Multi-Source and Multi-Scale Earth
Observation and Novel Machine
Learning for Mineral Exploration and
Mine Site Monitoring**

A Field Guide to the Kallyntiri Sb deposit, NE Greece

In the frame of the
MultiMiner Project 2nd Progress Meeting



by

***Dr. Constantinos Mavrogonatos, Dr. Marianthi Anastasatou,
Dr. Konstantinos Laskaridis***

April 2024



The MultiMiner project is funded by the European Union's Horizon Europe research and innovations actions program, under Grant Agreement No. 101091374.

Table of Contents

1.	Introduction	2
1.1.	Antimony as a Critical Raw Material	2
1.2.	Antimony – general information	3
1.3.	The Kallyntiri site	4
2.	Geological information	8
2.1.	Geology of Greece – The Rhodope Unit	8
2.2.	Geology of the Kallyntiri site	11
3.	Mineralization and Alteration	13
4.	References.....	18
	ANNEX I: CRM Hard rock deposits of Europe	23



Fig. 2. World map with the locations of selected antimony deposits, mines, and major occurrences (from Seal et al., 2017).

1.2. Antimony – general information

Antimony is a chemical element with atomic number 51 and symbol Sb. It is a brittle, grey-silver metalloid and is usually found in nature in the form of antimonite or stibnite (Sb_2S_3), a sulfide mineral. The usual interpretation of the term antimony is that it comes from the Greek words “anti” (opposed) and “monos” (solitude), which mean “against being alone” (Gibbson, 1998). Antimony is classified as a chalcophile element, has a strong affinity with sulfur, and most usually combines with other metals, such as copper, lead, and silver, commonly leading to sulfosalts (Miller, 1973).

Antimony resources are scattered around the world, as shown in Figure 2. More than 200 antimony minerals exist; however, apart from stibnite, other antimony minerals are relatively less common, such as the wide variety of sulfosalts (e.g., tetrahedrite, pyrargyrite, samsonite, boulangerite, jamesonite, berthierite, zinkenite, etc.). Moreover, antimony occurs in antimony sulfide minerals (i.e., other than stibnite, e.g., chalcostibite), rare antimonides (e.g., aurostibite), and as a trace element in sulfides (Boyle and Jonasson, 1984). Antimony has a low concentration in the continental thrust (0.2 – 0.4

ppm; Taylor and McLennan, 1995; Rudnick and Gao, 2014), however, it is associated with many types of mineral deposits and, therefore, is considered an important pathfinder element in geochemical prospecting surveys (Boyle and Jonasson, 1984; Seal et al., 2017).

The commodity of antimony is related to deposits with hydrothermal activity and is produced either as the primary product or as a by-product (Seal et al., 2017). Simple quartz-stibnite vein and replacement deposits can form in various types of hydrothermal systems, including intrusion-related gold deposits, outer parts of orogenic gold deposits, polymetallic vein deposits, copper and molybdenum porphyry deposits, sediment-hosted Carlin-type gold deposits and with no evident association with other mineral deposits (Hofstra et al., 2013; Seal et al., 2017).

According to Seal et al. (2017), there is limited information on antimony mining wastes, either historical or modern, and limited information on their acid-generating capability. Various studies of mine-drainage data from abandoned antimony mine wastes support the acid – acid-neutralization potential due to the frequent presence of carbonate minerals (e.g. Seal et al., 2017). However, various researchers support that some abandoned antimony mine sites can generate acid drainage, although the immediate downstream areas had almost neutral pH (Ritchie et al., 2013).

Today, antimony has a great variety of uses and applications. Some of the uses of antimony are in lead-acid storage batteries for backup power and transportation (containing 4-6% antimony alloyed with lead), in flame-retardant materials as an additive in adhesives, paints, papers, plastics, and sealants (mainly in the form of antimony trioxide - Sb_2O_3), in heat stabilizers and plastics, in infrared sensors and generally various applications in the field of microelectronics and pharmaceutical products, such as antiprotozoal drugs (e.g. Gibbson, 1998; Seal et al., 2017; Daigle and DeCarlo, 2021). Moreover, antimony has various military applications as it is a hardening agent in metals used in ball bearings, bullets, cable sheaths, chemical pumps, foils, plumbing fixtures and pipes, roofing sheets, and tank linings (e.g. Sean et al., 2017).

1.3. The Kallyntiri site

The Kallyntiri site has been declared as a Public Mining area (Fig. 3) through the ministerial decision 3304/11-3-88 (Gov. gazette

150/B/1988). It occupies 66.750 km² and is located to the northeast of Komotini (Municipality of Arriana, Regional Unit of Rhodopi, Prefecture of East Macedonia and Thrace).

Table 1: Coordinates (Greek Grid '87) of the Kallyntiri Public Mining Area. Point A marks the upper left corner of the polygon in Figure 3, with the rest of the points following a clockwise direction.

Point	X	Y
A	630991	4565066
B	639739	4565163
C	636228	4556954
D	625561	4557924
E	629963	4560799
F	631046	4561767

In the broad area of the Metallopigi stream, which is located at the southern edge of the Kallyntiri Public Mining Area, Sb-mineralization and exploitation have been documented since at least the previous century. No accurate information is available about when the extraction of Sb-rich ore took place, however, residents of the Kallyntiri village report that exploitation took place during World War II, but some of them claim that very small-scale workings might have taken place even earlier (e.g., at the beginning of the 20th century). A small number of galleries occur alongside the Metallopigi stream (mostly in the western part, Fig. 4), however, in the broad region quite a few areas with mining wastes have been identified.

Since the 1980s, the Kallyntiri Public Mining Area has been a subject of research by the Greek Geological Survey -at that time, the I.G.M.E.-Institute of Geology and Mineral Exploration. The research focused on mapping and the mineralogical characterization mainly of the Sb-mineralization, and to a lesser extent other mineralization types, e.g., chromitite bodies associated with ophiolitic rocks and Au mineralization related to listvenites (e.g., Dimou et al., 1985; Favas, 1992; Eliadis and Papadolopoulos 1998; Michael et al., 2013).

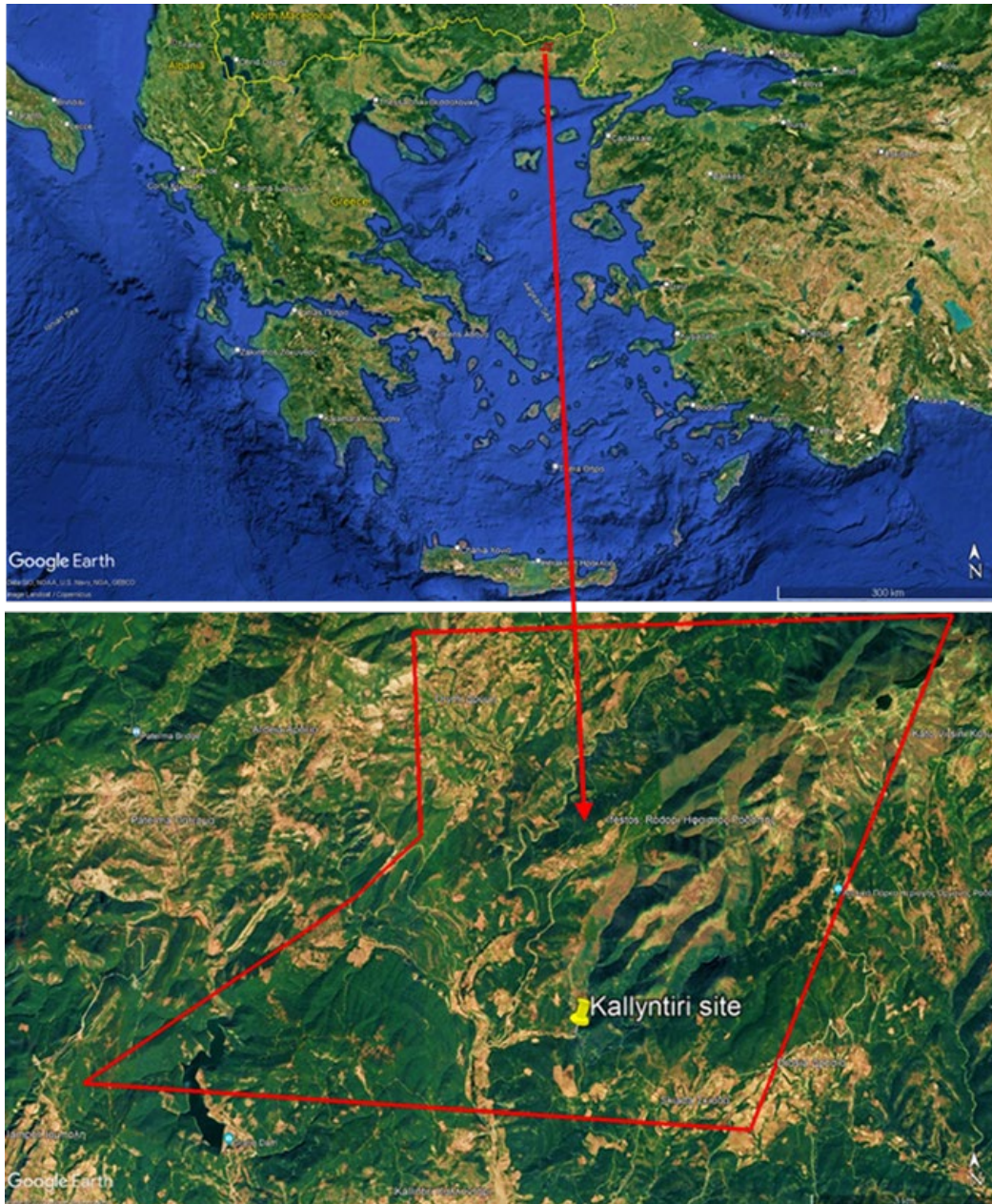


Fig. 3. The Kallyntiri Public Mining Area (marked with red polygon) and its location in the map of Greece (source: Google Earth).

Finally, over the last decade, a few academic researchers worked in the Kallyntiri area, producing new data and proposed a possible characterization for the Kallyntiri Sb-mineralization (Kanellopoulos et al., 2014; Melfos and Voudouris 2017; Voudouris et al., 2019).

However, to date, the Kallyntiri Sb-mineralization lacks a legitimate classification, due to the scarcity of available information and especially the lack of a systematic tectonic study and radiochronological data regarding the ore deposition.



Fig. 4. Field photographs from old galleries for extraction of stibnite (sbn) ore, located in the Kallyntiri area (Mavrogonatos et al., 2024).

In the frame of the EU-funded MultiMiner project, the Kallyntiri area is currently under re-evaluation regarding its metallogenetic potential. The collaborating partners are focusing on applying modern exploration techniques (e.g., acquisition of UAV-hyperspectral data, etc.) and cross-validating the results with ground-based information.

2. Geological information

2.1. Geology of Greece – The Rhodope Unit

Greece geologically belongs to the so-called Alpine Tethyan system and comprises the continuation of the Alpine orogenic chain, which, through various mountain ranges, including the Dinarides, the Hellenides, the Taurides, the Iranides, and the Afganides, reaches the mountainous complex of the Himalayas (Papanikolaou, 2021).

The Hellenic orogen or the “Hellenides” as it is mostly known, formed because of the (ongoing) collision between the African and Eurasian plates since the Late Jurassic, above the north-dipping Hellenic subduction zone. This procedure resulted in a SW-verging nappe-stacking (Fig. 5) of continental blocks, namely Adria, Pelagonia, and Rhodope, and the intervening Neotethyan oceanic crust, nowadays recognized as the Vardar- and Pindos Oceans (e.g., Jolivet and Brun, 2010; Ring et al., 2010; Jolivet et al., 2013).

The Hellenides are characterized by two major phases of deformation. The first one culminated during the middle Cretaceous times and is related to a compressional stage with south-verging thrusting and eclogite to amphibolite facies metamorphism. The second was initiated during the lower Eocene, lasts up to date, and comprises to a syn-, and post-orogenic extensional regime established in a back-arc setting (Jolivet et al. 2013).

An important characteristic of the Aegean region is the progressive migration of its magmatic activity towards the south: Magmatism occurred in the Rhodope region during Cretaceous-early Tertiary and gradually moved southwards through the northern Aegean islands (early Miocene) to the Attic-Cycladic region (late Miocene) and finally to its present position along the active South Aegean Volcanic Arc (since Pliocene times, Fig. 5). This migration is triggered by a slab roll-back mechanism occurring since the Cretaceous (45 Ma, Jolivet and Brun, 2010; Brun et al., 2016), which caused the collapse of the accretionary wedge that favored post-orogenic exhumation of deep-seated crustal lithologies and the opening of back-arc basins. Such large, crustal-scale structures are widely known as metamorphic core complexes (MCC) with prominent examples being the Rhodope and the Attic-Cycladic MCC. Such environments are commonly associated with voluminous magmatism with a pronounced post-collisional geochemical character (e.g., Menant et al., 2016, and references therein).

In the Rhodope region, four major metamorphic core complexes have been discriminated, namely the Southern Rhodope Core Complex/Domain, the Arda Metamorphic Dome, the Kesebir-Kardamos Dome, and the Biala Reka- Kechros Dome (Bonev et al. 2006; Wüthrich 2009).

The North Rhodope domain consists of (a) a lower high-grade unit of basement rocks, i.e., the Arda, Biala Reka-Kechros, and Kesebir-Kardamos domes/metamorphic core complexes; (b) an intermediate unit comprising high-grade basement rocks; and (c) an upper unit consisting of low-grade metamorphic sequences of the Circum-Rhodope belt and ophiolitic rocks (Bonev et al., 2015).

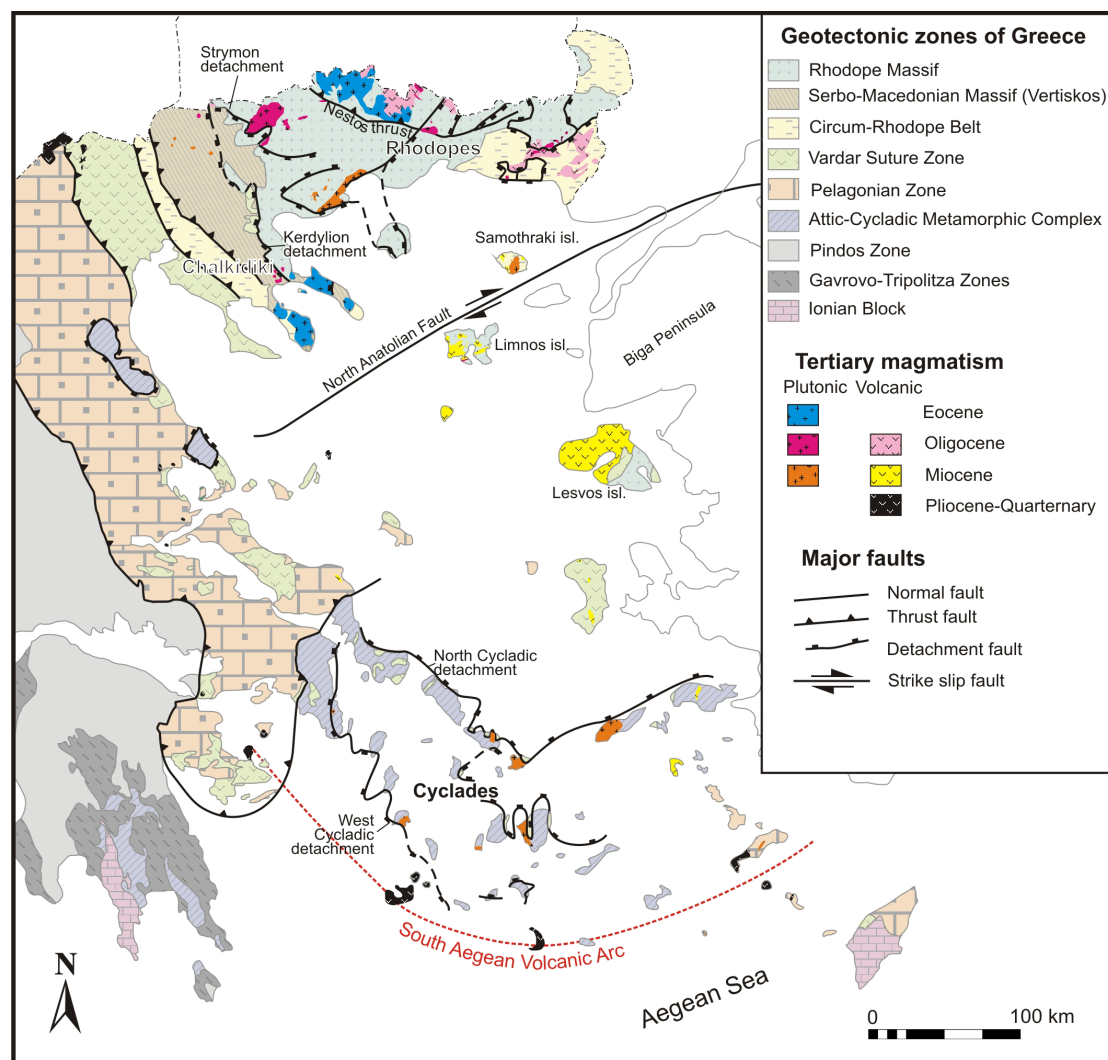


Fig. 5. Simplified geological map of Greece showing the main tectonic zones and the distribution of Cenozoic igneous rocks (from Voudouris et al., 2019).

The Southern Rhodope Core Complex comprises Paleozoic orthogneisses, Triassic marbles with intercalations of amphibolites and metapelites and minor migmatites. Finally, the Chalkidiki block represents a thrust system composed of NW-trending units, comprising various lithologies including ophiolitic rocks.

Lithologies of the Rhodope were exhumed by unroofing due to the activation of crustal-scale detachment-fault systems (Jolivet et al. 2013), during a late Cretaceous to Tertiary, syn- to post-orogenic collapse. The deep-seated metamorphic successions were uplifted along major detachment faults, resulting in the formation of metamorphic core complexes (MCC) and the opening of several E–W-trending, structurally controlled basins (Marchev et al., 2005; Jolivet et al., 2010). Syn-extensional sedimentation from Eocene to Miocene times, resulted in the formation of thick sequences of transgressive conglomerates, limestones, and sandstones (Kilias et al., 2013). At the same time, asthenospheric upwelling due to crustal thinning produced voluminous late Eocene to Miocene magmatism in the Rhodope and the Serbomacedonian domains (Ersoy and Palmer, 2013).

These magmatic rocks are mostly plutonic with minor volcanic equivalents and exhibit calc-alkaline to shoshonitic, and ultra-K affinities, imprinting the input of asthenospheric material. The latter is due to mantle upwelling, caused by a large-scale extension, and thermal disturbance of the crust and the underlying mantle (Pe- Piper and Piper 2002; Ersoy and Palmer, 2013; Menant et al., 2016). In NE Greece, magmatic activity culminated in two periods, ~34-26 Ma and from ~ 22 to 19 Ma (Gilg and Frei, 1994; Moritz et al., 2010; Kaiser-Rohrmeier et al. 2013; Siron et al., 2016), which roughly coincide with the two stages of post-orogenic, back-arc extension and metamorphic core complex formation (e.g., Brun and Faccenna, 2008; Jolivet et al., 2013).

Large-scale hydrothermal alteration associated with the above-mentioned magmatic activity has given rise to an important number of deposits and prospects, throughout the Rhodope and the Serbomacedonian domains. These areas, which have been recognized as a favorable exploration province for precious metals since ancient times (Voudouris et al., 2019), display a wide variety of ore types including polymetallic replacement, intrusion-related, porphyry, epithermal, and skarn-type ore deposits as well as stratiform volcano-sedimentary and fracture-controlled vein deposits,

some of which display a pronounced polymetallic character (e.g., Melfos and Voudouris, 2017; Voudouris et al., 2019). This unusual metal endowment of the deposits in the NE part of Greece, along with the magmatic/hydrothermal deposits of the Attic-Cycladic region account for Greece being one of the most significant metallogenic provinces in Europe (e.g., Marchev et al. 2005; Márton et al. 2010; Moritz et al. 2010, 2014; Melfos and Voudouris, 2017; Voudouris et al. 2019).

2.2. Geology of the Kallyntiri site

The Kallyntiri Sb deposit lies on the southwestern edge of the Biala Reka-Kechros metamorphic dome (Fig. 5, 6).

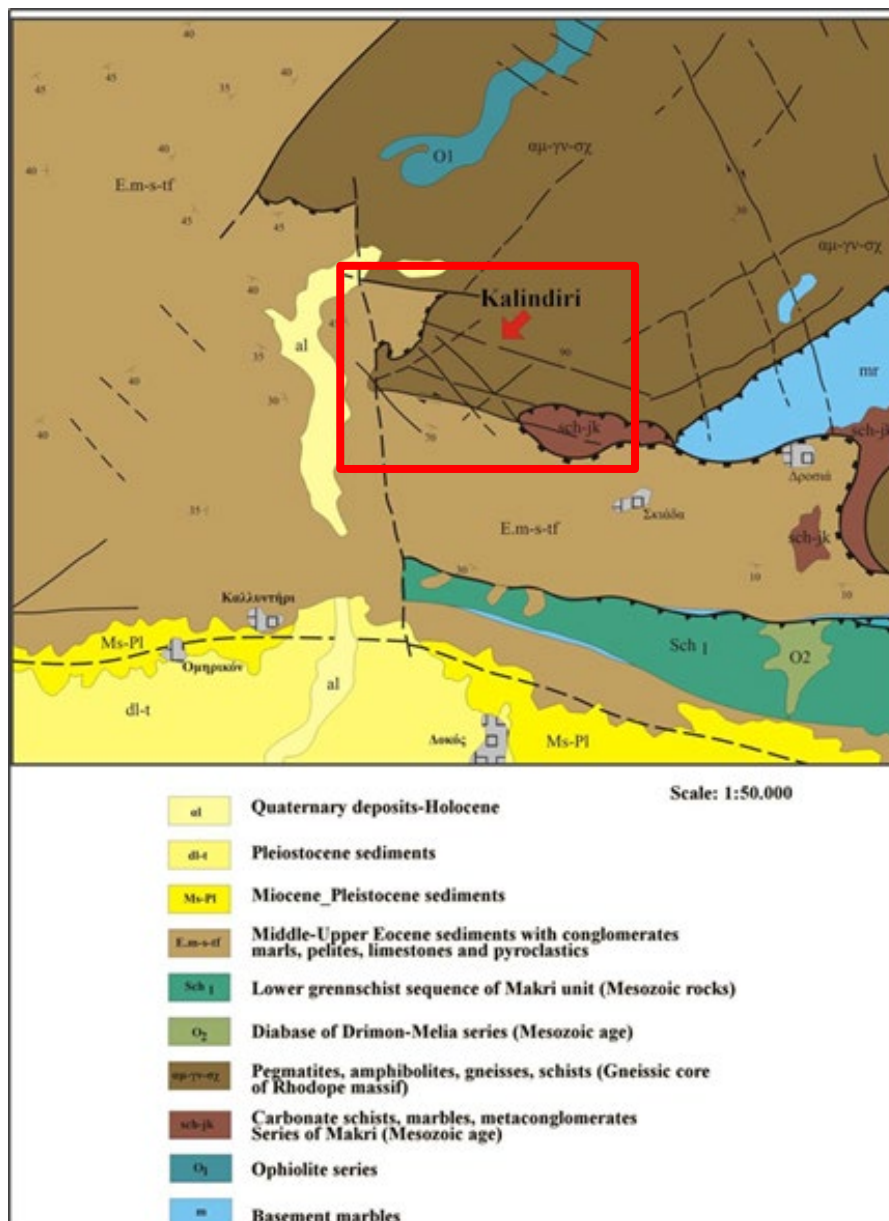


Fig. 6. Geological map of the Kallyntiri area (Michael et al., 2002; 2013).

In the northern and northeastern parts of the area, lithologies of the Rhope unit predominate. Orthogneisses are the most common lithotype and are intensely mylonitized. They exhibit a characteristic porphyroblastic texture and consist of K-feldspar, quartz, albite, biotite, white mica (mostly phengite), garnet, etc. At places, the gneisses enclose relatively large (e.g., hundreds of meters to km-scale) amphibolitic bodies which are interpreted as former eclogites. They comprise relict garnet and omphacite along with hornblende, tremolite, rare blue amphibole, kyanite, epidote/clinozoisite, albite, and minor quartz and opaque minerals. This unit is separated through a detachment fault system from the underlying Circum Rhodope Unit, known by a local name as "Makri Unit".

Locally, lithologies of the Circum-Rhodope Belt (Makri Unit) crop out. They consist of alternations of low-grade, mica- and calc-schists (i.e., metaclastic rocks) and marbles. The metaclastic rocks (metaflysch sequence) comprise fine alternations of calcitic and bituminous schists, quartzites, metaconglomerates, and olistholiths of metacarbonate rocks. The marbles are impure with colorful tints (whitish to greyish to yellowish/orange) and are mostly fine-grained, aligned in thin to medium-bedded sequences. At places, intercalations of metaclastic rocks occur.

Towards the south and western part of the area (Fig. 6), the volcanosedimentary sequence is widespread. The sequence transgressively (or tectonically at places) overlies the metamorphic lithologies. At its lower part, which is considered of Priabonian age, the sequence consists of alternating marls, sandstones and polymictic conglomerates, containing rubbles and boulders of Lutetian nummulitic limestones. At places, intercalations of clay and lignite horizons have also been found. Towards the upper part of the sequence, tuffs are intercalated with marls and sandstones, locally intruded by (sub)volcanic bodies of intermediate composition (e.g., two-pyroxene andesite). It must be noted though, that in the near vicinity of the Kallyntiri Sb deposit, no magmatic rocks have been identified.

3. Mineralization and Alteration

The Kallyntiri comprises a structurally controlled, Sb-rich deposit. The mineralization (Figs. 7 and 8) is characterized by a polymetallic assemblage that includes sulfides, sulfosalts, tellurides and native elements (Kanellopoulos et al., 2014, Voudouris et al., 2019). The main structural feature of the broader area is a low-angle detachment fault system, formed under a ductile-to-brittle regime, that is aligned to the regional ENE-WSW structural trend (Kanellopoulos et al., 2014). This detachment fault system marks the contact between the high-grade Rhodopian lithologies (in the footwall) and the low-grade Makri Unit (in the Hanging wall).

In the narrow area where the Sb-mineralization occurs (i.e., along the Metallopi stream), a detachment surface is observed (Fig. 7a), cutting through a sequence of alternating and thin-bedded marbles and metaclastic horizons, which exhibit significant mylonitization.

This sequence hosts the vast amount of the mineralization in the area. However, it must be noted that quartz-carbonate veins cutting through amphibolites and gneisses of the Rhodope Unit and hosting base metal mineralization have also been remarked (Fig. 7e, f and Fig. 8 e, f).

The marbles and calcschists of Makri Unit hosting the Sb-mineralization are strongly mylonitized and exhibit display varying alteration styles (commonly silicification which locally leads to the formation of networks of quartz veinlets/boxwork texture, carbonates, sericite, chlorite, kaolinite). At places, high-angle, commonly NW-, and E-trending faults and veins, possibly rooting to the detachment surface, host an important part of the mineralization (Fig. 7 b, c).

These faults and veins are up to 3 m wide and tens of meters long (Kanellopoulos et al., 2014) and consist of quartz and baryte and host a polymetallic assemblage dominated by stibnite (Fig. 9 a-e) which is at places replaced by its oxidation products (e.g., valentinite, stibiconite), leading to the formation of yellowish crusts. They are associated with silicification, sericitization, and Fe-oxides staining of the adjacent rocks (mostly the marble/calc-schist of the Makri unit, but also the volcano-sedimentary sequence at some places). Some of these veins exhibit banded/colloform textures (Fig. 8c).



Fig. 7. Field photographs of structural and mineralization features from the Kallyntiri area. (a) mineralized detachment-fault surface cutting through the upper parts of the Makri unit; (b,c) high-angle normal faults/veins, hosting stibnite (sbn) mineralization associated with quartz-carbonate-sericite alteration of the host Makri schists; (d) breccia mineralization cemented by base metal bearing quartz; (e, f) quartz-carbonate and base metal-bearing veins cutting through sericite-carbonate-altered lithologies (amphibolites) of the Rhodope Unit (Mavrogonatos et al., 2024).

Beyond the faults and veins, mineralization also forms disseminations, especially within the altered Makri Unit rocks, adjacent (mostly above) to the detachment surface, as well as breccias cemented by quartz and/or baryte (Fig. 8d).

The paragenetic sequence of the mineralization (Dimou et al., 1985; Kanellopoulos et al., 2014; Mavrogonatos et al., 2024) records the deposition of early pyrite, low-Fe sphalerite, galena, bournonite, chalcopyrite, and fahlore group minerals, in turn, followed by stibnite, Pb-Sb sulfosalts (e.g., semseyite, zinkenite, fülöppite, heteromorphite, senandorite, plagionite, etc.), and finally by realgar, native arsenic and native antimony.

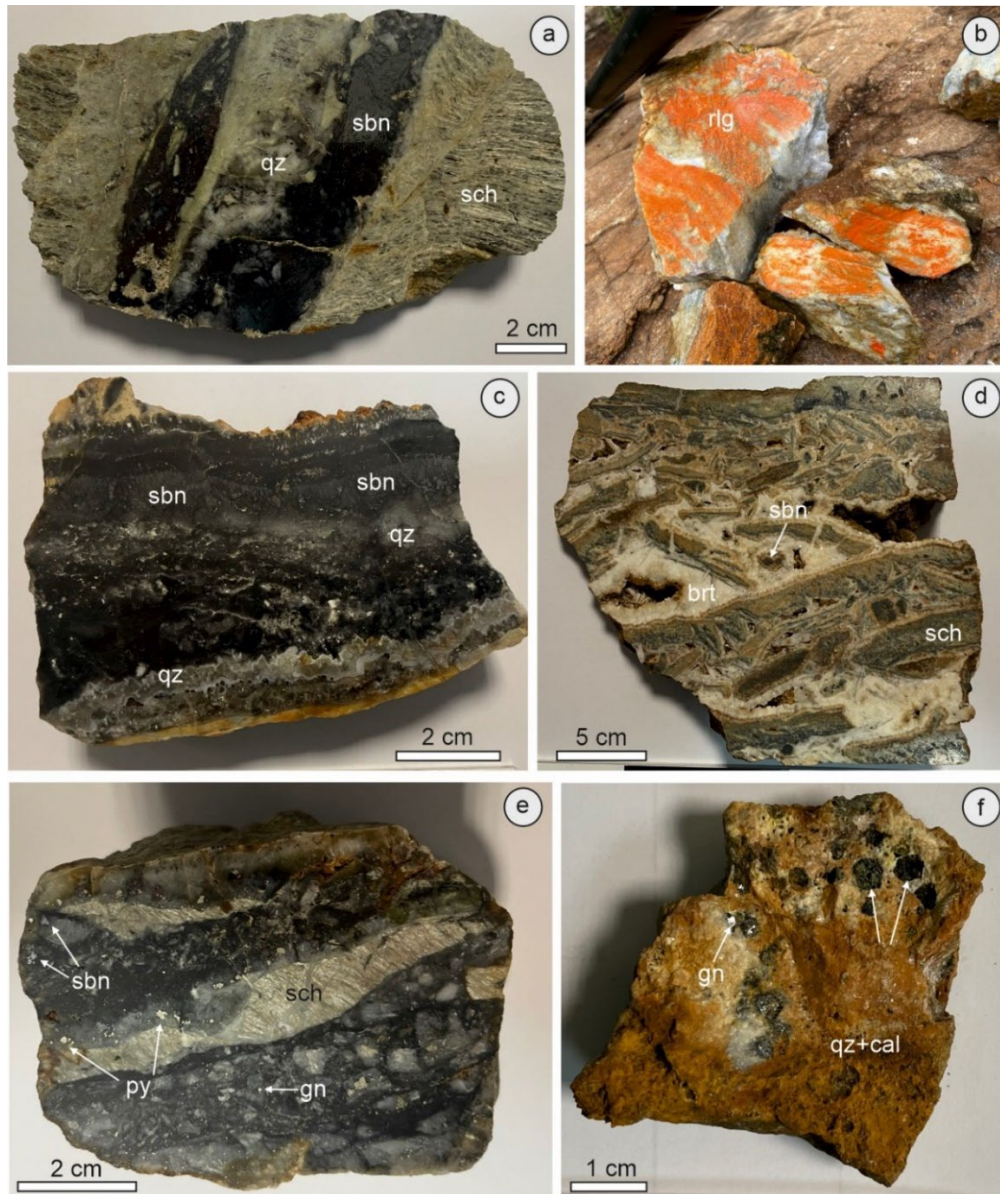


Fig. 8. Hand-specimen photographs of different mineralization styles from the Kallyntiri area. (a,c) quartz (qz) veins hosting stibnite (sbn) mineralization in sericite-altered schist (sch); (b) realgar (rlg) within fractures of Makri unit marble; (d) breccia-style stibnite (sbn) mineralization cemented by baryte (brt). The fragments comprise Makri schists; (e, f) stibnite (sbn) and galena-sphalerite (gn-sp) mineralization hosted within quartz-calcite veins, crosscutting sericite-altered schists (sch); (Mavrogonatos et al., 2024).

Stibnite often exhibits annealing textures/deformation twinning, a fact that implies deposition (partly?) contemporaneous to the tectonic activity (Dimou et al., 1985; Kanellopoulos et al., 2014). Realgar seems to have formed at the final stage, as it occurs exclusively in fractures within marbles or is associated with quartz in the veins.

Recently Kanellopoulos et al., (2014) reported the presence of native gold (electrum) and gold-silver tellurides occurring as inclusions in pyrite or in association with bornite, chalcopyrite, pyrrhotite, galena, and Fe-poor sphalerite.

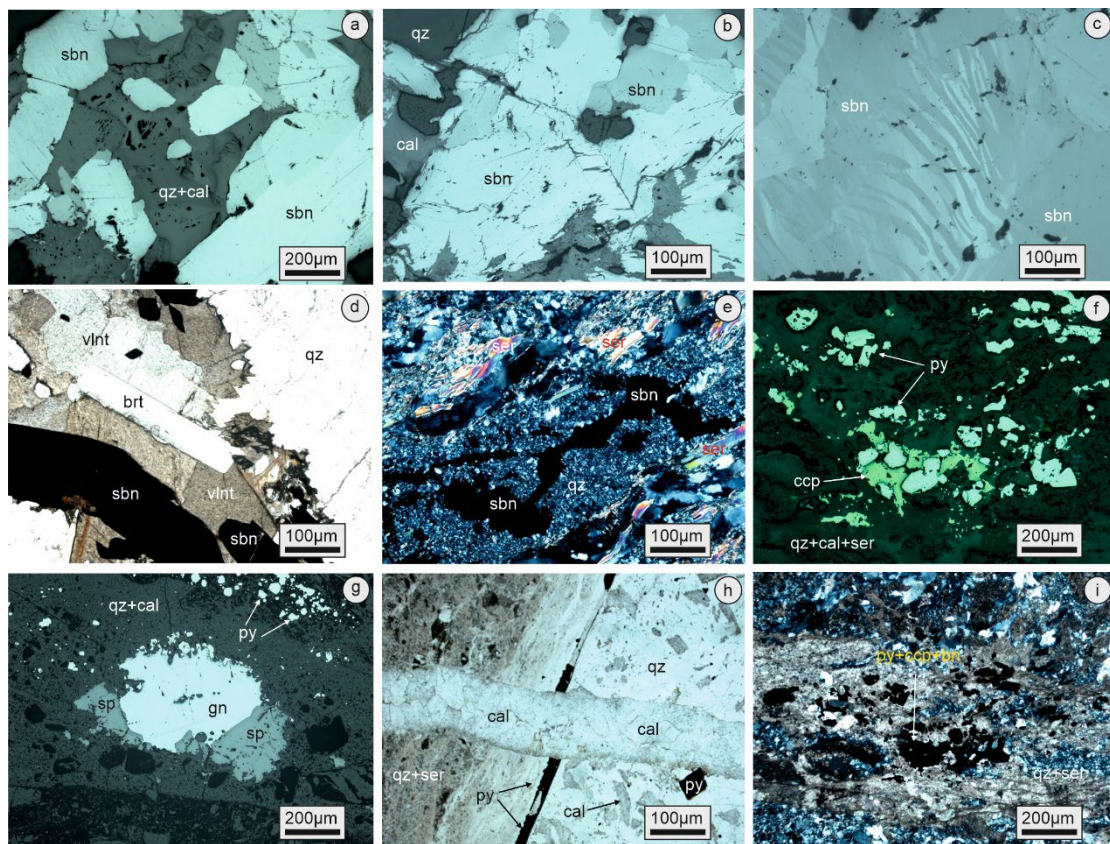


Fig. 9. Reflected (a-c and e-g) and transmitted (d-e and h-i) light photomicrographs of ore and alteration minerals from the Kallyntiri area: (a to c) euhedral to subhedral stibnite (sbn) crystals in a quartz (qz) and calcite (cal) matrix. Note the twinning in (b) and the bent, multiple twins in (d); quartz (qz) vein containing stibnite (sbn) valentinite (vlnt) and baryte (brt); (e) stibnite (sbn) in sericite-altered (ser) calc-schist; (f, g) pyrite (py), chalcopyrite (ccp), galena (gn) and sphalerite associated with quartz (qz)-carbonates (cal)-sericite (ser) alteration of the host rock; (h) late calcite (cal) vein crosscutting a quartz (qz)-pyrite (py) veinlet; (i) pyrite in association with chalcopyrite (ccp) and bornite (bn) in a quartz vein crosscutting sericite-altered schist (Mavrogonatos et al., 2024).

Geochemical analyses (Kanellopoulos et al., 2014) yielded elevated values for elements like Sb (>0.2 wt.%). Zn (>10.000 g/t), Pb (up to 2940 g/t) Ag (>100 g/t), and minor concentrations of elements like Hg (up to 16 ppm), Te (up to 6 g/t), Tl (up to 5 ppm)

Overall, The Kallyntiri Sb-mineralization remains to date poorly understood, owing both to its complex genetic features and the scarcity of available geological data (e.g., the absence of isotopic or geochronological data). However, it has been recently characterized as an epithermal s.l. type deposit (Kanellopoulos et al., 2014; Melfos and Voudouris, 2017; Voudouris et al., 2019), owing mostly to some similarities (e.g., both are hosted -at least in part- within a shear-zone/detachment fault, etc.) it shares with the low-sulfidation, detachment-related Ada Tepe deposit in Bulgaria (Marchev et al., 2004; Márton et al., 2010).

Fluid inclusion data (Michael et al. 2013) suggest that ore deposition took place under temperatures ranging from 190°C to 330°C and salinities from 0.2 to 7 wt.% NaCl equiv., from aqueous-carbonic fluids. In addition, a magmatic contribution is traced based on isotopic data ($\delta^{34}\text{S}=1.5$) from the Sb-mineralization (Michael et al., 2013). The presence of tellurides has also been interpreted as a possible magmatic contribution to the depositional system (Kanellopoulos et al., 2014). However, it must be pointed out that, to date, no magmatic rocks have been recognized to crop out in the close vicinity of the Sb-mineralization.

Further research is necessary to fully characterize the Kallyntiri deposit, which occurs in a favorable area for future discoveries regarding the presence of precious and critical metals, especially since it has never been a subject of research using modern exploration techniques.

4. References

- Bonev, N., Burg, J.P., Ivanov, Z., 2006a. Mesozoic- Tertiary structural evolution of an extensional gneiss dome - the Kesebir-Kardamos dome, E. Rhodopes, Bulgaria. *International Journal of Earth Sciences* 95, 318-340.
- Bonev, N., Marchev, P., Moritz, R., Collings, D., 2015. Jurassic subduction zone tectonics of the Rhodope Massif in the Thrace region (NE Greece) as revealed by new U–Pb and $^{40}\text{Ar}/^{39}\text{Ar}$ geochronology of the Evros ophiolite and high-grade basement rocks. *Gondwana Research* 27, 760–775.
- Boyle R.W., Jonasson I.R., 1984. The geochemistry of antimony and its use as an indicator element in geochemical prospecting: *Journal of Geochemical Exploration*, v. 20, no. 3, p. 223–302. [Also available at [http://dx.doi.org/10.1016/0375-6742\(84\)90071-2](http://dx.doi.org/10.1016/0375-6742(84)90071-2).]
- Brun, J.-P., Faccenna, C., 2008. Exhumation of high-pressure rocks driven by slab roll-back. *Earth Planetary Science Letters* 272, 1-7.
- Brun J.P., Faccenna C., Gueydan F., Sokoutis D., Philippon M., et al., 2016. The two-stage Aegean extension, from localized to distributed, a result of slab rollback acceleration. *Canadian Journal of Earth Sciences*, 53, 11, <https://doi.org/10.1139/cjes-2015-0203>.
- Canadian Ministry of Natural Resources, 2022. The Canadian Critical Minerals Strategy. ISBN 978-0-660-46339-1.
- Daigle B. and DeCarlo S., 2021. Antimony: A Critical Material You’ve Probably Never Heard Of, U. S. International Trade Commission.
- Deady E., Goodenough K.M., Currie D., Lacinska A., Grant H., Patton M., Cooper M., Josso P., Shaw R.A., Everett P., Bide T., 2023. Potential for Critical Raw Material Prospectivity in the UK British Geological Survey CR/23/024 57pp.
- Dimou E., Papastaurou S., Serment R., 1985. Study of Sb-rich ore deposits in Greece. Institute of Geology and Mineral Exploration (IGME unpubl. Report, in Greek).
- Ersoy, E.Y., Palmer, M.R., 2013. Eocene-Quaternary magmatic activity in the Aegean: implications for mantle metasomatism and magma genesis in an evolving orogeny. *Lithos* 180-181, 5-24.
- Eliadis A., Papadopoulos P., 1998. New occurrences of antimony, and discoveries of chromititic bodies NE of Komotini. (IGME internal report, in Greek).
- European Commission, Directorate-General for Internal Market, Industry, Entrepreneurship and SMEs, Grohol, M., Veeh, C., Study on the critical raw materials for the EU 2023 – Final report,

- Publications Office of the European Union, 2023, <https://data.europa.eu/doi/10.2873/725585>
- Favas N., 1992. Research for primary gold in the silicified rocks of the Kallyntiri-Skiada area, Prefecture of Rhodopi. (HSGME internal report, in Greek).
- Gibson R.I., 1998, Type-cast—Antimony, the metallic sidekick, sets the world on fire and puts it out: *Geotimes*, February, p. 58. [Also available at <http://www.gravmag.com/antimony.shtml>.] (*Geotimes* magazine became *Earth* magazine on September 1, 2008.)
- Gilg, H.A. Frei, R., 1994. Chronology of magmatism and mineralization in the Kassandra mining area, Greece: The potentials and limitations of dating hydrothermal illites. *Geochimica et Cosmochimica Acta*, 58(9), 2107-2122
- Hofstra A.H., Marsh E.E., Todorov T.I., Emsbo, P., 2013, Fluid inclusion evidence for a genetic link between simple antimony veins and giant silver veins in the Coeur d'Alene mining district, ID and MT, USA: *Geofluids* 13, 4, p. 475–493. <http://dx.doi.org/10.1111/gfl.12036>.
- Hughes A., Britt A., Pheeney J., Morfiadakis A., Kucka C., Colclough H., Munns C., Senior A., Cross A., Summerfield D., Hitchman A., Cheng Y., Walsh J., Thorne J., Sexton M., 2024. Australia's Identified Mineral Resources 2023. *Geoscience Australia*, Canberra. <https://dx.doi.org/10.26186/149056>
- India, Ministry of Mines, 2023. Report of the Committee on Identification of Critical Minerals
- Jolivet, L., Brun, J.-P., 2010. Cenozoic geodynamic evolution of the Aegean region. *International Journal Earth Science* 99, 109-138.
- Jolivet, L., Lecomte, E., Huet, B., Denèle, Y., Lacombe, O., Labrousse, L., Le Pourhiet, L., Mehl, C., 2010. The North Cycladic detachment system. *Earth and Planetary Science Letters* 289, 87-104.
- Jolivet, L., Faccenna, C., Huet, B., Labrousse, L., et al., 2013. Aegean tectonics: Strain localization, slab tearing and trench retreat. *Tectonophysics* 597, 1–33.
- Kanellopoulos C., Voudouris P., Moritz R., 2014. Detachment-related Sb-As-Au-Ag-Te mineralization in Kallintiri area, Northeastern Greece: Mineralogical and geochemical constraints: *Buletini i Shkencave Gjeologjike Special Issue 1, Proceedings 20th CBGA Congress, Tirana, Albania*, p. 162-165.
- Kaiser-Rohrmeier, M., von Quadt, A., Driesner, T., Heinrich, C.A., Handler, R., Ovtcharova, M., Ivanov, Z., Petrov, P., Sarov, S., Peytcheva, I., 2013. Post-orogenic extension and hydrothermal ore

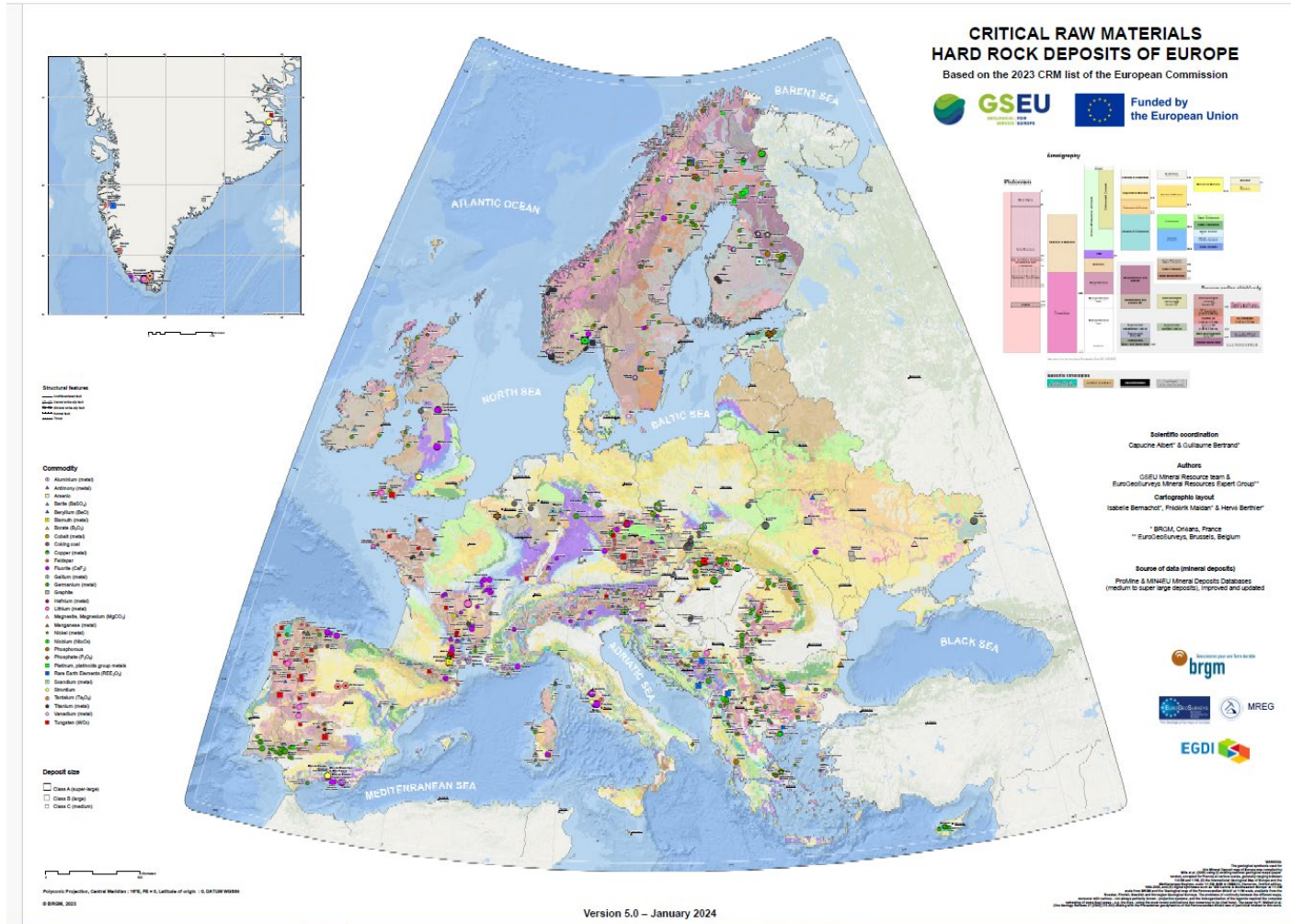
- formation: high precision geochronology of the Central Rhodopian metamorphic core complex (Bulgaria-Greece). *Economic Geology* 108, 691–718.
- Kilias A., Falalakis G., Sfeikos A., Papadimitriou E., Vamvaka A., Gkarlaouni C., 2013. The Thrace basin in the Rhodope province of NE Greece - a Tertiary supra-detachment basin and its geodynamic implications. *Tectonophysics* 595-596, 90-105.
- Laznicka P., 2010. Giant metallic deposits—Future sources of industrial metals: Berlin, Germany, Springer-Verlag, 834 p.
- Lee K., Cha J., 2021. Towards Improved Circular Economy and Resource Security in South Korea. *Sustainability* 2021, 13, 17. <https://dx.doi.org/10.3390/su13010017>
- Marchev P., Kaiser-Rohrmeier B., Heinrich C., Ovtcharova M., von Quadt A., Raicheva R., 2005. Hydrothermal ore deposits related to post-orogenic extensional magmatism and core complex formation: The Rhodope Massif of Bulgaria and Greece. *Ore Geology Reviews* 27, 53-89.
- Marchev P., Singer B., Jelev D., Hasson H., Moritz R., Bonev N., 2004. The Ada Tepe deposit: a sediment-hosted, detachment fault-controlled, low-sulfidation gold deposit in the Eastern Rhodopes, SE Bulgaria. *Schweizerische Mineralogische und Petrographische Mitteilungen* 84, 59-78.
- Márton I., Moritz R., Spikings R., 2010. Application of low-temperature thermochronology to hydrothermal ore deposits: Formation, preservation and exhumation of epithermal gold systems from the Eastern Rhodopes, Bulgaria. *Tectonophysics* 483/3–4, 240-254.
- Mavrogonatos C., Anastasatou M., Laskaridis K., 2024. Preliminary results from exploration activities at the Kallyntiri area, NE Greece, in the frame of the MultiMiner Project. Unpubl. Internal Report, HSGME.
- Melfos V., Voudouris P., 2022. Ore deposits of Greece Kallipos Open Academic Editions, <http://dx.doi.org/10.57713/kallipos-32>.
- Melfos V., Voudouris P., 2017. Cenozoic metallogeny of Greece and potential for precious, critical and rare metals exploration, *Ore Geology Reviews* 89, 1030-1057
- Menant A., Jolivet L., Vrielynck B., 2016. Kinematic reconstruction and magmatic evolution illuminating crystal and mantle dynamics of the eastern Mediterranean region since the late Cretaceous. *Tectonophysics* 675, 103-140.

- Michael C., Arvanitidis, N.D., Iliadis, A., Papavasiliou, K., Christidis, C., 2013. Orogenic mineralizations – A new exploration target for gold-polymetallic ore deposits in Greece. *Proceed. 6th Conf. Sustain. Devel. Min. Industry, Milos Island, Greece*, pp. 139-145.
- Michael C., 2002. Evaluation of primary gold deposits in Eastern Rhodope zone. Internal report, IGME (in Greek).
- Miller M.H., 1973. Antimony, in Brobst, D.A., and Pratt, W.P., eds., *United States mineral resources: U.S. Geological Survey Professional Paper 820*, p. 45–50, accessed October 6, 2015, at <http://pubs.er.usgs.gov/publication/pp820>.
- Moritz R., Márton I., Ortelli M., Marchev P., Voudouris P., Bonev N., Spikings R., Cosca M., 2010. A review of age constraints of epithermal precious and base metal deposits of the tertiary Eastern Rhodopes: coincidence with late Eocene-early Oligocene tectonic plate reorganization along the Tethys. *Proceedings of the XIX CBGA Congress, Thessaloniki*, vol. 1, pp. 351-358.
- Moritz R., Noverraz C., Márton I., Marchev P., Spikings R., Fontignie D., Spangenberg J.E., Vennemann T., Kolev K., Hasson S., 2014. Sedimentary-rock-hosted epithermal systems of the Tertiary Eastern Rhodopes, Bulgaria: new constraints from the Stremtsi gold prospect. *Geological Society, London, Special Publications 402*, <http://dx.doi.org/10.1144/SP402.7>.
- Papanikolaou D.I., 2021. *The Geology of Greece. Regional Geology Reviews*. doi:10.1007/978-3-030-60731-9, Springer Nature Switzerland.
- Pe-Piper, G., Piper, D.J. W, 2002. The igneous rocks of Greece. The anatomy of an orogen, *Beiträge der regionalen Geologie der Erde 30*. Berlin-Stuttgart. 573 p.
- Ritchie V.J., Ilgen A.G., Mueller S.H., Trainor T.P., Goldfarb R.J., 2013. Mobility and chemical fate of antimony and arsenic in historic mining environments of the Kantishna Hills district, Denali National Park and Preserve, Alaska: *Chemical Geology*, v. 335, January, p. 172–188., <http://dx.doi.org/10.1016/j.chemgeo.2012.10.016>.]
- Rudnick R.L., Gao S., 2014. *Composition of the Continental Crust, Treatise on Geochemistry, 2nd ed.*; Elsevier Ltd.: Amsterdam, The Netherlands.
- Seal R.R., Schulz K.J., DeYoung, J.H., Jr., with contributions from David M. Sutphin, Lawrence J. Drew, James F. Carlin, Jr., and Byron R. Berger, 2017. Antimony, chap. C of Schulz, K.J., DeYoung, J.H., Jr., Seal, R.R., II, and Bradley, D.C., eds., *Critical mineral resources of*

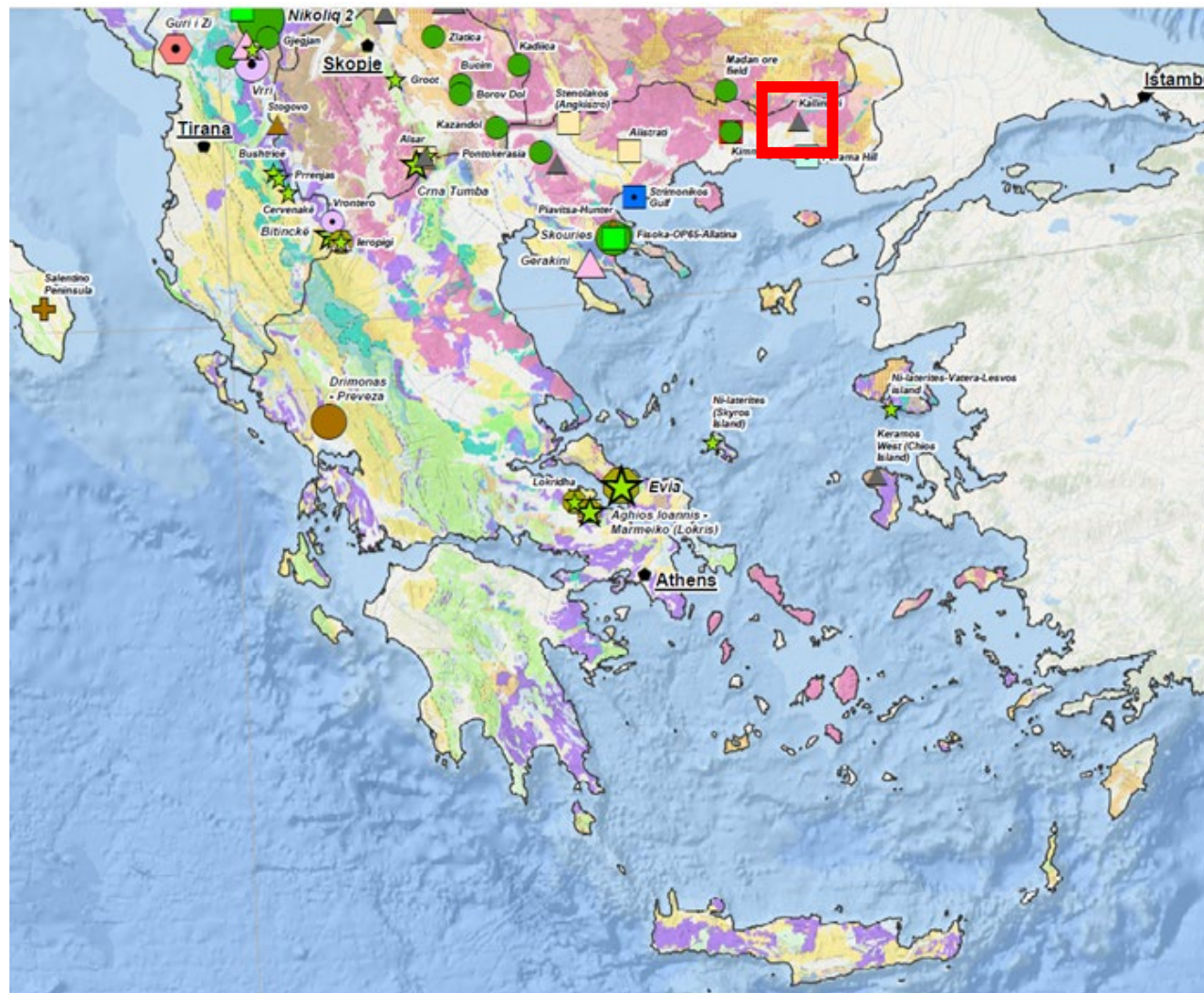
- the United States—Economic and environmental geology and prospects for future supply: U.S. Geological Survey Professional Paper 1802, p. C1– C17, <https://doi.org/10.3133/pp1802C>.
- Siron, C.R., Thompson, J.F.H., Baker, T., Friedman, R., Tsitsanis, P., Russell, S., Randall, S., and Mortensen, J., 2016, Magmatic and metallogenic framework of Au-Cu porphyry and polymetallic carbonate-hosted replacement deposits of the Kassandra mining district, northern Greece: Society of Economic Geologists Special Publication 19, p. 29–55
- Taylor S.R., and McLennan, S.M., 1995. The geochemical evolution of the continental crust: *Reviews of Geophysics*, v. 33, no. 2, p. 241–265. [Also available at <http://dx.doi.org/10.1029/95rg00262>.]
- U.S.G.S., 2022. United States Geological Survey - Final List of Critical Minerals 2022.
- U.S.G.S., 2023. Antimony - Mineral Commodity Summaries.
- U.S.G.S., 2024. Antimony - Mineral Commodity Summaries.
- Voudouris P., Mavrogonatos C., Spry, P.G., Baker, T., et al., 2019. Porphyry and epithermal deposits in Greece: An overview, new discoveries, and mineralogical constraints on their genesis. *Ore Geology Reviews*, Volume 107, pages 654-691, <https://doi.org/10.1016/j.oregeorev.2019.03.019>. This article was published in the special issue: Metallogeny of the eastern Mediterranean Realm, (Uysal i., Moritz r., Yiğit Ö, eds), Copyright Elsevier 2019.
- Wüthrich, E., 2009. Low temperature thermochronology of the Northern Aegean Rhodope Massif. Unpublished Doctoral thesis, Zürich, Switzerland, ETH Zürich. 216 p.

ANNEX I: CRM HARD ROCK DEPOSITS OF EUROPE (GSEU, v.5, January 2024)

Find text or tools    



Extract from the previous map showing the location of the Kallyntiri Sb-deposit.



Grant agreement	101091374
Project title	Multi-Source and Multi-Scale Earth Observation and Novel Machine Learning for Mineral Exploration and Mine Site Monitoring
Project acronym	MultiMiner
Project coordinator	Dr. Maarit Middleton, GTK
Project start date	Jan 1, 2023
Project duration	42 months
Related work packages	WP 4 – Site Demonstrations
Related task(s)	Task 4.1 In situ data standardization and databases
Lead organization	Geosphere Austria
Contributing partners	GTK, BGR, VTT, RHI, MUL, EFTAS, HSGME, CGS
Submission date	June 30, 2024
File name	Appendix 4 GUIDELINES FOR SPECTRAL DATA ACQUISITION – Field (D4_1_MultiMiner_Field_Guidebook_V1_4.docx)
Organisation responsible for deliverable	BGR
Author name(s)	Michaela Frei, Martin Schodlok, Patrick Reschke, Kai Hahne
Date	June 30, 2024
Version	1.0
Status	Complete
Dissemination Level	Public



Table of contents

1. Background	4
2. Motivation	4
3. Methodology Field Measurements	5
3.1 Field Spectroscopy	5
3.1.1 Required field equipment.....	5
3.1.2 Site description	6
3.1.3 Spectral field measurements.....	6
3.1.4 Collection of transect/profile reflectance measurements	8
3.1.5 Collection of target reflectance measurements/ Calibration measurements	8
3.1.6 Field/data sheet management	8
3.1.7 Field data storage	9
References	11

Acronyms / Glossary of terms

ASD	Analytical Spectral Devices, now owned by Malvern Panalytical
ASD3	ASD FieldSpec Pro 3
ASD4	ASD FieldSpec Pro 4
ASTER	Advanced Spaceborne Thermal Emission and Reflection Radiometer
BRDF	Bidirectional Reflectance Distribution Function
BRF	Bidirectional Reflectance Function
Cal	Calibration
CSIRO	Commonwealth Scientific and Industrial Research Organization
EO	Earth observation
FOV	Field of view
GPS	Global positioning system
GSD	Ground Sampling Distance
GUI	Graphical user interface
Lat	Latitude
Long	Longitude
QA	Quality assurance
QC	Quality control
SN	Serial number
SR	Surface reflectance
SWIR	Shortwave infrared



TBD	To be determined
UTC	Coordinated universal time
USB	Universal serial bus
UV	Ultraviolet
VNIR	Visible and near infrared



1. Background

This guide has been designed to support the systematic collection of *in situ* field spectroscopic data for the purposes of calibration and validation of surface reflectance of different scale products such as drone, airborne and satellite products and for that as input for spectral libraries. These data form archives of measurements suitable for validation and quantification of different reflectance products.

This handbook provides guidelines to ensure a high level of consistency between spectroscopy teams in MultiMiner project, including the selection of specific sites for measurement and in the systematic collection of both site description data and of spectral radiance and reflectance measurements using field spectrometers.

2. Motivation

Calibration and **validation** achieve independent verification of satellite/UAV surface reflectance and products and their uncertainties; they establish the link between the satellite/UAV products and measurements made on the ground (see box below for appropriate definitions). Without calibration, uncertainties can only be derived from pre-launch and on-board sensor calibrations (e.g. Thome 2001). To enable for the verification of the reflectance and products, conventional ground-based observations are required using calibrated and traceable field instrumentation and associated methods. It is only when we can quantify the uncertainty of the data products using **validation**, improved algorithms to reduce the uncertainty can be developed (Malthus et al. 2014).

The definition of Cal/Val key terms (Malthus et al., 2014)

- Calibration - The process of quantitatively defining the responses of a system to known, controlled signal inputs;
- Validation - The process of assessing, by independent means, the quality of the data products derived from the system outputs;

Optical satellite sensors of medium resolution such as the Multispectral Instruments (MSI) on board the Sentinel-2 series satellites (S2a and S2b) or Hyperspectral Instruments (HSI), are passive optical instruments measuring a combination of atmospheric and surface radiance at the top of the atmosphere (TOA) in discrete spectral bands in the 400 – 2500 nm range. The surface radiance in each band is calibrated to absolute physical measurements of $\text{mW m}^{-2} \text{sr}^{-1} \text{nm}^{-1}$. Each spectral band of each satellite has a spectral response function (SRF); in order to take specific SRFs into account measurements of surface reflectance at each calibration/validation site need to be made using a high spectral resolution instrument.

The techniques and methods of data measurement described here are mainly assembled to support calibration and validation of medium spatial/spectral Satellite data as well as high spatial/spectral resolution (i.e. hyperspectral) remote sensing instruments (e.g. Satellite, airborne and UAV) and to develop further spectral libraries.

Scale and homogeneity – Cal/Val sites should contain homogeneous features e.g. at the Sentinel-2 pixel scales, 10 to 60 m of a minimum of 30x30 up to 180 x 180 m or HS Instruments e.g. EnMAP 30x30 a minimum of 90x90 site scale or representative for airborne or drone sensors within a larger homogeneous region. Sites should be as homogeneous as possible in terms of background color and

vegetation cover to minimize within-site variation such that field reflectance values measured are representative over the scale of several satellite/airborne or UAV pixels in the imagery to be validated. In addition, spectral ground truth measurements are investigated to characterize targets spectrally and to link in situ field spectral measurements with laboratory and mineralogical and chemical analysis for spectral library development and Satellite and airborne product development and validation.

3. Methodology Field Measurements

This section outlines the method and equipment needed for collecting the field measurements. The minimum amount of equipment needed for the collection of field spectral data and the characterization of the site is outlined below.

3.1 Field Spectroscopy

While this handbook deals with the practical steps of obtaining high quality field spectral data it is important that anyone intending to undertake a field program be aware of the physics, nomenclature and measurement issues associated. It is relatively easy to get good field spectra – and easier still to get bad spectra.

3.1.1 Required field equipment

Equipment

Spectrometer (recently wavelength checked and radiometrically calibrated) with Visible, Near Infrared (VNIR)-Shortwave Infrared (SWIR) wavelength range, e.g. Spectral Evolution PSR+, with all relevant accessories and spare batteries	 <p>Fotos BGR</p>
Pistol grip for optical fibre with 8 degree foreoptic	 <p>Foto BGR</p>
Minimum 24.5 cm square Spectralon ⁺ reflectance panel (recently calibrated) and if relevant levelling tripod	 <p>Foto BGR</p>

Field sheets (Fig. 1);
 Camera for sky and site photos;
 Global positioning system (GPS) (+/-compass);
 100 m measuring tape

3.1.2 Site description

An example of the site description/field sheets can also be found in the Appendix. Field sheets for 'Target', 'Profile' and 'Cal/Val' are available including a predefined drop-down menu (Fig. 1).

field sheet - TARGET -

Project	date	page	start time	end time	coordinates latitude		coordinates longitude			
MultiMiner										
Target ID	picture start	picture end	Operator	referenz	type of measurement		device	contact probe	Foreoptic	
Country	general comment overview									
Location	Sublocation	Lithology /Formation					Main surface Target			
Path- Folder/File/ Photo										
meas- ment nr.	comment measurement		Photo Start	Photo End	Comment Photo		°C	sample number	scetch	
001										
002										
003										
004										
005										
006										
007										
008										

Figure 1. An example of a field sheet.

For cal/val measurements for e.g. UAV or proximal sensing a site of 1-2 m² with 5 to 9 measurements is appropriate. Spectral measurements are taken either in the center and at each corner or as 3x3 parallel measurements.

For transect layout for e.g. Cal/Val measurements for Satellite data with 30x30 spatial resolution pixel e.g. EnMAP a min of 60x60 m field with 6 to 10 parallel profiles is appropriate.

3.1.3 Spectral field measurements

Spectrometers must be warmed up before operation. Time for warm up varies between 15 to 30 minutes to 1 hour for different instruments and age of manuals. Findings from long-term operation by expert users has found that the detectors are known to drift considerably with different internal temperatures. It is not completely clear if a long warm up time is greatly beneficial, but a warm up of **at least 30 minutes** will show an improvement in instrument stability. Older instruments may have difficulty cooling the detectors in extremely hot weather conditions and may require strict timing of warm up and measurement.

Spectrometer optimization/calibration

Optimization of the spectrometer is required at the start of the measurements. This must be done as close in time as possible to the collection of data. To account for changing solar conditions, **at the start of each new profile/transect a re-optimization of the spectrometer needs to be performed, but at least every 15 minutes or if sky cloud conditions change.**

Setting up of the Spectralon reference panel

Larger panels are ideal (i.e. 500 x 500 mm) but are very expensive. Thus a **250 x 250 mm panel** should be the minimum size used.

DO NOT TOUCH THE PANEL SURFACE. The Spectralon panel should be clean and free of dirt, dust and visible marks. Ideally, it should not have any damage to the surface, such as deep scratches or indentations, which will cause shadowing. The panel should not have a shiny surface when viewed from a low angle, which would indicate that the panel surface is not as Lambertian as when it was manufactured and calibrated. When the panel is not in immediate use, it should be covered; this greatly reduces its exposure to the sun and air and its subsequent degradation.

The reflectance characteristic of the Spectralon panel and its factory calibration should be known. If the panel has been in use for a long period of time, its reflectance characteristics should be re-measured in the calibration laboratory.

While white reference measurements the panel is orientated towards the sun and is horizontal, ideally on a tripod but handheld is also convenient.

A panel should not be placed at ground level, due to the increased likelihood of contamination from dust and debris from footsteps and the prevailing wind.

Reference panel measurement

Measurement of the reference panel (including saving of the panel measurement) is made **before and after** each transect/profile/series of point measurements. Re-optimization should be conducted each time before the panel measurement is made at the start of a new profile/transect. Measurements of the panel should be conducted with the operator facing the sun and standing alongside the panel (i.e. to the east or west of the panel).

The FOV should be considered when setting the **height** of the foreoptic from the panel. It is important that the reading is from the center of the panel.

For example, a 8 degree FOV will capture a 210x210 mm panel edge at 1.5 m. An overview for the field of view with different foreoptics /bare fibre at different height is given in Table 1. The head of the spectrometer (i.e. foreoptic) should point directly downward (**nadir**).

As the spectrometer is set to collect 10 spectra per spacebar push, only one spacebar push is required to collect the 10 panel spectra.

Table 1. A reference table of distances to the target and the resulting GSD's (GSD=ground sampling distance).

Device e.g. ASD	Bar fibre FOV: 25 degree	FOV 8 degree
Distance to target	GSD (m)	GSD (m)

0.5	0.22	0.07
1	0.44	0.13
1.5	0.67	0.21
2	0.88	0.28
5	2.22	0.70
8	3.55	1.12
15	6.65	2.09

3.1.4 Collection of transect/profile reflectance measurements

The ground data collection will be performed using the continuous sampling approach. The head of the spectrometer is to be held at shoulder height, level and pointed directly downward (nadir), similar to that as described for the panel measurement. The spectrometer operator walks at a constant speed along the transect. The spacebar should be pushed at the location of each flag marking 20 m for a cal/val aerial measurement or in case of profile measurements every meter (or few meters as decided before hand).

At the end of each transect/profile re-acquire white reference panel spectra.

3.1.5 Collection of target reflectance measurements/ Calibration measurements

Follow the same setting as described in 3.1.4 but instead of walking take measurements while standing above or in front of the investigated surface area. The space bar is pushed and minimum 10 spectra are acquired. If sun conditions are not ideal but it is relevant to take field spectra measurements can be acquired by using the contact probe (see 3.1.1). Please make sure that lens is always clean while using the contact probe. For calibration/validation measurements for UAV or proximal sensing with e.g. Fenix it can be decided that a m^2 to several m^2 surface is measured by at least 5 target points (center, and each corner).

3.1.6 Field/data sheet management

While the operator is using the spectrometer, the second person, acting as the spotter, note taker and panel mover and if relevant as well as sample collector, has a very important role during data acquisition. As the operator acquires the measurements, the note taker is filling out the data sheet. The information that should be recorded include: measurement IDs, site information, the operator's names, the instrument, panel type, site, conditions, date, time, weather, clouds, wind, cover and surface conditions, topography etc. This list needs to be extended depending on specific questions and project goals. The note taker will also collect weather and sky condition information during the measurement period and track anomalous incidents. Sky condition information includes taking sky photo. An example of the field sheet is shown in the Appendix.

The note taker needs to be in communication with the spectrometer operator and ask what spectrum number they are up to during the collection, especially at the end of transects and after panel measurements. The note take should record the number of spectra acquired during each transect/profile/target measurement as well as the type of spectra (target or panel). The note taker watches the operator to ensure that the foreoptic is kept at nadir, that the field of view is being held in a stable position, that they follow the correct path along the predefined area of acquisition and

measure the reference panel when required.

For the spectral data the naming shall be short including site name, type of acquisition (cal/val, profile, target etc.

Example MultiMiner: *Country_Location_Sublocation_acquisition type_looping
number/AF_HF_LK_Tar_01*

3.1.7 Field data storage

At the end of each day's fieldwork, the measured data must be checked. In all cases, copies of the data must be saved to a local hard drive or USB drive or remote drive. Best attaching additional notes recorded on the field sheet, photographs, GPS locations, etc. and, any other QA/QC parameters recorded.

At the end of the campaign, data must be uploaded to relevant projects file database.

Field Guide Step by Step

Pre-visit:

Check the weather conditions.

Organize staff availability, travel arrangements, vehicles, equipment, accommodation and health and safety plans.

Inform landholders of intention to access. Pre-print field data recording sheets/ or use handheld tablet.

Make sure all batteries are charged and spares for instruments are packed.

Check your relevant packing and equipment lists. Make sure that all relevant cables, adaptors, etc. are packed.

On arrival:

Ensure times on all devices have been set to UTC.

Take photographs of the surface and the surroundings sufficient to characterize the site, its scale and the context of its surrounding environment (slope, distance to horizons, sky, vegetation type and height, soil colour)

Evaluate overhead atmospheric conditions. Take photos (preferably geotagged) of the sky conditions.

Warm up spectrometer and prepare for measurements.

Check GPS and tracker are working

Spectrometer settings (example)

The spectrometer (e.g. ASD) should be set up as follows:

- Dark current (if a VNIR shutter is present): 20
- Spectrum averaging: 20
- Radiance mode
- Number of files to save: 10
- Time between saves: 0 sec
- New file format
- Mode: Radiance
- Time on the laptop controller should be set to UTC
- GPS should be activated
- Fore optic set to bare fibre or 8 degrees

Fore optic set bare fibre or to 8 degrees

Start filling in the Site Description and Field Data Collection Form.

Set up the Spectralon panel, level and oriented to the sun. Consider keeping the panel covered when not being viewed by the ASD.

Field equipment checklist (each team has its own check lists)

Field record forms

Each team has their own check list.

Spectralon panel care

Spectralon reference panels are easy to damage due to their soft nature. Care should be taken with the panels so that they are not scratched or gouged in any way. Impacts on the panel surface will

cause dents and therefore shadowing. Dirt, fingerprints and insect gunk can all be removed by proper cleaning.

If the panel does need abrasive or significant cleaning then the panel's reflectance factor will have to be re-determined. Ideally, this should be undertaken in the calibration laboratory but if necessary it can be performed in the field using the ratio of downwelling irradiance made using an RCR foreoptic followed by a panel reading made using the 8 degree foreoptic. These measurements should ideally be made at solar noon. Defining a new reflectance factor can wait until after the field campaign so long as users note which data are impacted.

It is important to note that reference panels change properties with temperature (coefficient of thermal expansion) and that this may potentially affect their reflectance. Any significant changes in temperature should be noted.

References

Malthus, TJ, Ong, C, Lau, I, Fearn, P, Byrne G and Thankappan, M., Chisholm, L., Suarez, M., Clarke, K., Scarth, P., Phinn, S. (2018) A community approach to the standardised validation of surface reflectance data. A technical handbook to support the collection of field reflectance data. Release version 1.0. CSIRO, Australia. ISBN: 978-1-4863-0991-7

Grant agreement	101091374
Project title	Multi-Source and Multi-Scale Earth Observation and Novel Machine Learning for Mineral Exploration and Mine Site Monitoring
Project acronym	MultiMiner
Project coordinator	Dr. Maarit Middleton, GTK
Project start date	Jan 1, 2023
Project duration	42 months
Related work packages	WP 4 – Site Demonstrations
Related task(s)	Task 4.1 In situ data standardization and databases
Lead organization	Geosphere Austria
Contributing partners	GTK, BGR, VTT, RHI, MUL, EFTAS, HSGME, CGS
Submission date	June 30, 2024
File name	Appendix 5 GUIDELINES FOR SPECTRAL DATA ACQUISITION – Laboratory (D4_1_MultiMiner_Field_Guidebook_V1_4.docx)
Organisation responsible for deliverable	BGR
Author name(s)	Michaela Frei, Martin Schodlok, Patrick Reschke, Kai Hahne, Kati Laakso
Date	June 30, 2024
Version	1.0
Status	Complete
Dissemination Level	Public

Contents

1	Point spectrometer.....	2
1.1	General.....	2
1.2	Handheld instruments ASD/ Spectral Evolution	3
1.3	Agilent FTIR instruments	3
2	Imaging Instruments.....	4
2.1	SisuRock.....	4
2.2	Measurement – Sample preparation	5
3	ASD FieldSpec (Spectral Evolution etc.) measurement protocol for rock, soil and tailings samples including the Internal Soil Standard (ISS).....	7
3.1	Sample preparation.....	7
3.2	Sample container.....	7
3.3	Measurement setup	7



3.4 ASD software settings.....	8
3.5 Measurement White Reference.....	8
3.6 Measurement Standard Sand (SSAN) for soil samples.....	9
3.7 Measurement of soil samples	9
3.8 Internal Soil Standard (ISS).....	9

Acronyms:

ASD	Analytical Spectral Devices, now owned by Malvern Panalytical
FTIR	Fourier Transform Infrared Spectroscopy
GSD	Ground Sampling Distance
ISS	Internal Soil Standard
LB	Lucky Bay
SSAN	Standard Sand
WB	Wiley Bay
WR	White Reference
WS	Weißstandard

These guidelines apply to point spectral measurements and imaging spectral measurements conducted in a laboratory in the MultiMiner project. The samples can be rock samples, soil samples or tailings samples. The spectrometers used in the project are listed in Table 1.

1 Point spectrometer

1.1 General

- Prior to any spectral measurements, let the samples adjust to room temperature.
- Spectral Laboratory (especially for spectral library standard measurements) has ideally a black coating all over to avoid scatter light from walls etc... (Fig. 1).
- Make sure the samples are free of dust and organic material prior to spectral measurements (Fig. 2).
- Sample surfaces must be arranged parallel to the instrument head independent of sample type.
- Photos of the measured areas must be recorded and measurement logs kept.
- Ensure that the field of view of the spectrometer is completely covered by the sample. Ensure that the sample is optically thick, i.e. light is not transmitted because the sample is so thin.
- Always ensure that the instrument batteries are left charged after use. Leaving batteries flat for long periods of time may damage them permanently.



1.2 Handheld instruments ASD/ Spectral Evolution

- Turn the spectrometer on at least 30 min prior to spectral measurements.
- Use the same measurement set up for the white reference and sample measurements.
- In cases where the white reference readings are done with a contact probe or similar foreoptic, make sure to wipe the contact point (e.g. the contact probe) with lint free and non-scratching towels prior to any white reference measurements.
- Conduct white reference measurements as often, or more often than what suggested by the instrument manual (see Table 1 for reference).
- Make sure the foreoptics of the instrument is clear at all times.

1.3 Agilent FTIR instruments

These instruments are used in direct contact with the sample. The surface must be even to avoid effects off scattering light from surrounding area contaminating the measurement. Surface that can be measured with one measurement is 2 mm diameter. The instrument has its own internal calibration.

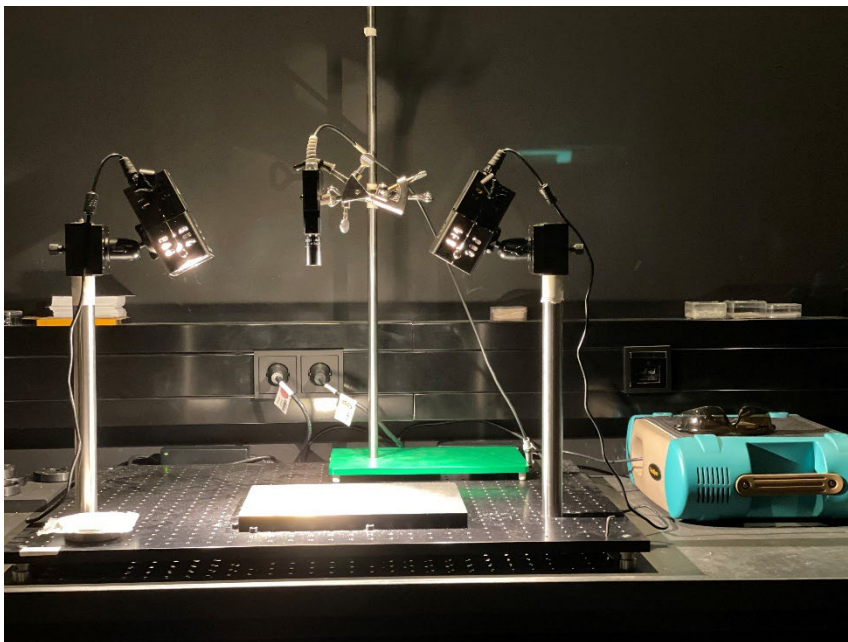


Figure 1. A data acquisition setup



Figure 2. A sample with a ruler for scale.



Table 1. The essential parameters of different point spectrometers.

	Malvern Panalytical TerraSpect Halo	ASD-FieldSpec 4	Spectral Evolution PSR+	Spectral Evolution RS8800	Agilent FTIR 4300
Wavelength range	350-2500 nm	350-2500 nm	350-2500 nm	350-2500 nm	4500-650 cm^{-1}
Number of scans	50-100	Default setting Min 10	Default setting Min 10	Default setting Min 10	128
Frequency of white reference measurements (minutes)	The instrument prompts when a white reference measurement is required.	30 minutes			every 10 minutes

2 Imaging Instruments

2.1 SisuRock

The system consists of three cameras (VNIR, SWIR and LWIR), which are operated with three corresponding computers (Fig. 3, Table 2). Pixel resolution is for the VNIR/SWIR max. $25 \mu\text{m} - 1.5 \text{mm}$ for the LWIR max. $400 \mu\text{m}$. The essential parameters of the system cameras are given in Table



Figure 3. The SisuROCK drill core scanner setup.



Start the systems 30 min before the measurements, and keep the room temperature at ca. 21 degrees. The samples should have room temperature at the time of measurements.

Table 2. The essential parameters of different cameras of the SisuROCK drill core scanner.

	FENIX	OWL
Manufacturer	Specim	Specim
Wavelength range	380 – 2500 nm	8000-12000 nm
Frequency of white reference measurements (minutes)	Every measurement	Every measurement

Calibration

Dark current and white balance run is set automatic with measurements start.

Focus setting

Software prompts via screen if focus is ok (Fig. 4).

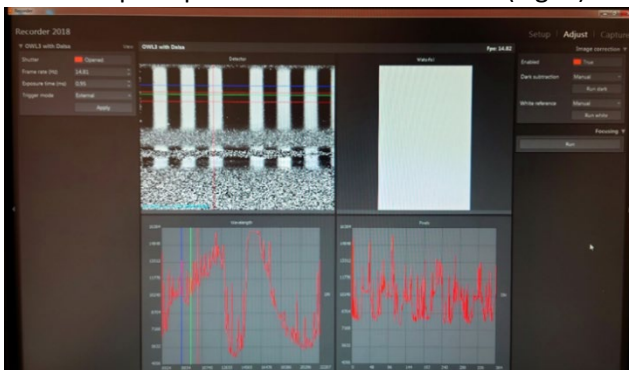


Figure 4. Focus settings of the SisuROCK drill core scanner.

The black and white grid is sharp and therefore the focus is set correctly.

2.2 Measurement – Sample preparation

The sample/samples to be measured are first brought to the same height using the parallel press and kneading mass (Fig. 5).





Figure 5. A sample measurement setup.

The sample table is adjusted so that the sample surfaces match the marking on the "sample surface" spirit level. In case of very irregular samples, e.g. the weathering crust on the outside of a sample disk, the height is adjusted using a box filled with quartz sand (Fig. 6).



Figure 6. A sample measurement setup.

Make sure that the samples are positioned as centrally as possible on the table (e.g. marked with the magnetic spheres provided) so that they are fully captured by all three cameras. Storage location on all three computers parallel.

Generate/measure data:

Capture of data starts with file name setting, several measurements with length of 1 m and width of 4.5 cm are set by default. Switch off the room light during the measurement!



3 ASD FieldSpec (Spectral Evolution etc.) measurement protocol for rock, soil and tailings samples including the Internal Soil Standard (ISS)

3.1 Sample preparation

- a. Air-dry samples for 48 hours (record room temperature and humidity)
- b. Switch on air conditioning and leave switched on (also during measurements)
- c. Sieve samples to <2 mm (fine soil) if possible and if following the ISS is required
- d. Leave the two reference samples Standard Sand (SSAN) Wylie Bay (WB) and Lucky Bay (LB) open for at least 24 hours under the same atmospheric conditions in the laboratory so that a moisture equilibrium can be established that corresponds to the soil samples to be measured

3.2 Sample container

- a. Material: plastic, glass, stainless steel
- b. Sample area should be at least 2 x ground distance size
- c. Fill the sample container to the top and smooth the surface (e.g. knife, spatula, glass jar)

3.3 Measurement setup

- a. 2 artificial light sources, each at a 45° angle to the sample (Fig. 7).
- b. Allow lamps and spectrometer to warm up for at least 1 hour
- c. Use the same white standard for the entire measurement, no contact between the white standard and the sample
- d. The distance of the white standard must correspond to that of the sample
- e. The GSD (ground sampling distance) can be calculated using the following formula. See also table 3.

$$GSD = \tan\left(\frac{\alpha}{2}\right) \times h \times 2$$

GSD = ground sampling distance in m

α = Sensor FOV (23° for ASD bare fiber measurements, otherwise the angle of the foreoptic)

h = height of the sensor in m (see also Table 3)

- f. Keep the door closed during the measurement

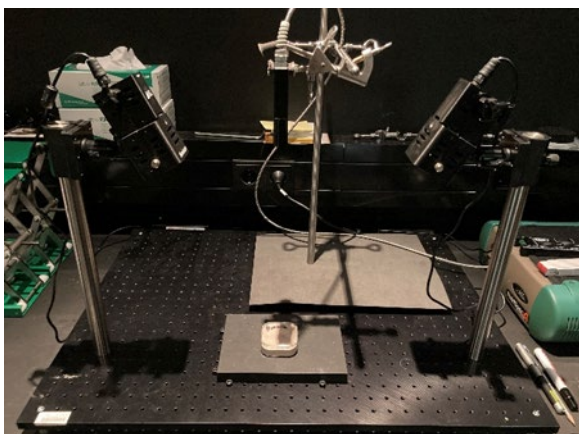


Figure 7. A data acquisition setup.

3.4 ASD software settings

- a. Start ASD software RS³
- b. Create a new folder for the measurements under C:\... create or alternate
- c. Change the save path under *Control* → *Spectrum Save* to the folder created
- d. Change the numbering from 0 to 1 under *Control* → *Spectrum Save* → *Starting Spectrum Name*
- e. Make the following settings under *Control* → *Adjust Config*:
 - Used foreoptic: 8°
 - Spectrum: 100
 - Dark current (DC): 100
 - White reference (WR): 100
- f. Save spectrum with space bar

3.5 Measurement White Reference

- a. Position the white reference in the center (align the foreoptic using a laser pointer) and mark the position
- b. In RS³ select **Opt** to optimize the measurements
- c. In RS3 select **WR** to perform a white balance. The maximum reflectance values of the white reference for each spectral band are recorded in order to estimate the relative reflectance of the subsequent measurements
- d. Measure the white reference, wait 2-4 minutes and repeat the measurement (reflectance should be 100%) to guarantee the stability of the spectrometer and the light sources
- e. Use a corrected transfer standard with the aid of a master standard

Correction of the transfer standard

- $Cts = Cst(Vts/Vst)$

Cst - calibration of master reference

Vts - response of transfer standard

Vst - response of master reference

Cts - Calibration factor transfer standard

Conversion to reflectance with the calibration factor

- $Rs = Cts(Vs/Vts)$

Cts - calibration transfer standard

Vs - response sample target

Vts - response transfer standard

Rs - calibrated reflectance sample target



3.6 Measurement Standard Sand (SSAN) for soil samples

- Fill LB and WB samples each into a sample container and smooth out
- Same height sample surface and white standard
- Carry out the measurement
- Mix the sample, smooth it, turn it 90° and measure again
- Repeat d
- For each sample, take 3 measurements from different sides (270°) (maintain direction of rotation)
- LB and WB are measured both before and after the sample measurement, so that at the end there are 6 spectra each (6 x LB and 6 x WB)
- The spectra of the 6 measurements must not differ from each other by more than 5 % (proposal IEEE SA P4005 WG: < 5 % at 1650 nm)/ the variation of the 6 measurements must be < 7 % percent

3.7 Measurement of soil samples

- Procedure according to the SSAN measurement
- Measure 5 soil samples per batch
- After each batch, measure WB and LB again according to the procedure from 5.
- Measure white reference
- Measurement sequence per batch (29 measurements): WS, LB, LB, LB, WB, WB, WB, samples (5 samples, measure 3x per sample), LB, LB, LB, WB, WB, WB, WS

3.8 Internal Soil Standard (ISS)

Background: Correction of soil sample spectra to the international CSIRO (Commonwealth Scientific and Industrial Research Organization) standard for comparability of different measurements

$$CF_{\lambda} = 1 - ((S\rho_{\lambda} - M\rho_{\lambda}) / S\rho_{\lambda})$$

$$Rc_{\lambda} = Ro_{\lambda} \times CF_{\lambda}$$

Sr_{λ} is the reflectance of the *Slave* reference (SSAM – user- standard)

Mp_{λ} is the reflectance of the *Master* reference (SSAN – CSIRO - standard)

Ro_{λ} is the original sample reflectance (SOIL -user)

Rc_{λ} is the corrected sample reflectance (SOIL – user – normalized to CSIRO Master)

CF_{λ} – A CORRECTION FACTOR

Table 3. the distance (in cm).

A reference table of ground sampling (GSD) at different instrument heights (in

Height (cm)	GSD (cm)		
	1 degree	8 degree	Bare fiber
10	0,17	1,39	4,06



15	0,26	2,09	6,10
20	0,35	2,79	8,13
25	0,44	3,49	10,17
30	0,52	4,19	12,20
35	0,61	4,89	14,24
40	0,70	5,59	16,27
45	0,78	6,29	18,31
50	0,87	6,99	20,34

